

Contract No. DTFACT-15-D-00007
Task Order Number 005

Construction Cycle 7 Post-Traffic Report - Field Testing
DELIVERABLE 4.9.3.1

September 3, 2019

Composed by:
Gemini Technologies Inc., for General Dynamics Information Technology

GENERAL DYNAMICS
Information Technology

TABLE OF CONTENTS

	Page
1. INTRODUCTION	1
2. P-401: ASPHALT CONCRETE	5
2.1 PSPA	5
2.2 Asphalt Cores	10
3. ASPHALT TREATED DRAINABLE BASE	12
3.1 Field Cores	12
4. P-209: CRUSHED STONE BASE	13
4.1 D-PSPA	13
4.2 LWD	15
4.3 Nuclear Gauge Density and Sand Cone	17
5. P-154: AGGREGATE SUBBASE	22
5.1 D-PSPA	22
5.2 LWD	30
5.3 Nuclear Gauge Density and Sand Cone	34
6. P-152 DUPONT CLAY SUBGRADE	43
6.1 D-PSPA	43
6.2 LWD	46
6.3 CBR and Vane Shear	47
6.4 Drive Cylinder and Nuclear Density	50
6.5 DCP	53
7. PROFILE	66
8. SUMMARY	74
9. REFERENCES	74
APPENDICES	

LIST OF FIGURES

Figure	Page
1 CC7 Post Traffic Trench Locations	3
2 Layer Profile Measurement on Trench Wall	4
3 PSPA Test Locations	6
4 Comparison of Seismic Modulus Between Traffic And Non-Taffic Areas (CC7 North Side)	6
5 Comparison of Seismic Modulus Between Traffic And Non-Taffic Areas (CC7 South Side)	7
6 PSPA Results Along The Trench Line (CC7 South Side, longitudinal direction)	8
7 PSPA Results Along The Trench Line (CC7 South Side, transverse direction)	8
8 PSPA Results Along The Trench Line (CC7 North Side, longitudinal direction)	9
9 PSPA Results Along The Trench Line (CC7 North Side, transverse direction)	9
10 CC7 Post Traffic Coring Locations.	11
11 D-PSPA Results on P-209 (CC7 North Side)	14
12 D-PSPA Results on P-209 (CC7 South Side, transverse direction)	14
13 D-PSPA Results on P-209 (CC7 South Side, longitudinal direction).	15
14 LWD Tests on P-209	16
15 LWD Results on P-209 (CC7 South Side)	16
16 LWD Results on P-209 (CC7 North Side).	17
17 LWD Tests on P-209	18
18 12 in. Sand Cone Tests on P-209	18
19 Nuclear Tests on P-209 (CC7 South Side)	19
20 Nuclear Tests on P-209 (CC7 North Side)	20
21 Sand Cone Tests on P-209 (CC7 South Side)	20
22 Sand Cone Tests on P-209 (CC7 North Side)	21
23 Sand Cone Tests on P-209 (CC7 North Side)	21
24 D-PSPA Results on P-154 for LFS6-N and LFC5-N (CC7 North Side, longitudinal direction)	22
25 D-PSPA Results on P-154 for LFS6-N and LFC5-N (CC7 North Side, transverse direction)	23
26 D-PSPA Results on P-154 for LFP1-N (CC7 North Side, longitudinal direction)	23
27 D-PSPA Results on P-154 for LFP1-N (CC7 North Side, transverse direction)	24
28 D-PSPA Results on P-154 for LFP2-N (CC7 North Side, longitudinal direction)	24
29 D-PSPA Results on P-154 for LFP2-N (CC7 North Side, transverse direction)	25
30 D-PSPA Results on P-154 for LFP3-N (CC7 North Side, longitudinal direction)	25
31 D-PSPA Results on P-154 for LFP3-N (CC7 North Side, transverse direction)	26
32 D-PSPA Results on P-154 for LFP4-N (CC7 North Side, longitudinal direction)	26
33 D-PSPA Results on P-154 for LFP4-N (CC7 North Side, transverse direction)	27
34 D-PSPA Results on P-154 (CC7 South Side, longitudinal direction): (a) Layer Surface, (b) 10'' below Surface	28
35 D-PSPA Results on P-154 (CC7 South Side, transverse direction): (a) Layer Surface, (b) 10'' below Surface	29
36 LWD Results on P-154 for LFC5-N and LFS6-N (CC7 North Side)	30
37 LWD results on P-154 for LFP1-N to LFP4-N (CC7 North Side): (a) Layer Surface, (b) 12'' below Surface	31
38 LWD results on P-154 for LFC5-S and LFC6-S (CC7 South Side)	32

39 LWD results on P-154 for LFC1-S to LFC4-S (CC7 South Side): (a) Layer Surface, (b) 10'' below Surface	33
40 Sand Cone Results on P-154 for LFC5-N and LFS6-N (CC7 North Side)	34
41 Sand Cone Results on P-154 for LFP1-N to LFP4-N (CC7 North Side): (a)Layer Surface, (b) 10'' below Surface	35
42 Sand Cone Results on P-154 for LFC5-S and LFC6-S (CC7 South Side)	36
43 Sand Cone Results on P-154 for LFC1-S to LFC4-S (CC7 South Side): (a)Layer Surface, (b)10'' below Surface	37
44 Nuclear Density Results on P-154 for LFC5-N and LFS6-N (CC7 North Side)	38
45 Nuclear Density Results on P-154 for LFP1-N to LFP4-N (CC7 North Side): (a)Layer Surface, (b)12'' below Surface	39
46 Nuclear Density Results on P-154 for LFC5-S and LFC6-S (CC7 South Side)	40
47 Nuclear Density Results on P-154 for LFC1-S to LFC4-S (CC7 South Side): (a)Layer Surface, (b)10'' below Surface	41
48 P-154 Gradation LFC5-S	42
49 P-154 Gradation LFC5-N	42
50 P-154 Gradation LFC6-S	43
51 D-PSPA Results on P-152 (CC7 North Side, longitudinal direction)	44
52 D-PSPA Results on P-152 (CC7 North Side, transverse direction)	44
53 D-PSPA Results on P-152 (CC7 South Side, longitudinal direction)	45
54 D-PSPA Results on P-152 (CC7 South Side, transverse direction)	45
55 LWD Results on P-152 (CC7 North Side)	46
56 LWD Results on P-152 (CC7 South Side)	47
57 CBR Results on P-152: (a)North Side, (b)South Side	48
58 Vane Shear Results on P-152: (a)North Side, (b)South Side	49
59 Drive Cylinder Results on P-152 for LFS6-N and LFC5-N (CC7 North Side)	50
60 Drive Cylinder Results on P-152 for LFP1-N to LFP4-N (CC7 North Side)	51
61 Drive Cylinder Results on P-152 (CC7 South Side)	51
62 Nuclear Density Results on P-152 for LFS6-N and LFC5-N (CC7 North Side)	52
63 Nuclear Density Results on P-152 for LFP1-N to LFP4-N (CC7 North Side)	52
64 Nuclear Density Results on P-152 (CC7 South Side)	53
65 DCP Results for LFC1-S	54
66 DCP Results for LFC2-S	55
67 DCP Results for LFC3-S	56
68 DCP Results for LFC4-S	57
69 DCP Results for LFC5-S	58
70 DCP Results for LFC6-S	59
71 DCP Results for LFP1-N	60
72 DCP Results for LFP2-N	61
73 DCP Results for LFP3-N	62
74 DCP Results for LFP4-N	63
75 DCP Results for LFC5-N	64
76 DCP Results for LFS6-N	65
77 Pavement Layer Profiles, LFS6-N	66
78 Pavement Layer Profiles, LFC5-N	67
79 Pavement Layer Profiles, LFP4-N	67

80	Pavement Layer Profiles, LFP3-N	68
81	Pavement Layer Profiles, LFP2-N	68
82	Pavement Layer Profiles, LFP1-N	69
83	Pavement Layer Profiles, LFC6-S	69
84	Pavement Layer Profiles, LFC5-S	70
85	Pavement Layer Profiles, LFC4-S	70
86	Pavement Layer Profiles, LFC3-S	71
87	Pavement Layer Profiles, LFC2-S	71
88	Pavement Layer Profiles, LFC1-S	72
89	Percent Contribution to Rut Depth (LFS6-N LFC5-N)	72
90	Percent Contribution to Rut Depth (LFP1-N to LFP4-N)	73
91	Percent Contribution to Rut Depth (CC7 South)	73

LIST OF TABLES

Table	Page
1 CC7 South Maximum Rut Depth at the End Of Traffic Test	1
2 Summary of Trench Locations	2
3 PSPA Test Locations on P-401 Surface	5
4 CC7 North P401-Nontraffic Area Coring Locations	10
5 CC7 South P401-Nontraffic Area Coring Locations	10
6 CC7 South P401-Cracking Area Coring Locations	10
7 P-401 Material Laboratory Test Plan for CC7 North Cores	12
8 P-401 material laboratory test plan for CC7 south cores	12
9 CC7 North ATDB Non-traffic Area Coring Locations	12
10 ATDB Material Laboratory Test Plan	13

LIST OF ACRONYMS

2D	Dual Tandem
AC	Advisory Circular
ACN-PCN	Aircraft Classification Number–Pavement Classification Number
APA	Asphalt Pavement Analyzer ATDB
ATDB	Asphalt Treated Drainable Base
AV	Air Voids
CC1	Construction Cycle 1
CC7	Construction Cycle 7
CDF	Cumulative Damage Factor
D	Dual
FAA	Federal Aviation Administration
FN	Flow Number
GSD	Grain Size Distribution
G/S	Gravel-to-Sand
HMA	Hot-Mix Asphalt
ICAO	International Civil Aviation Organization
JMF	Job Mix Formula
LVDT	Linear Vertical Displacement Transducers
NAPTF	National Airport Pavement Test Facility
NAPTV	National Airport Pavement Test Vehicle
NCHRP	National Cooperative Highway Research Program
SCI	Structural Condition Index
TSR	Tensile Strength Ratio
UCS	Unconfined Compressive Strength
VMA	Voids in Mineral Aggregates

1. INTRODUCTION

CC7 traffic testing was completed in December 2016. Severe rutting was observed in all six test items on the south side, as shown in table 1. Comprehensive analyses of HWD data were performed, and the largest deflections were found in either or both of the intermediate granular material layers above the subgrade and below the surface layer (base and subbase). On the north side of CC7, MDD data showed the majority of the observed rutting was in the subbase P-154 layer.

Table 1. CC7 South Maximum Rut Depth at the End of Traffic Test

Test Item	Test Item Passes	STA, ft	Maximum Rut Depth, in
LFC1-S	27522	10	3.51
	27522	25	3.62
LFC2-S	27522	60	3.98
	27522	75	4.39
LFC3-S	26136	110	5.33
	26136	125	5.59
LFC4-S	22836	160	4.00
	22836	175	3.78
LFC5-S	22836	210	4.15
	22836	225	4.53
LFC6-S	14520	260	4.65
	14520	275	5.06

Trenching provides a viable option to examine failed test items, confirmation of the contribution of each pavement layer to the total rutting, characterization of the material properties for each layer of the pavement structure, evaluation of the effect of traffic load on the pavement material properties, and allows samples to be retrieved for laboratory material characterization.

One 60-ft long, 4-ft wide trench was excavated perpendicular to the centerline of NAPTF for each test item. Trenches in test items LFP1-N, LFP2-N, LFP3-N and LFP4-N were excavated to an approximate depth of 49 inches, including the removal of the P-154/P-152 interface. All remaining trenches in both north and south side were excavated to an approximate depth of 49 inches. Table 2 lists the start station and end station for each trench. As shown in figure 1, the proposed trenches are located between the MDD sensors and profile stations where the maximum rut depth was measured.

The trenching involved removing the surface P-401 HMA layer, ATDB, P-209 base, and P-154 subbase (in multiple lifts) to reveal the subgrade interface. Removal of P-401 layer required a saw cut deep enough to penetrate through the HMA surface, while minimizing the disturbance to base and subbase materials. Tests and measurements then were performed on the various pavement layers.

Table 2. Summary of Trench Locations

Test Item	Start STA, ft	End STA, ft
LFP1-N/LFC1-S	20	24
LFP2-N/LFC2-S	70	74
LFP3-N/LFC3-S	120	124
LFP4-N/LFC4-S	165	169
LFP5-N/LFC5-S	220	224
LFP6-N/LFC6-S	270	274

Upon the completion of all tests, transverse trench walls (at base, subbase and subgrade levels) were smoothed using shovels, chisels, and brooms. Once a clean trench wall was achieved, chalk and string lines were used to differentiate pavement layers. The profile of each layer was measured at regular intervals to determine its contribution to the total deformation and upheaval of the pavement structure (figure 2).

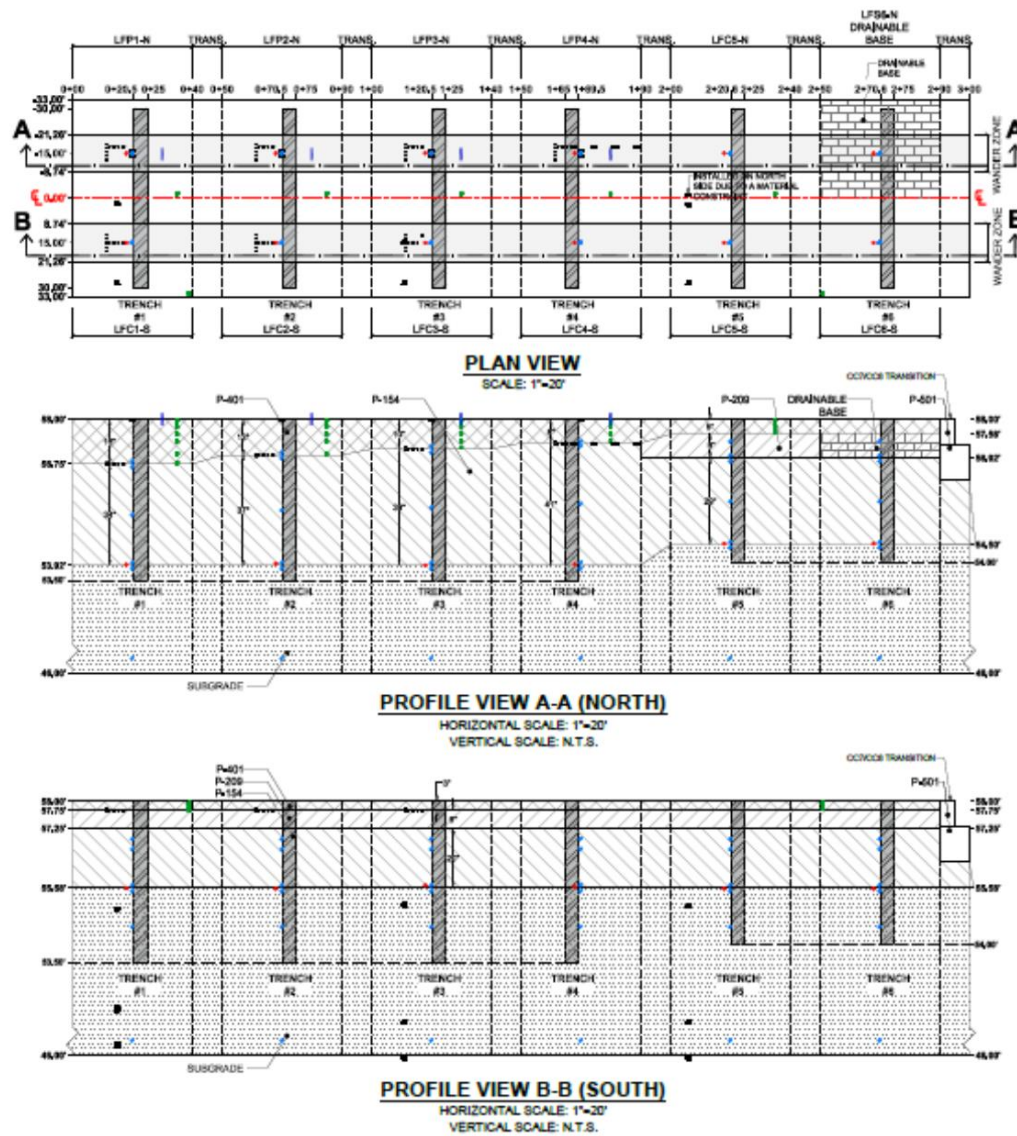


Figure 1. CC7 Post Traffic Trench Locations



Figure 2. Layer Profile Measurement on Trench Wall

2. P-401: ASPHALT CONCRETE

Before trenching, Portable Seismic Property Analyzer (PSPA) tests were performed on top of the P-401 asphalt layer to evaluate the effect of the traffic load on the modulus of the P-401 materials. PSPA is a non-destructive testing method based on wave propagation theory. The PSPA is set on the test surface and a source initiates highly repeatable seismic waveforms that are recorded by three accelerometers. These waveforms are transferred back to the computer for analysis. The modulus of the pavement materials can be determined based on compression or shear wave velocity. The modulus value obtained from PSPA is low-strain elastic modulus. The seismic modulus is normally higher than laboratory dynamic modulus at the same temperature. The repeat traffic load induced micro cracking that can reduce the modulus of P-401 materials. The PSPA testing results are summarized in the following sections.

2.1 PSPA

PSPA tests were performed on the surface of the P-401 as detailed in table 3. PSPA test was conducted at all the offsets in each station indicated in table 3. A typical layout of the test locations considered for trench surface testing is illustrated in figure 3.

Table 3. PSPA Test Locations on P-401 Surface

General Surface Testing		Trench Surface Testing	
Station (ft.)	Offset (ft.)	Station (ft.)	Offset (ft.)
15	-25	20	-25
30	-15	70	-22
65	-5	120	-20
80	+5	170	-15
115	+15	220	-10
130	+25	270	-8
165			-5
180			+5
215			+8
230			+10
265			+15
280			+20
			+22
			+25

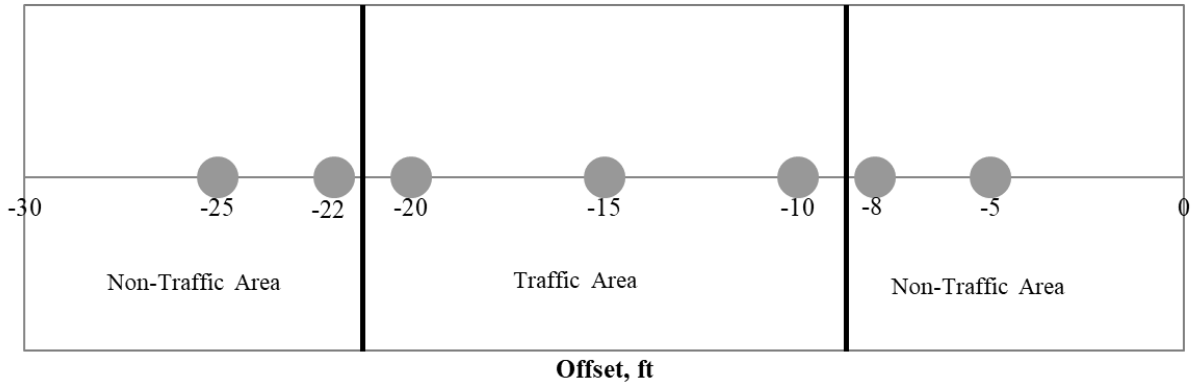


Figure 3. PSPA Test Locations

Figures 4 and 5 show the comparison of seismic modulus collected from traffic area and non-traffic area. The results appear to indicate that seismic moduli of P-401 in the non-traffic area is higher than traffic area in most test items. There was no significant difference in LFP1-N, because the P-401 layer was thicker than the other test items and the traffic did not produce much damage in the surface layer. Since the seismic wave cannot travel through macro cracks and there was a large amount of cracking in LFC6-S, the PSPA tests were performed on a traffic area without cracking. The seismic modulus in non-traffic area was close to the traffic area in test item LFC6-S. In summary, the modulus of P-401 materials reduced due to the traffic induced micro cracks.

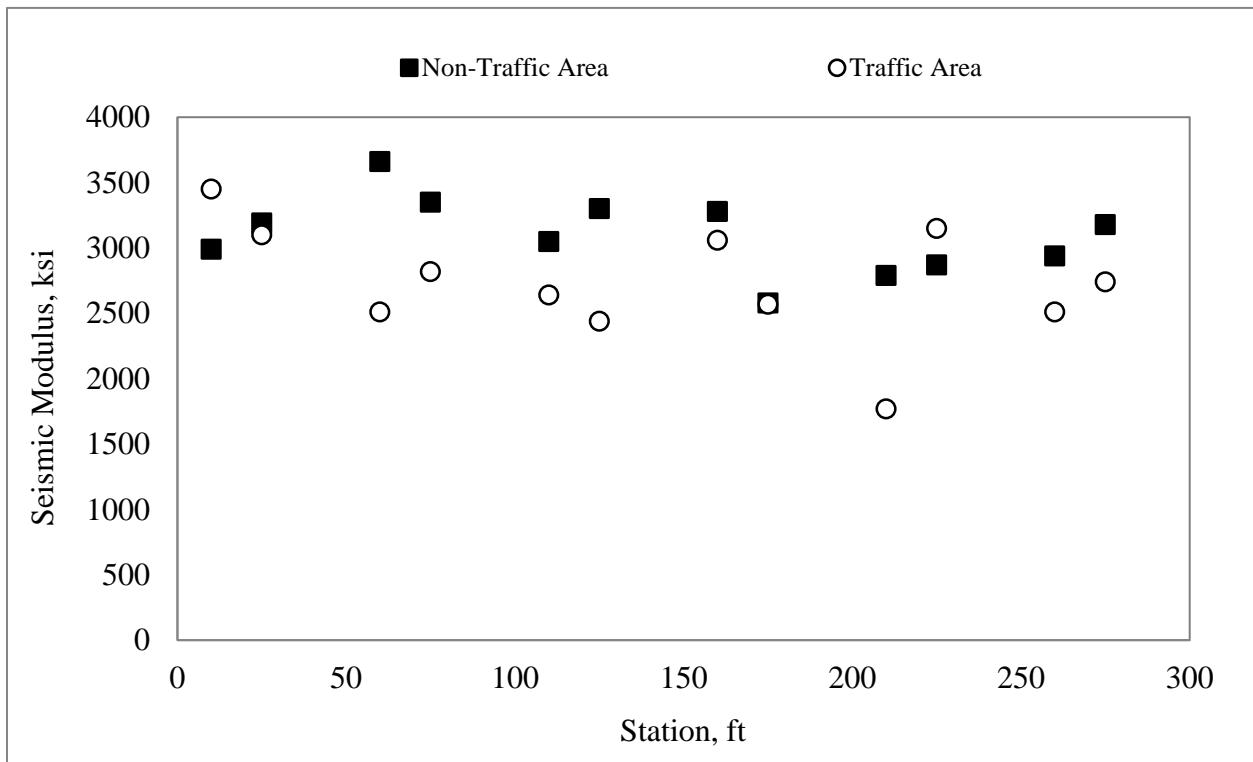


Figure 4. Comparison of Seismic Modulus Between Traffic And Non-Traffic Areas (CC7 North Side)

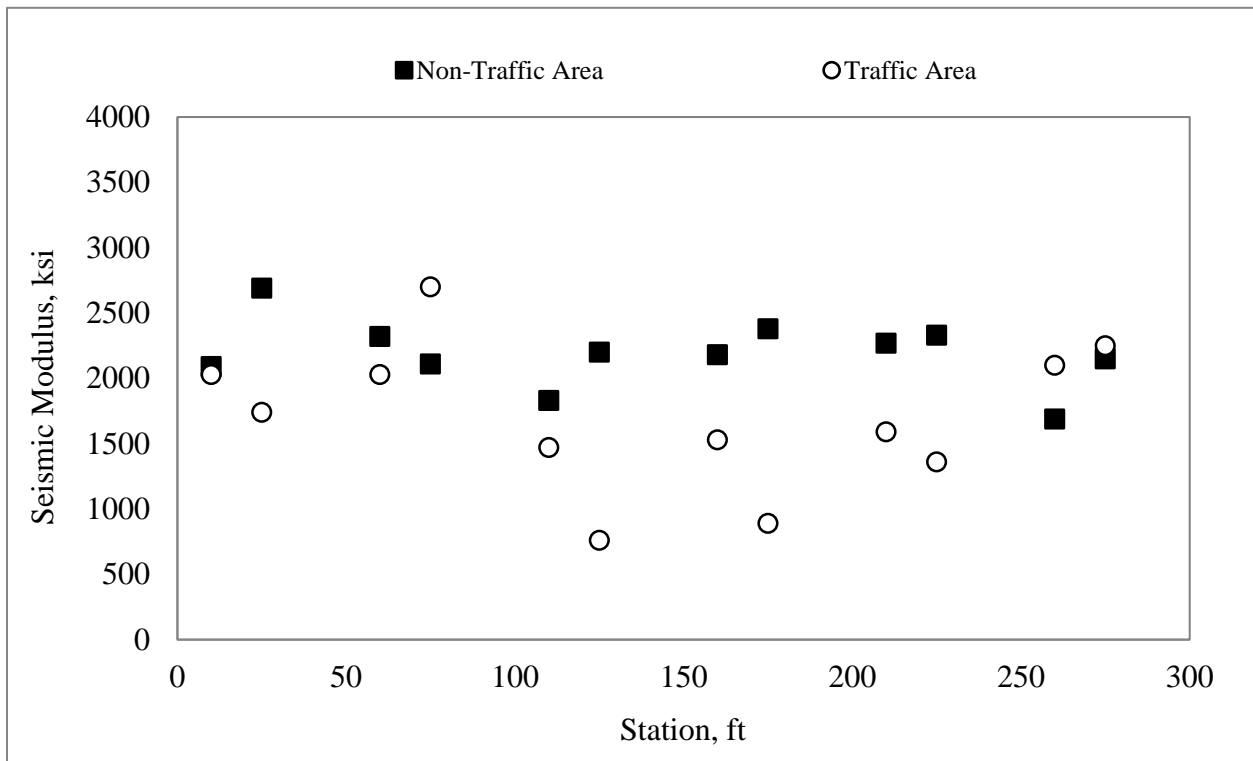


Figure 5. Comparison of Seismic Modulus Between Traffic And Non-Taffic Areas (CC7 South Side)

Figures 6-9 represent PSPA results that were performed along each of the trench lines. PSPA tests were performed in both longitudinal and transverse directions. All the figures show the same trend as mentioned previously for figures 4 and 5. Generally, the seismic moduli of P-401 in traffic areas were lower than non-traffic areas on both sides and both directions.

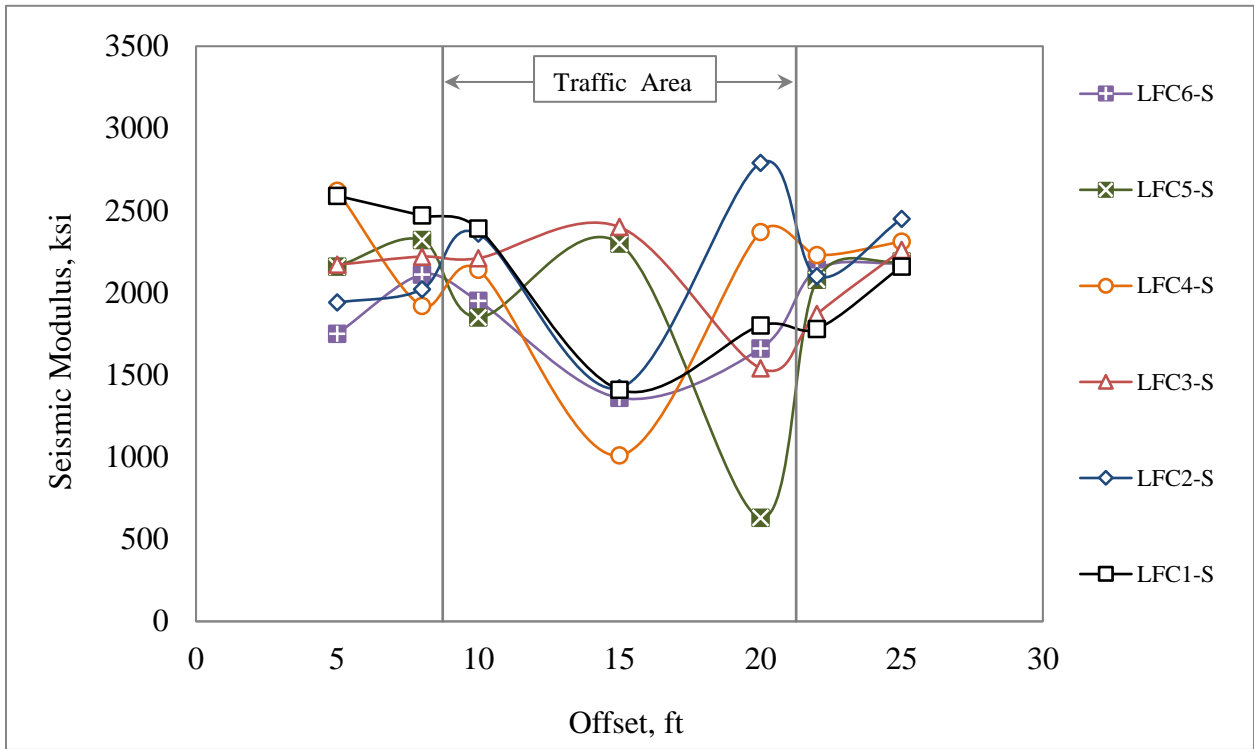


Figure 6. PSPA Results along the Trench Line (CC7 South Side, longitudinal direction)

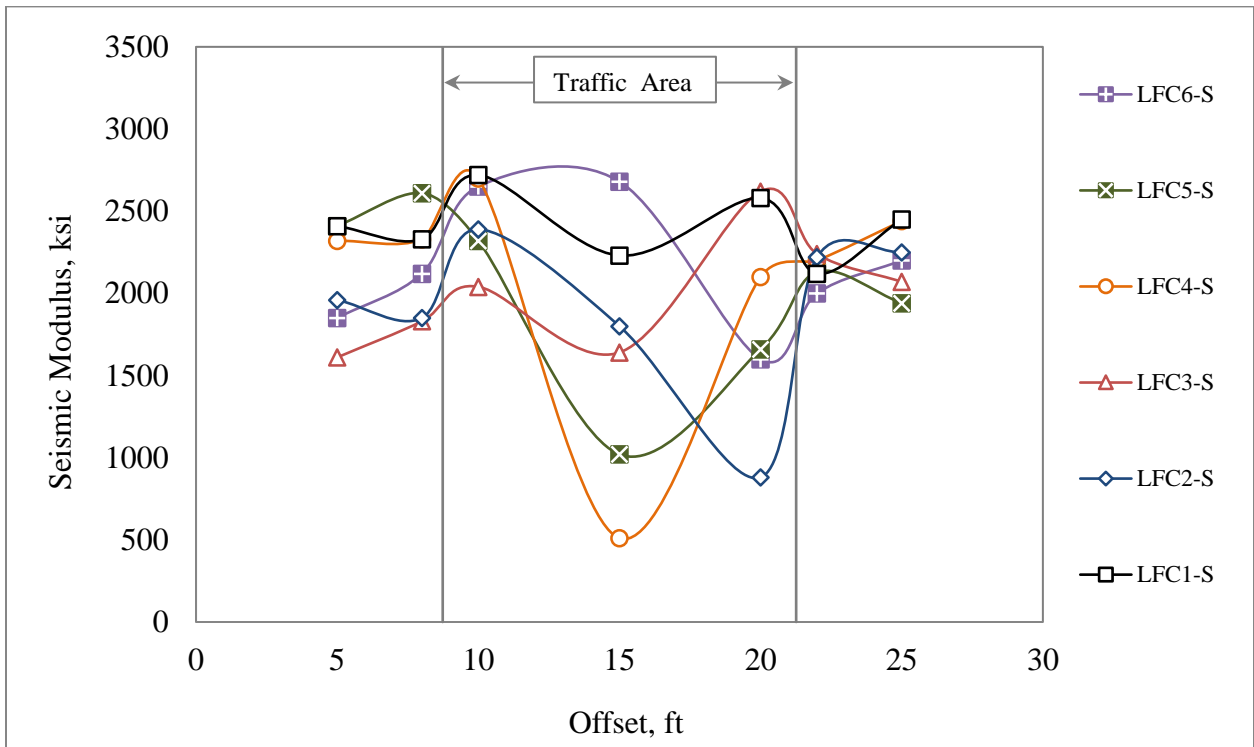


Figure 7. PSPA Results along the Trench Line (CC7 South Side, transverse direction)

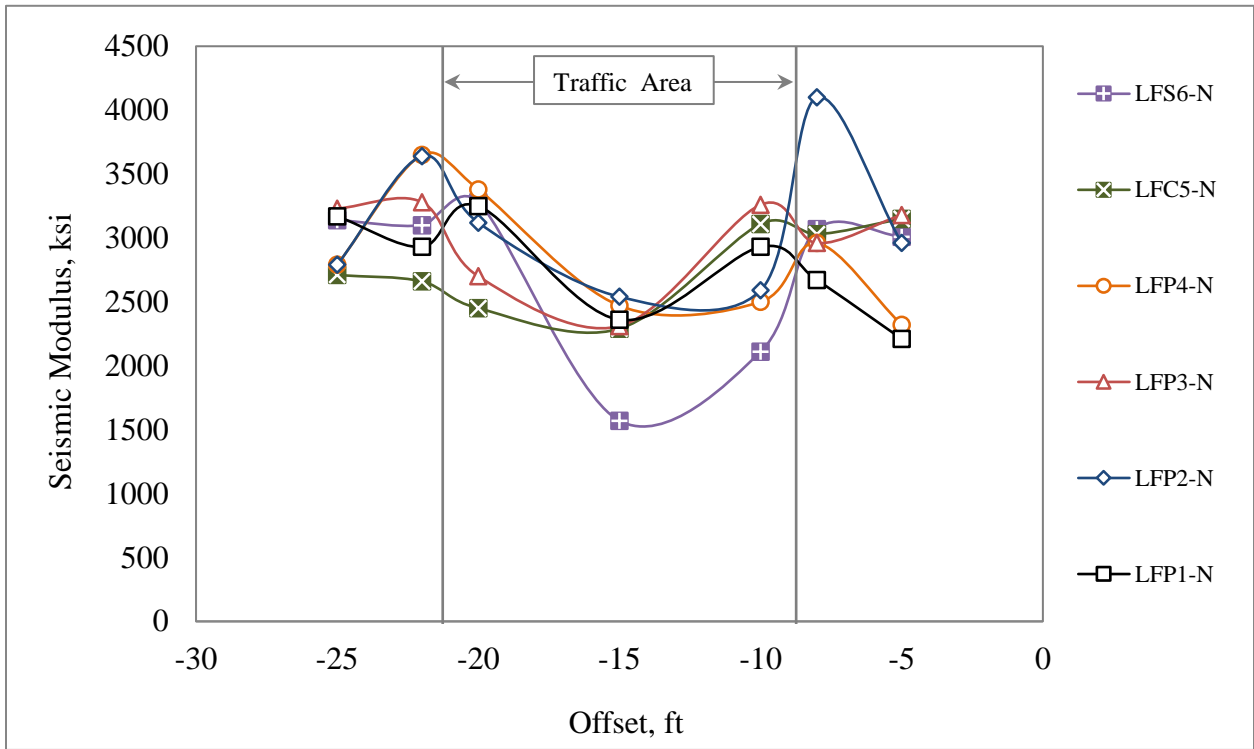


Figure 8. PSPA Results along the Trench Line (CC7 North Side, longitudinal direction)

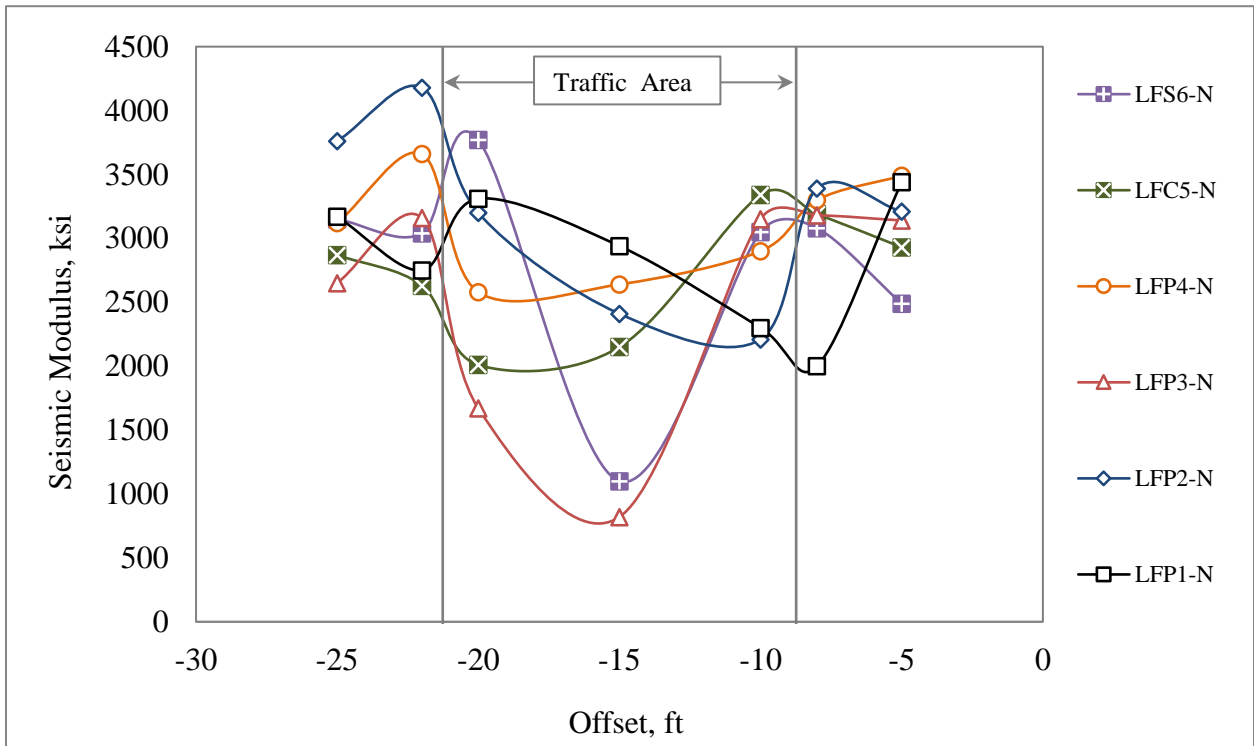


Figure 9. PSPA Results along the Trench Line (CC7 North Side, transverse direction)

2.2 ASPHALT CORES

There were 6” Cores (Inner diameter of core bit=6”) collected from the non-traffic areas away from upheaval. Additional field cores were also extracted at crack locations in each south side test item. The detailed coring locations are shown in tables 4-6 and figure 10 (tables 7 and 8 show the laboratory test plans). Six and five cores were collected at each non-traffic location (figure 10) in the north and south side, respectively. Only one core per crack location was collected in the south side. The data analysis was provided in a separate CC7 Post-Traffic Report - Laboratory Testing (I).

Table 4. CC7 North P401-Nontraffic Area Coring Locations

Test Item	Core #	Station (ft.)	Offset (ft.)
LFP1-N	1-6	30	-5
LFP2-N	7-12	85	-5
LFP3-N	13-18	120	-5
LFP4-N	19-23	180	-5
LFC5-N	24-28	220	-5
LFS6-N	29-33	265	-5

Table 5. CC7 South P401-Nontraffic Area Coring Locations

Test Item	Core #	Station (ft.)	Offset (ft.)
LFC1-S	1-5	20	4
LFC2-S	6-10	70	4
LFC3-S	11-15	120	4
LFC4-S	16-20	165	4
LFC5-S	21-24	220	4
LFC6-S	25-28	265	4

Table 6. CC7 South P401-Cracking Area Coring Locations

Test Item	Cracking Direction	Core #	Station (ft.)	Offset (ft.)
LFC6-S	Longitudinal	C1	258	18
	Transverse	C2	252	14
LFC5-S	Longitudinal	C3	206	14
	Transverse	C4	215	13
LFC4-S	Longitudinal	C5	165	11
	Transverse	C6	170	18
LFC3-S	Longitudinal	C7	115	15
	Transverse	C8	120	11
LFC2-S	Longitudinal	C9	69	13
	Transverse	C10	77	12
LFC2-S	Transverse	C11	18	19
	Longitudinal	C12	14	14

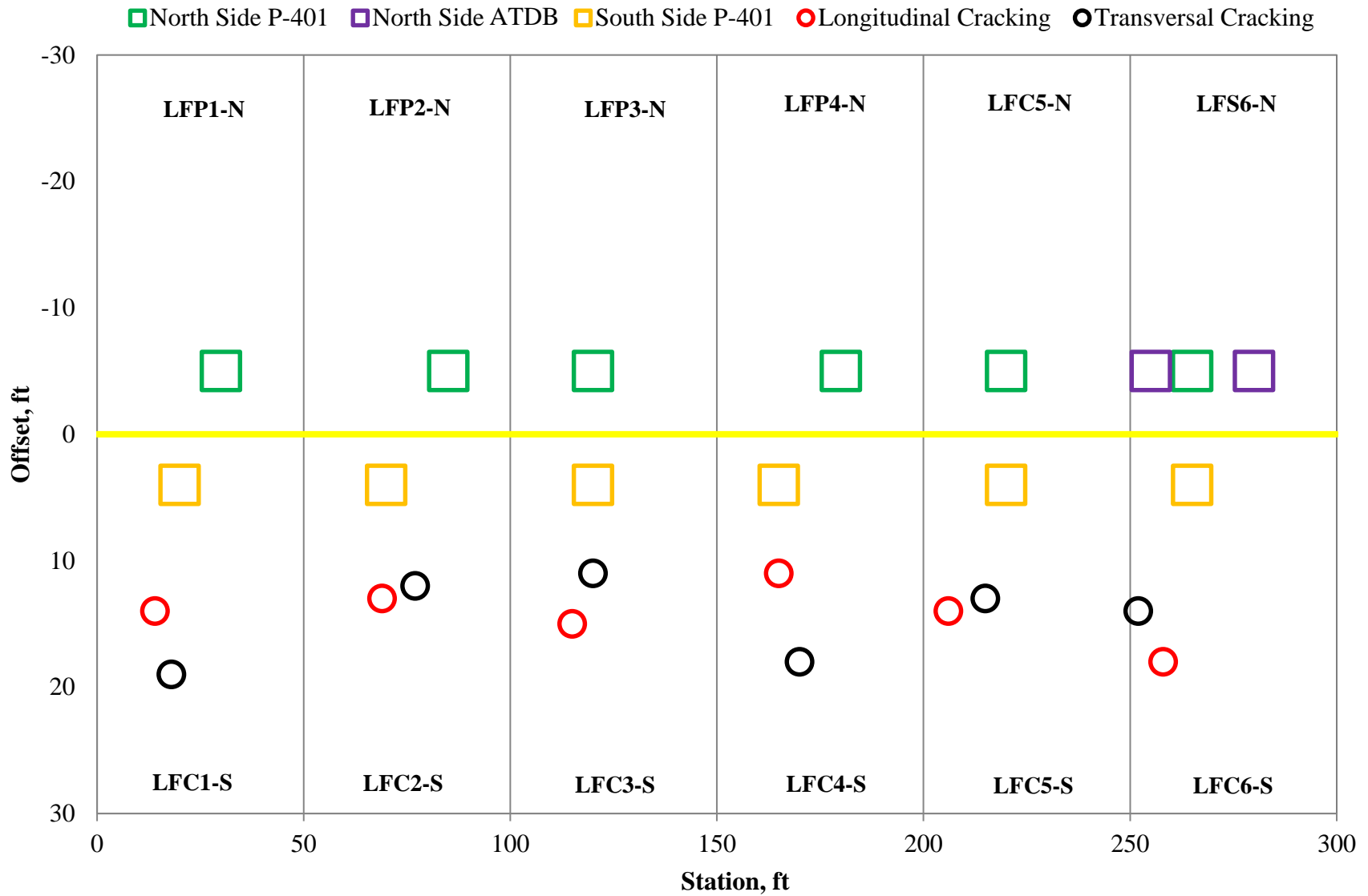


Figure 10. CC7 Post Traffic Coring Locations.

Table 7. P-401 Material Laboratory Test Plan for CC7 North Cores

Property	Test	Standards	Quantities
Modulus	AMPT Dynamic Modulus	AASHTO T342	5*
	IDT Dynamic Modulus	ASTM D7369	5*
Permanent deformation	AMPT Flow Number	AASHTO TP79	5
	High Temperature IDT	ASTM D6931	5
	APA(100psi and 254psi)	AASHTO T340	12
Cracking resistance	IDT Creep and Strength	AASHTO T322	5
Moisture sensitivity	Tensile Strength Ratio	ASTM D4867	3
Air Voids	Gmb and Gmm	ASTM D3203	3
Total Core Samples			33

*Since AMPT and IDT Dynamic Modulus tests are non-destructive tests, the specimens fabricated for AMPT Flow Number and IDT Creep and Strength can be used to perform those tests.

Table 8. P-401 material laboratory test plan for CC7 south cores

Property	Test	Standards	Quantities
Modulus	IDT Dynamic Modulus	ASTM D7369	5*
Permanent deformation	High Temperature IDT	ASTM D6931	5
	APA	AASHTO T340	12
Cracking resistance	IDT Creep and Strength	AASHTO T322	5
Moisture sensitivity	Tensile Strength Ratio	ASTM D4867	3
Air Voids	Gmb and Gmm	ASTM D3203	3
Total Core Samples			28

*Since IDT Dynamic Modulus tests are non-destructive tests, the specimens fabricated for IDT Creep and Strength can be used to perform those tests.

3. ASPHALT TREATED DRAINABLE BASE

3.1 FIELD CORES

There were 6” Cores (Inner diameter of core bit=6”) collected from non-traffic areas away from upheaval (Offset: -6 ft. to -2 ft.). The detailed coring locations are shown in table 9. These cores included the P-401 surface materials. Table 10 shows the laboratory test plan. The data analysis was provided in a separate CC7 Post-Traffic Report - Laboratory Testing (1).

Table 9. CC7 North ATDB Non-traffic Area Coring Locations

Test Item	Core #	Station	Offset
LFS6-N	D1-D8	255	-5
LFS6-N	D9-D18	280	-5

Table 10. ATDB Material Laboratory Test Plan

Property	Test	Standards	Quantities
Modulus	AMPT Dynamic Modulus	AASHTO T342	5*
Permanent deformation	AMPT Flow Number	AASHTO TP79	5
	APA(100psi and 254psi)	AASHTO T340	12
Permeability	Falling Head Permeability Test	N/A	3
Air Voids	Gmb and Gmm	ASTM D3203	3
Total Core Samples			23

*Since AMPT Dynamic Modulus tests are non-destructive tests, the specimens fabricated for AMPT Flow Number can be used to perform those tests.

4. P-209: CRUSHED STONE BASE

On the CC7 south side, there was a 6 in. P-209 layer underneath the P-401 surface layer for all six test items. On CC7 north side, only test item LFC5-N had a 5 in. P-209 layer. The P-209 crushed aggregate base course was clean crushed calcium carbonate (limestone) aggregate purchased from a local aggregate supplier conforming to the FAA Advisory Circular AC 150/5370-10G. The material was placed in a single lift with a paver and compacted to at least 98.0% of the laboratory maximum dry density (γ_{dmax}). Sand cone testing yielded an average of 2.7% moisture content (dry of the 5.7% optimum condition) with a dry density of 156.8 lb/ft³. When the P-401 HMA layer was removed, D-PSPA, LWD, Nuclear Gauge Density and 12-in Sand Cone tests were performed on top of P-209 along the trench line. The following sections summarize the field test results.

4.1 D-PSPA

D-PSPA tests were done at offsets -15ft, -10ft, -8ft, -5ft, +5ft, +8ft, +10ft, and +15ft for LFC-5-N and all the test items on CC7 south side to determine seismic moduli of the base material. Figures 11-13 summarize the PSPA results.

Figures 12 and 13 showed that on the south side, regardless of test direction (i.e., transverse or longitudinal), the seismic modulus of P-209 material in traffic areas was higher than non-traffic areas. This can be attributed to additional densification of the P-209 material resulting from traffic load. The velocity of the seismic wave in the solid materials increased with the increased density.

On the north side, the P401 pavement is 5 inches thick, which is 2 inches thicker than the south side. Also, the maximum wheel load on the north side was higher than the south side. The data in figure 11 indicates that, on the north side, the seismic modulus was higher than the average measured during construction.

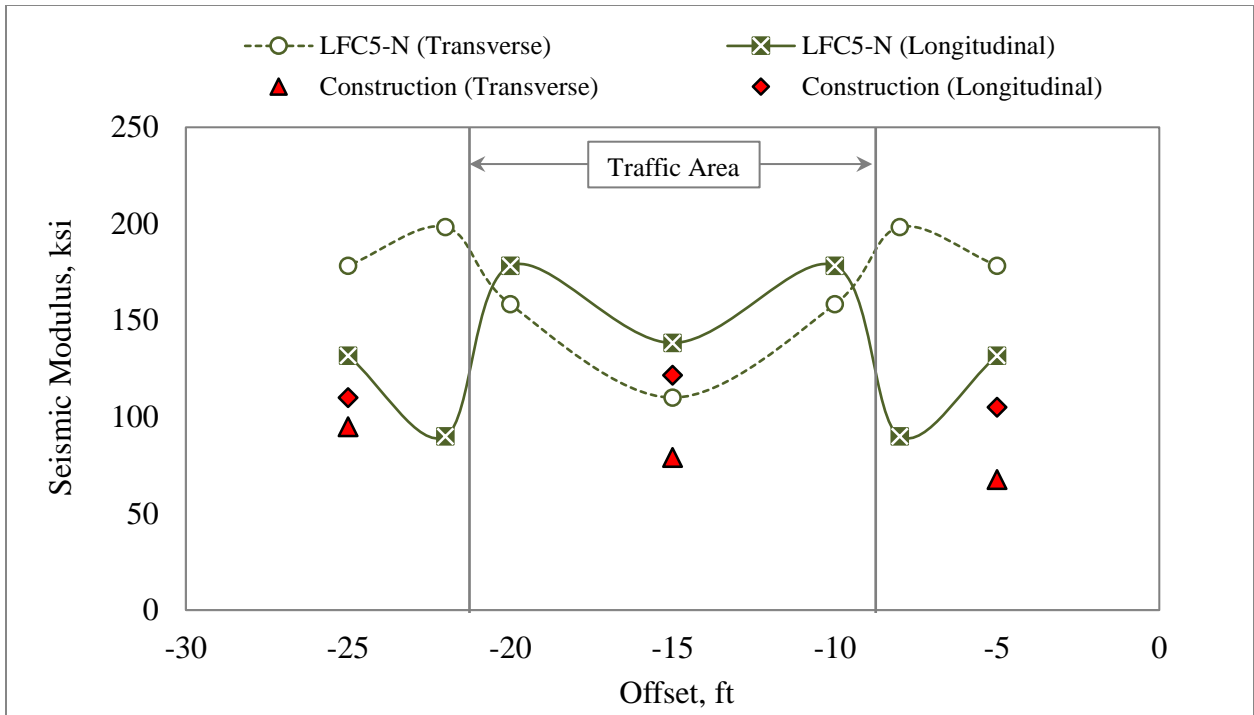


Figure 11. D-PSPA Results on P-209 (CC7 North Side)

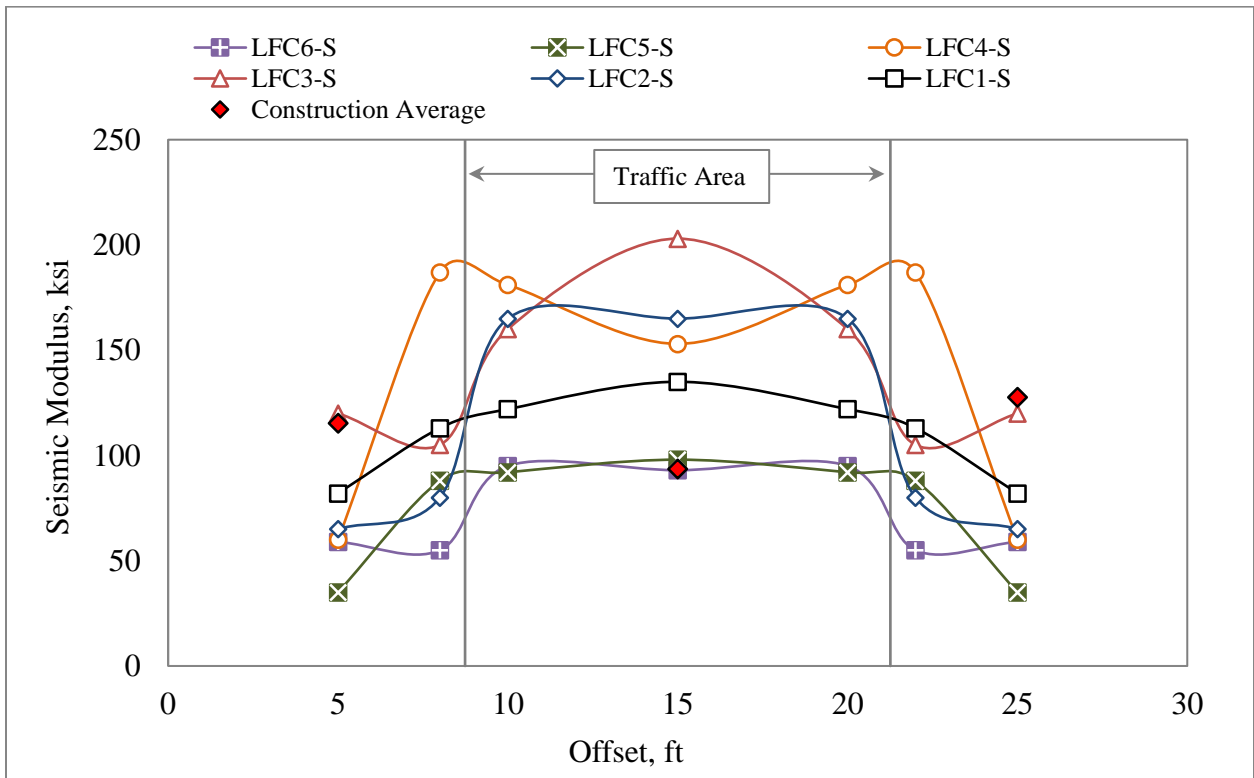


Figure 12. D-PSPA Results on P-209 (CC7 South Side, transverse direction)

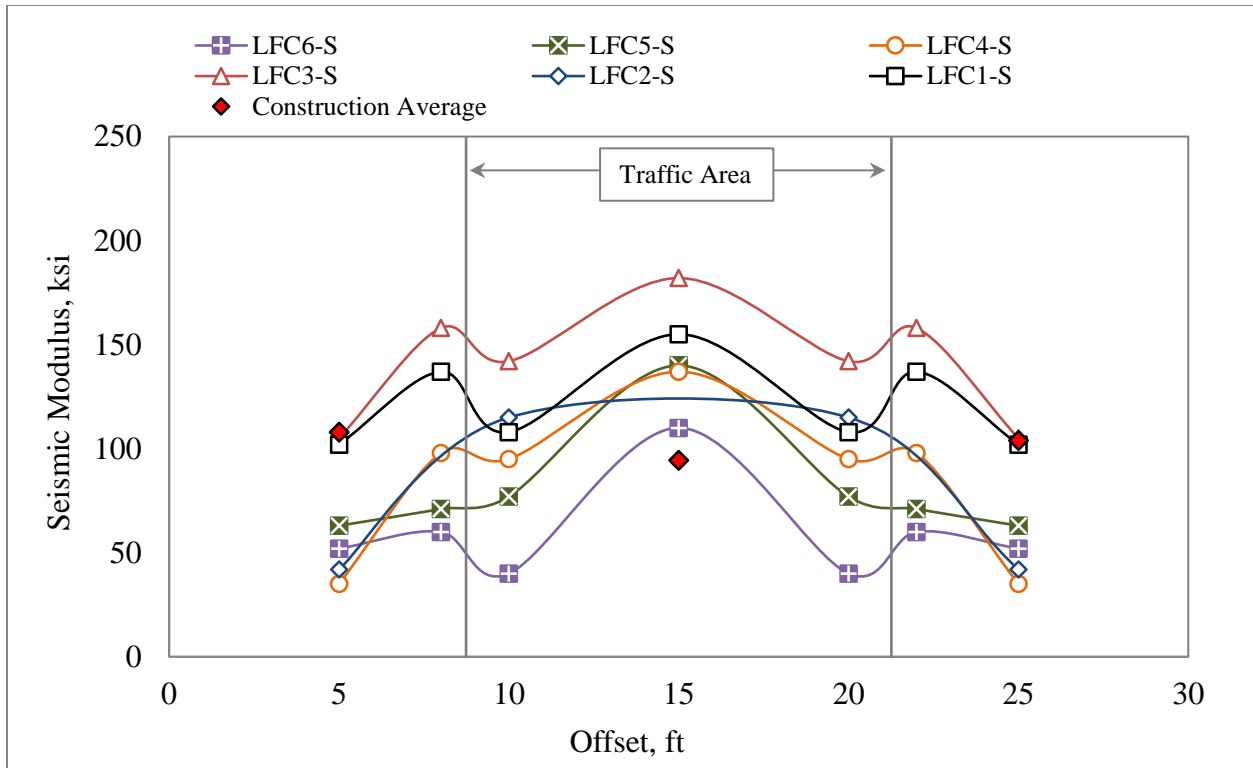


Figure 13. D-PSPA Results on P-209 (CC7 South Side, longitudinal direction).

4.2 LWD

Light Weight Deflectometer (LWD) is a portable version of the HWD. LWD measures the deflection from a falling weight and estimates the modulus. LWD (figure 14) tests were done at offsets -15ft, -10ft, -8ft, -5ft, +5ft, +8ft, +10ft, and +15ft atop of P-209 on both the north and south side. Figures 15 and 16 summarize the LWD results. The LWD results show a similar trend as PSPA results. On the CC7 south side, the LWD modulus in traffic areas was higher than non-traffic areas. Post-traffic LWD modulus were higher than pre-traffic LWD modulus. Additional post-construction compaction from full-scale traffic test increased the density of P-209 material in traffic areas.



Figure 14. LWD Tests on P-209

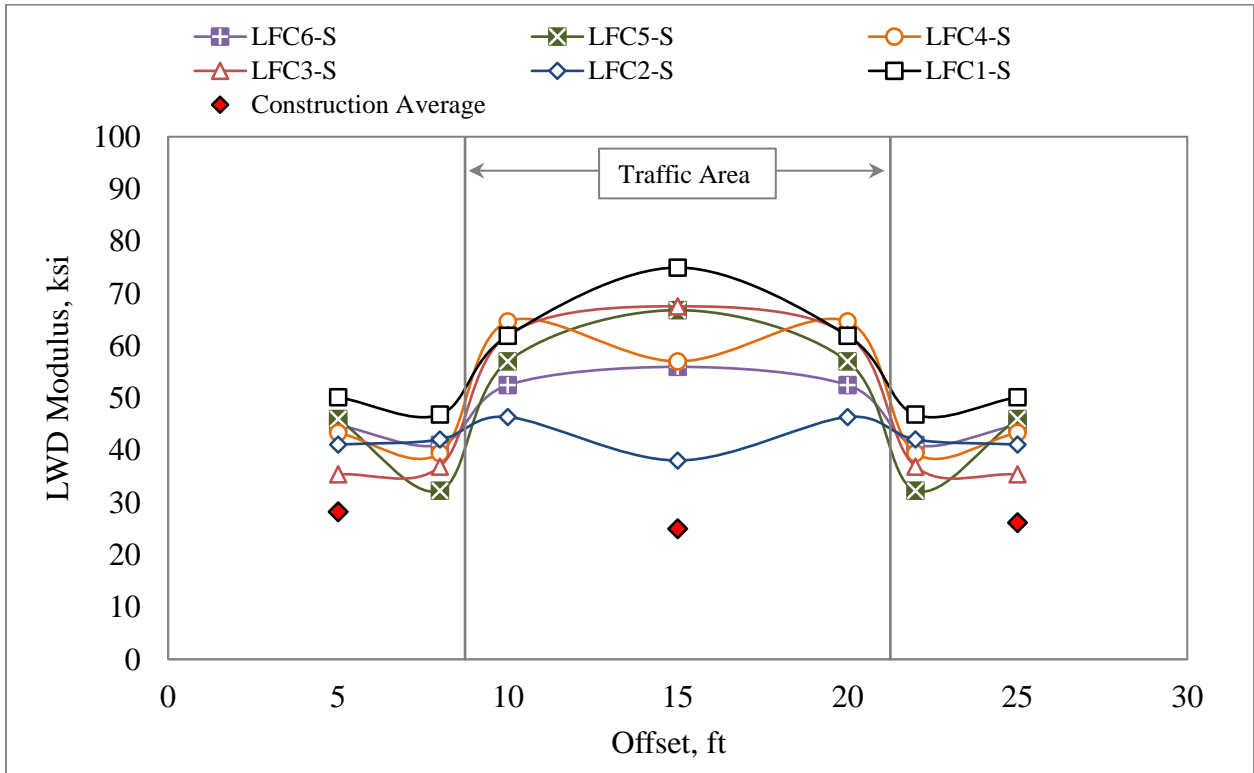


Figure 15. LWD Results on P-209 (CC7 South Side)

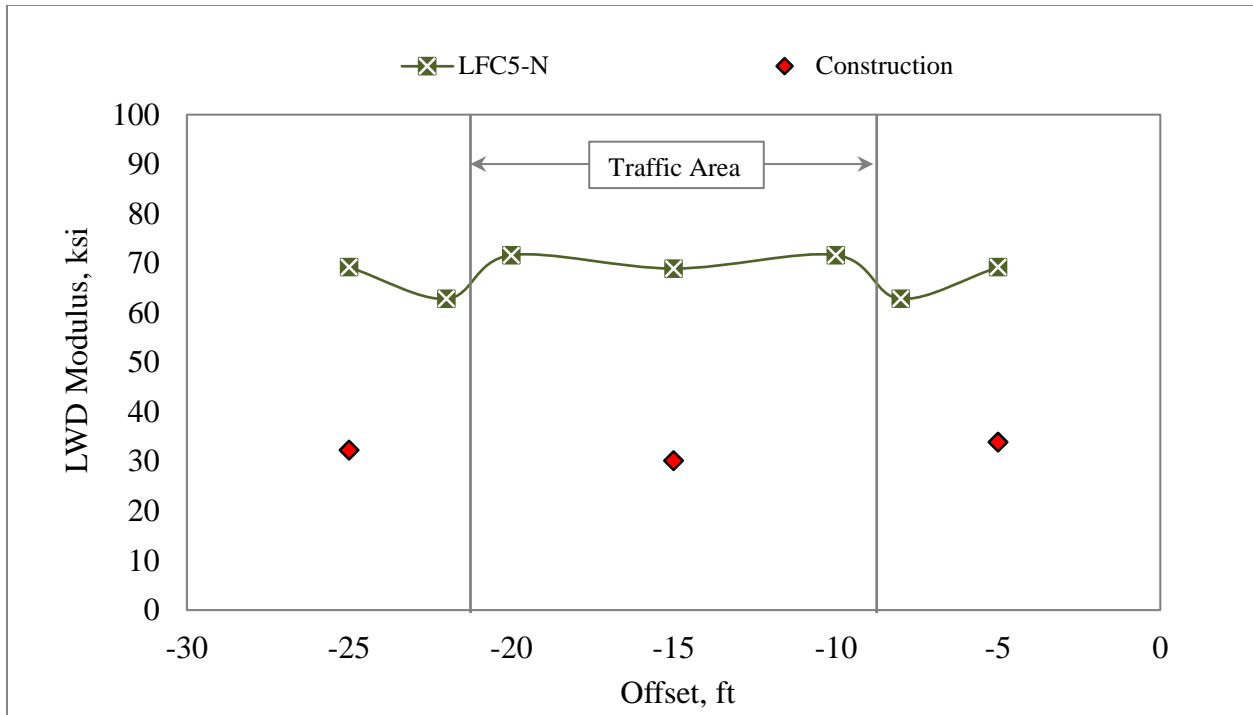


Figure 16. LWD Results on P-209 (CC7 North Side).

4.3 NUCLEAR GAUGE DENSITY AND SAND CONE

Nuclear gauge density and 12-in sand cone tests were performed on the top of P-209 materials to determine the density and moisture content. Nuclear density tests (figure 17) were conducted at offsets -25ft, -22ft, -20ft, -15ft, -10ft, -8ft, -5ft, +5ft, +8ft, +10ft, +15ft, +20ft, +22ft, and +25ft on top of P-209 at each trench locations. The 12-in sand cone tests (figure 18) were also performed on P-209 at offsets -15ft, -10ft, -8ft, -5ft, +5ft, +8ft, +10ft, and +15ft at CC7 trench locations.

The average moisture content of P-209 on the north side was 1.9% (Sand Cone) and 2.4% (Nuclear Density). The average moisture content of P-209 on south side was 2.1% (Sand Cone) and 2.8% (Nuclear Density). During the construction, sand cone testing yielded an average of 2.7% moisture content.



Figure 17. LWD Tests on P-209



Figure 18. 12 in. Sand Cone Tests on P-209

Figures 19 and 20 summarize the nuclear density test results. The laboratory maximum dry density, $\gamma_{d\ max}$, and densities collected during construction are also plotted in those two figures. The results indicate that the traffic load densified the P-209 materials. The post-traffic density in traffic areas was higher than construction values. Furthermore, in some test items, the post-traffic density was even higher than $\gamma_{d\ max}$.

The sandcone results are shown in figures 21 and 22. The surface of P-209 was quite stiff and rough especially in the traffic area. Figure 23 shows the gradation of the P-209 in traffic area, non-traffic area and pre-traffic tests results. From the figure we can see that there was no significant changes on the gradation.

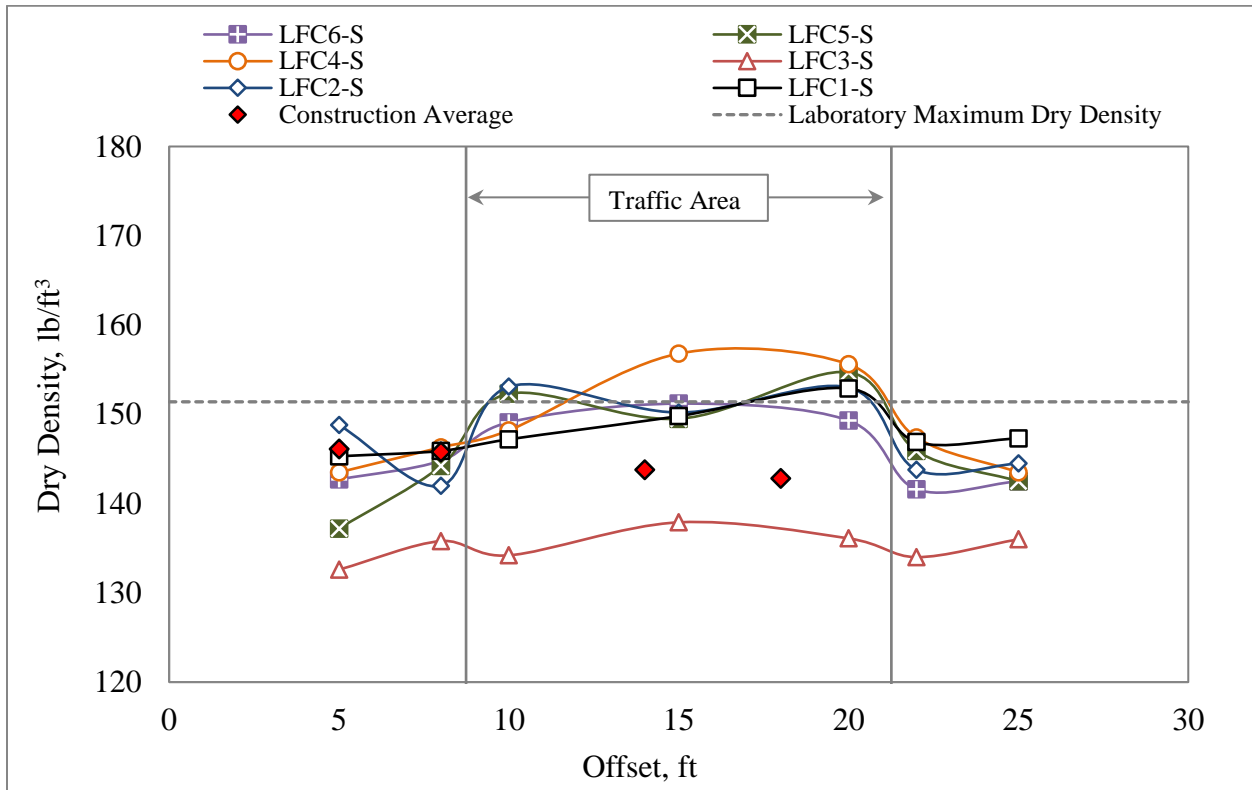


Figure 19. Nuclear Tests on P-209 (CC7 South Side)

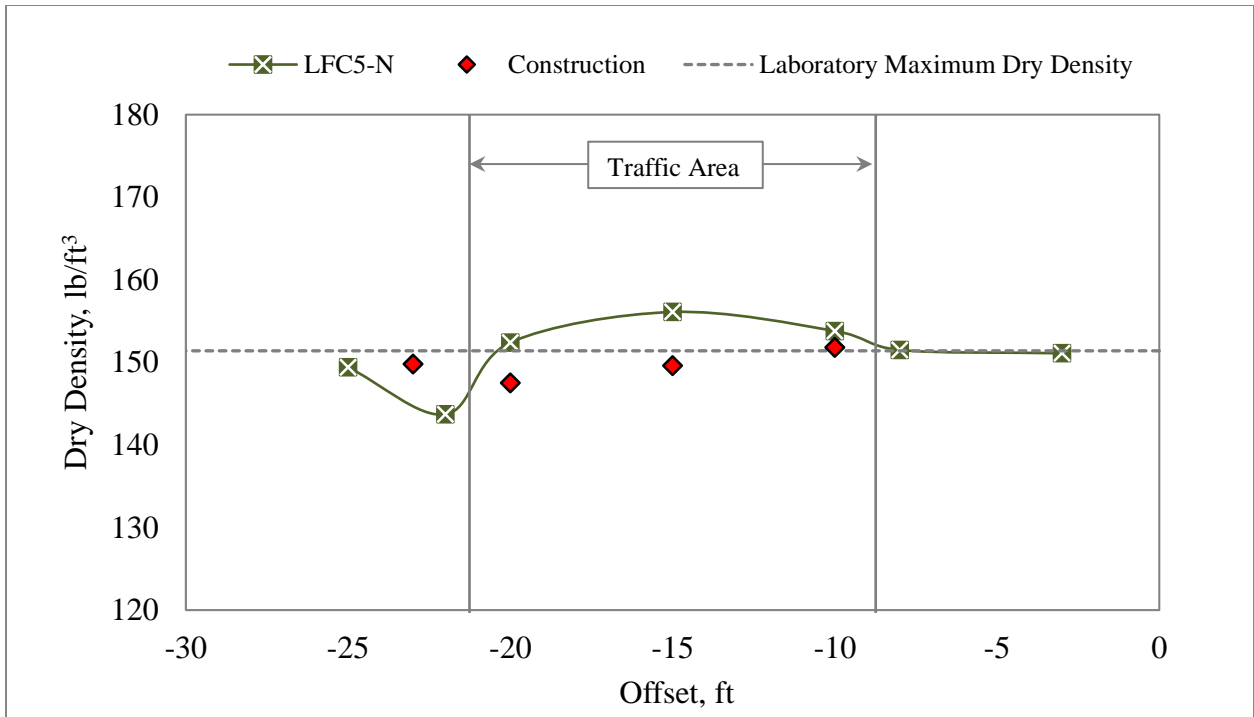


Figure 20. Nuclear Tests on P-209 (CC7 North Side)

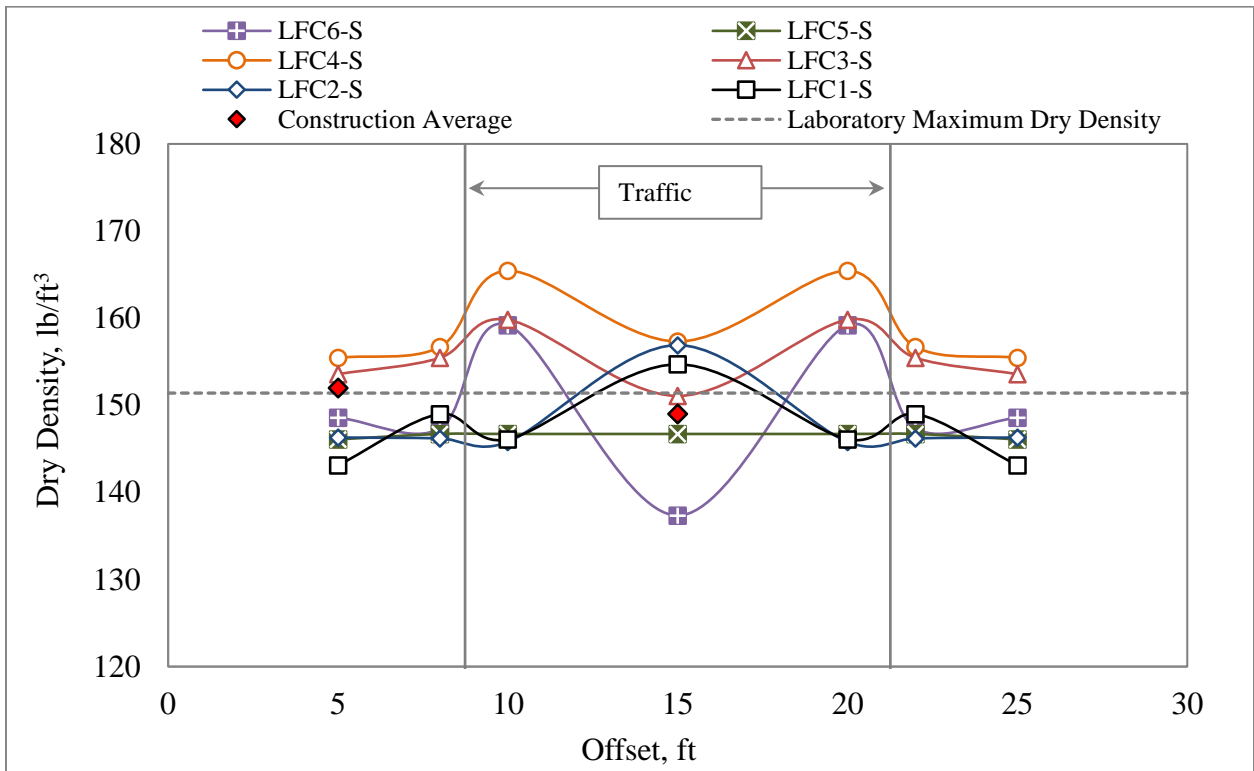


Figure 21. Sand Cone Tests on P-209 (CC7 South Side)

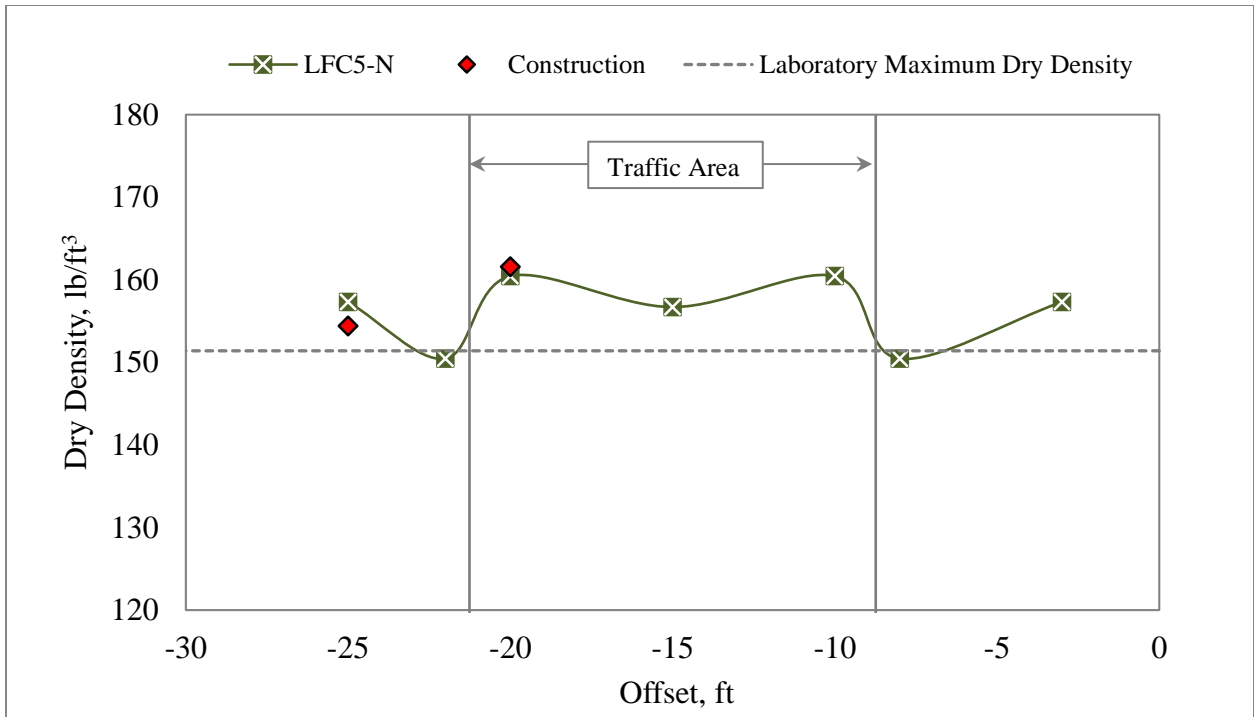


Figure 22. Sand Cone Tests on P-209 (CC7 North Side)

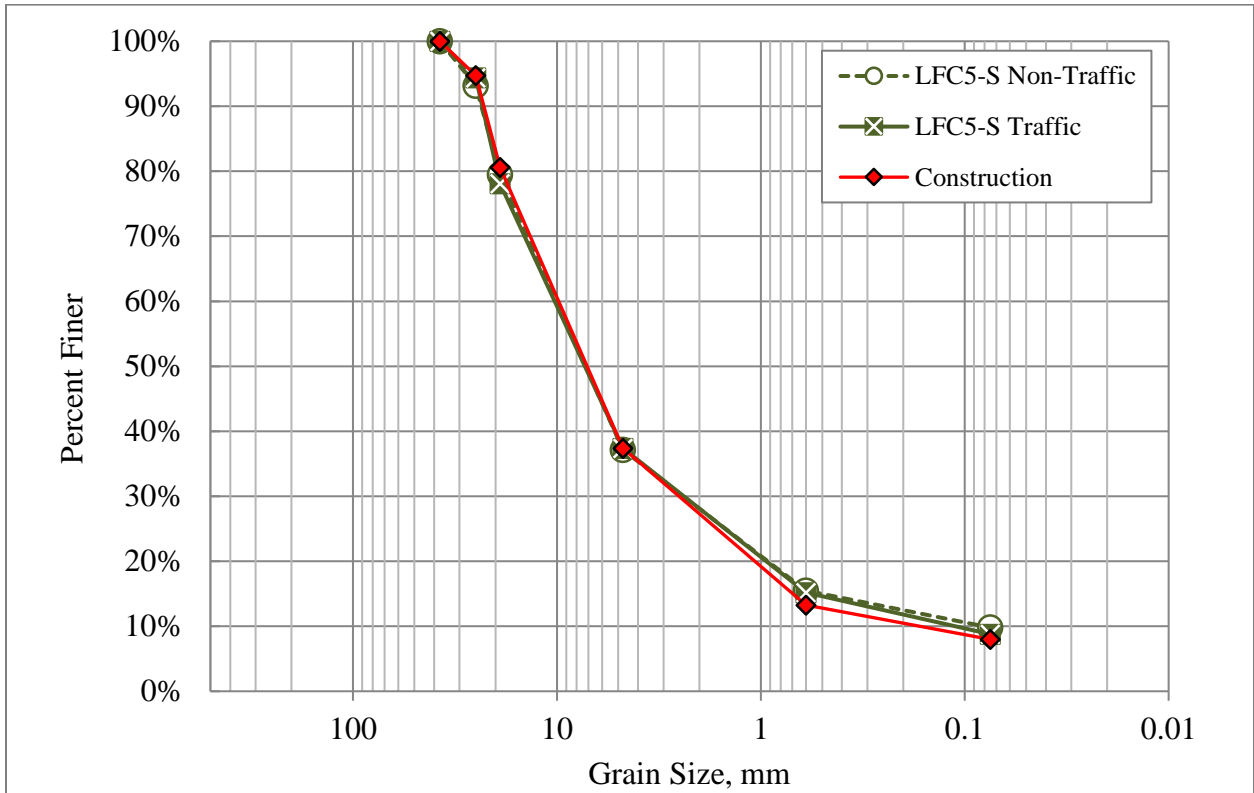


Figure 23. Sand Cone Tests on P-209 (CC7 North Side)

5. P-154: AGGREGATE SUBBASE

After P-209 and ATDB were removed, the P-154 layer was exposed. The P-154 subbase course was a granular argillite material purchased from a local supplier conforming to the FAA Advisory Circular AC 150/5370-10G. The material was placed in approximately 10-inch compacted lifts to a percent compaction at least 95% of $\gamma_{d\ max}$. Sand cone testing yielded an average of 4.1% moisture (dry of the 7.6% optimum moisture content) with an average dry density of 136.18 lb/ft³. The tests discussed in this section were performed on the surface of P-154 layer as well as at additional depths.

5.1 D-PSPA

D-PSPA tests were done at offsets -15ft, -10ft, -8ft, -5ft, +5ft, +8ft, +10ft, and +15ft for on P-154 to determine seismic moduli of the subbase material. Figures 24-35 summarize the D-PSPA results.

In the figures, it can be observed that the PSPA data had a relatively high variation, which made it impossible to investigate the modulus differences between surface and deeper layers and the differences between traffic area and non-traffic area.

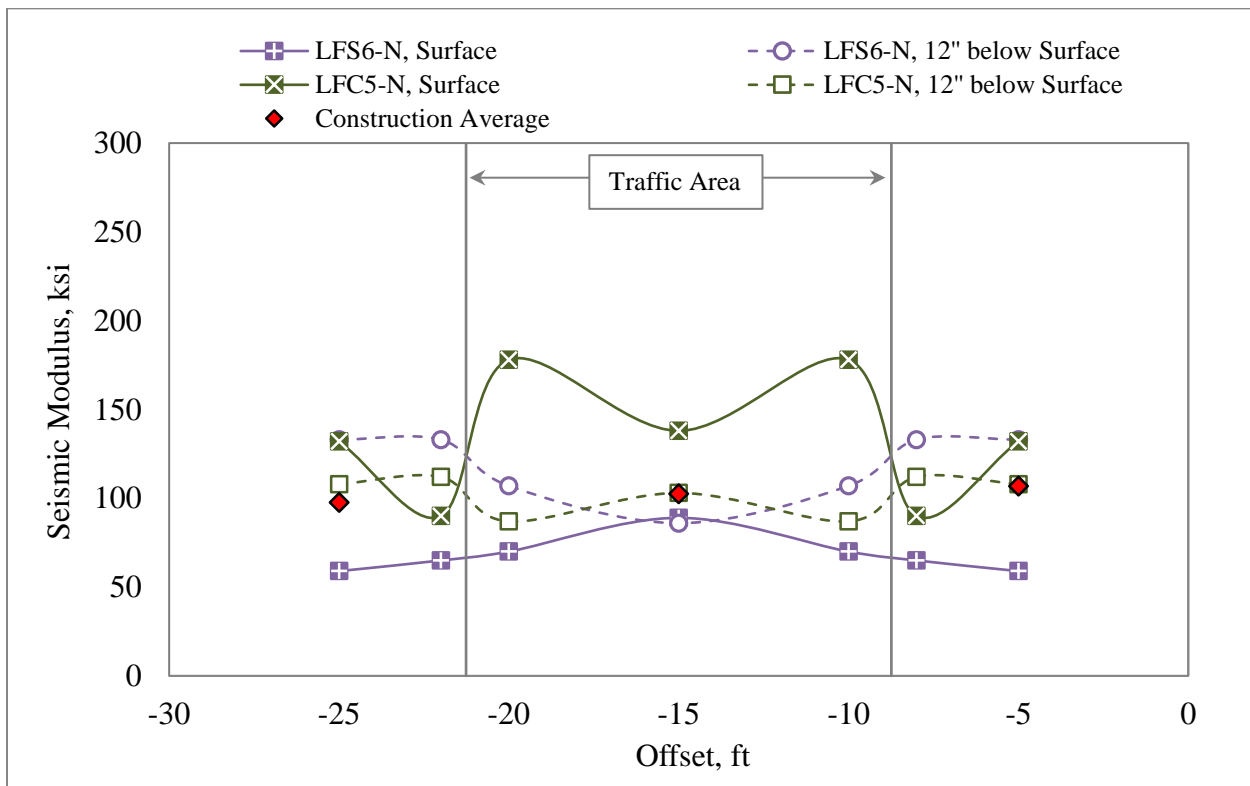


Figure 24. D-PSPA Results on P-154 for LFS6-N and LFC5-N (CC7 North Side, longitudinal direction)

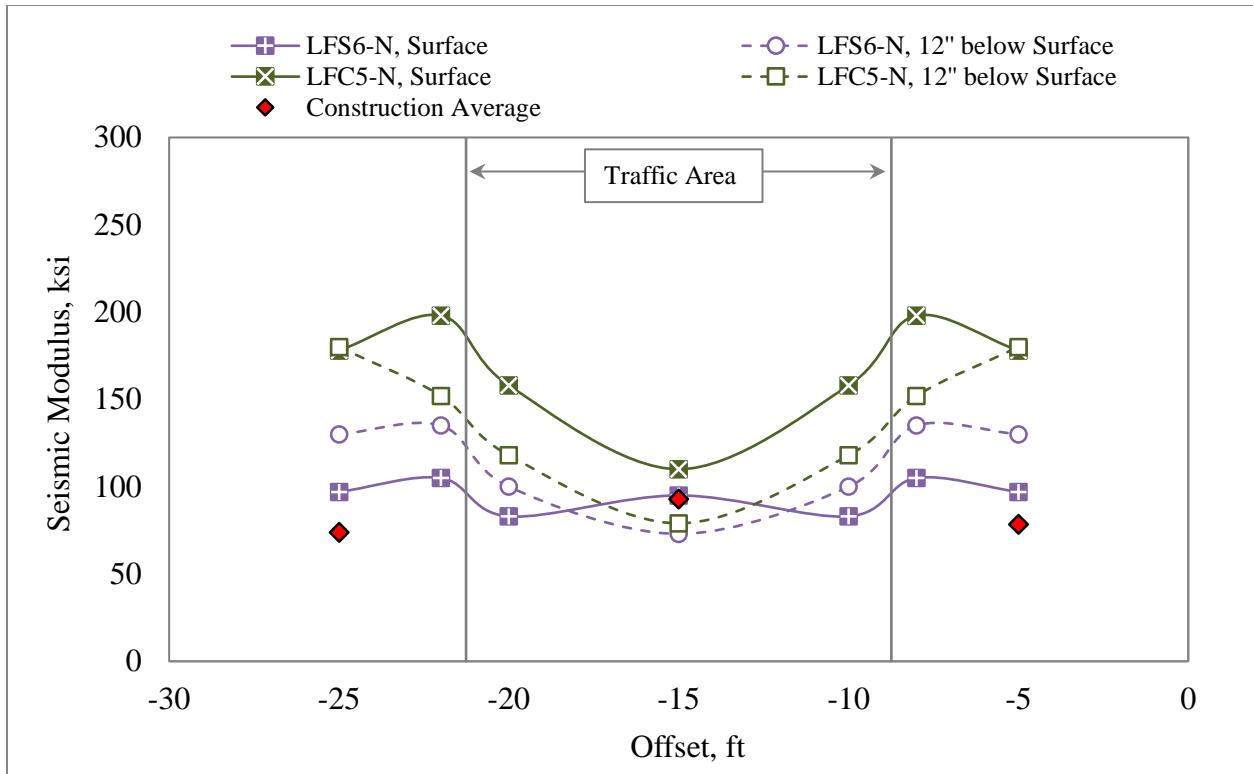


Figure 25. D-PSPA Results on P-154 for LFS6-N and LFC5-N (CC7 North Side, transverse direction)

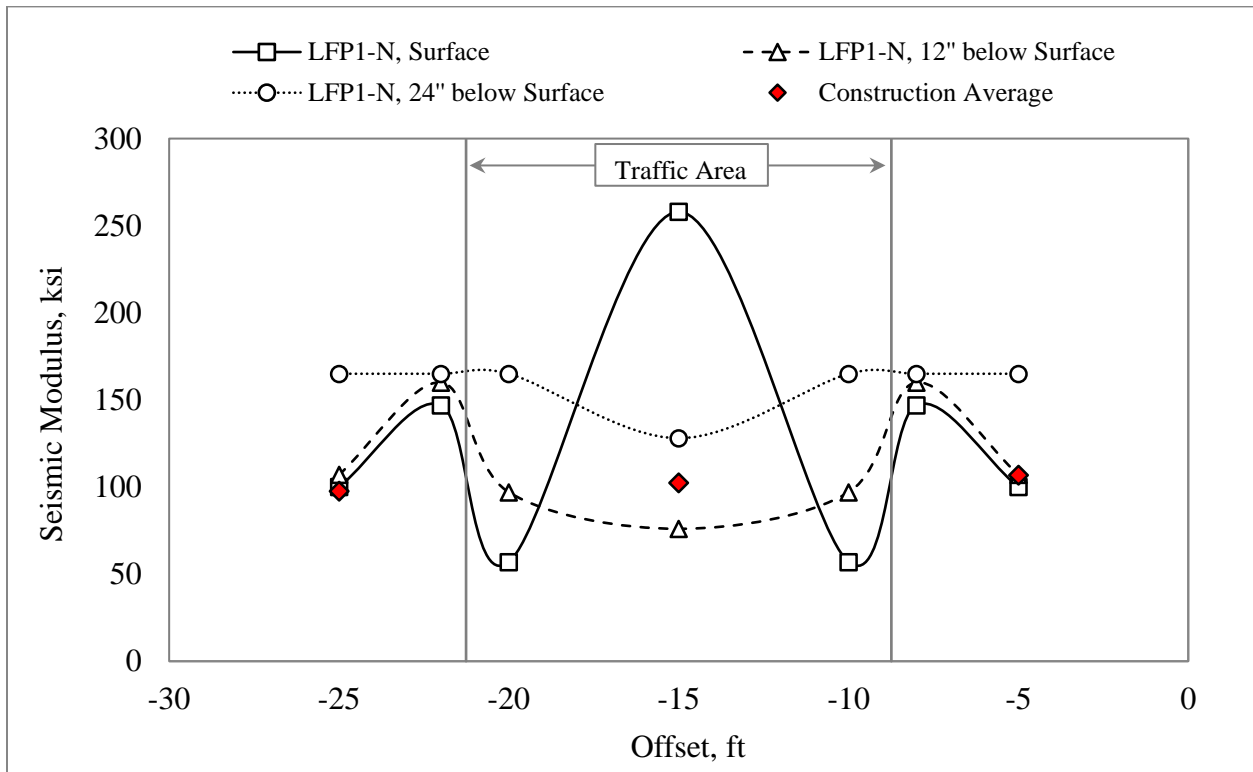


Figure 26. D-PSPA Results on P-154 for LFP1-N (CC7 North Side, longitudinal direction)

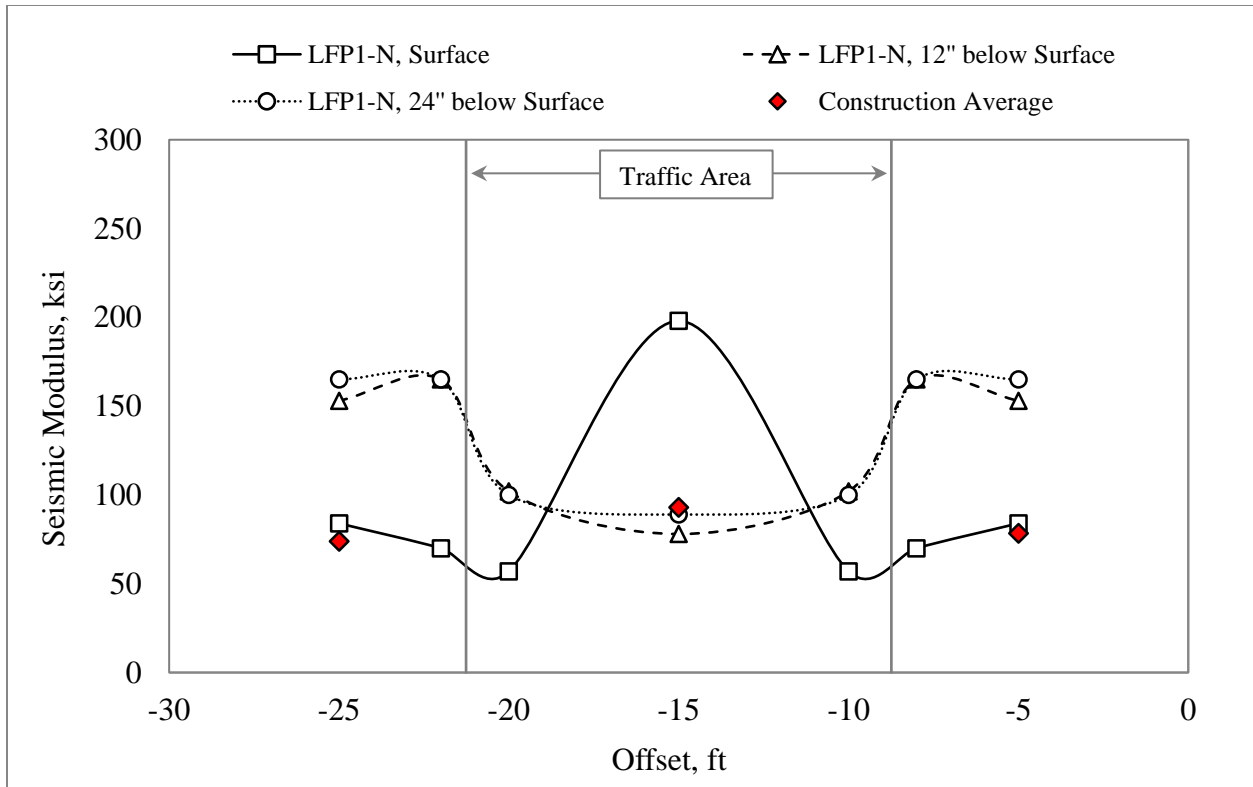


Figure 27. D-PSPA Results on P-154 for LFP1-N (CC7 North Side, transverse direction)

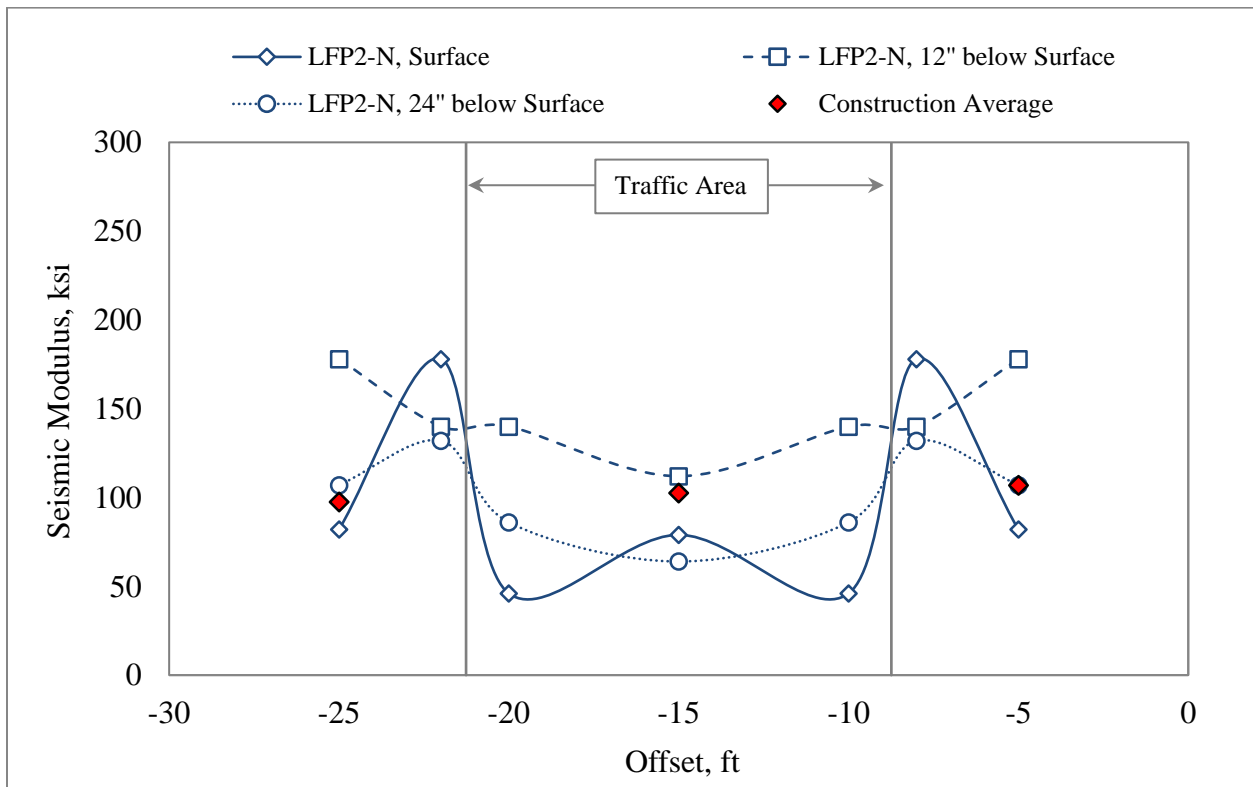


Figure 28. D-PSPA Results on P-154 for LFP2-N (CC7 North Side, longitudinal direction)

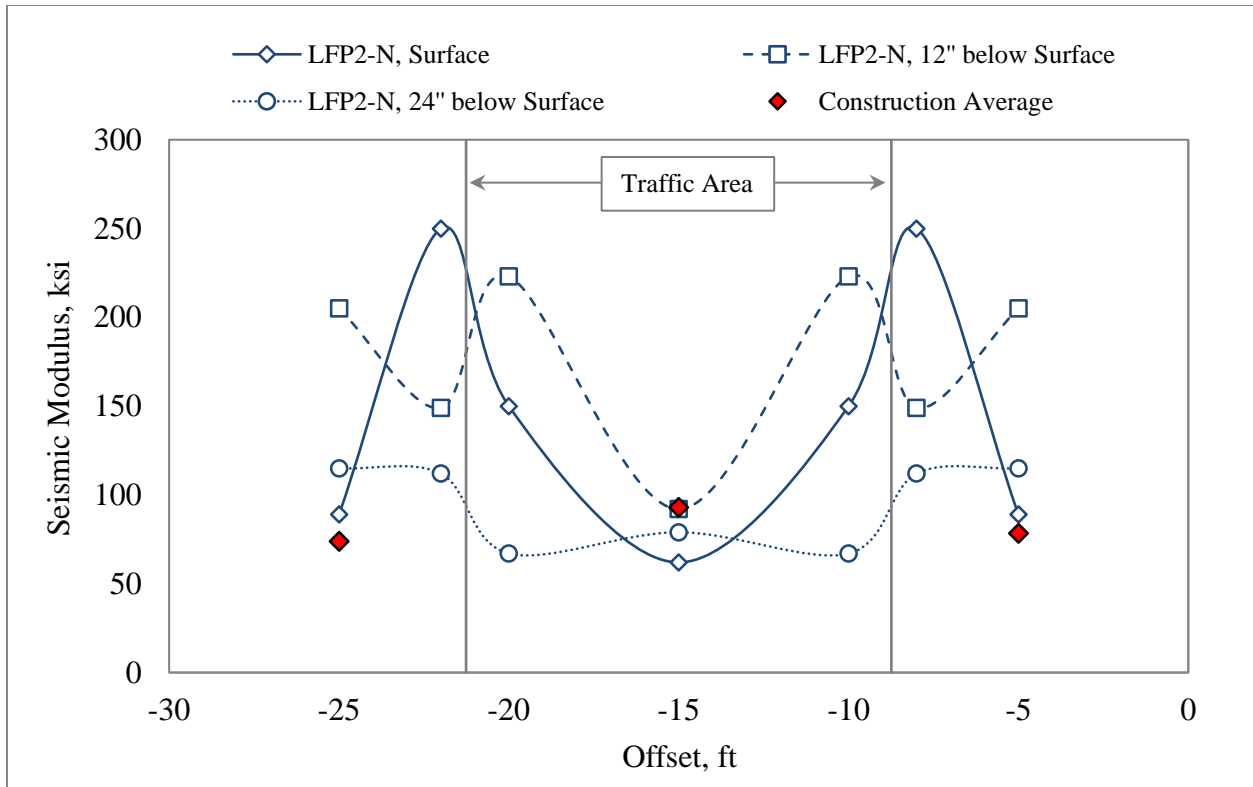


Figure 29. D-PSPA Results on P-154 for LFP2-N (CC7 North Side, transverse direction)

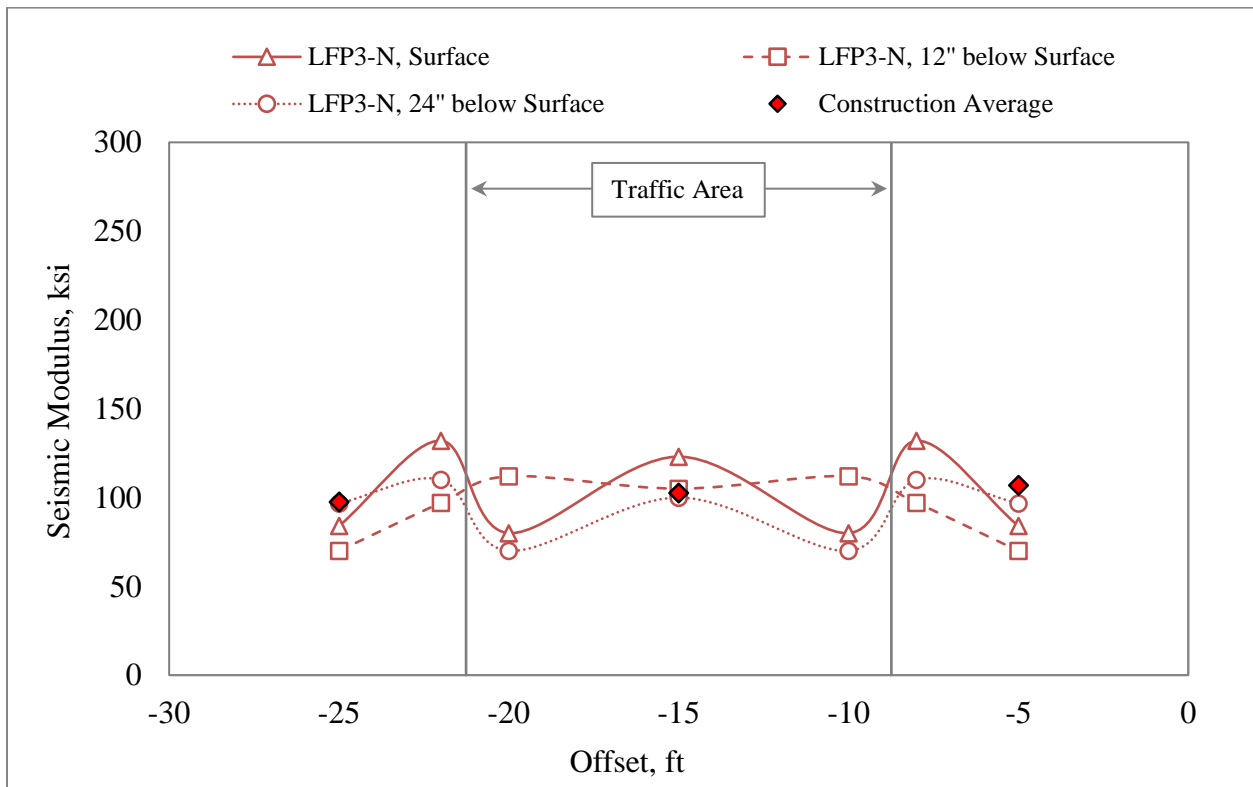


Figure 30. D-PSPA Results on P-154 for LFP3-N (CC7 North Side, longitudinal direction)

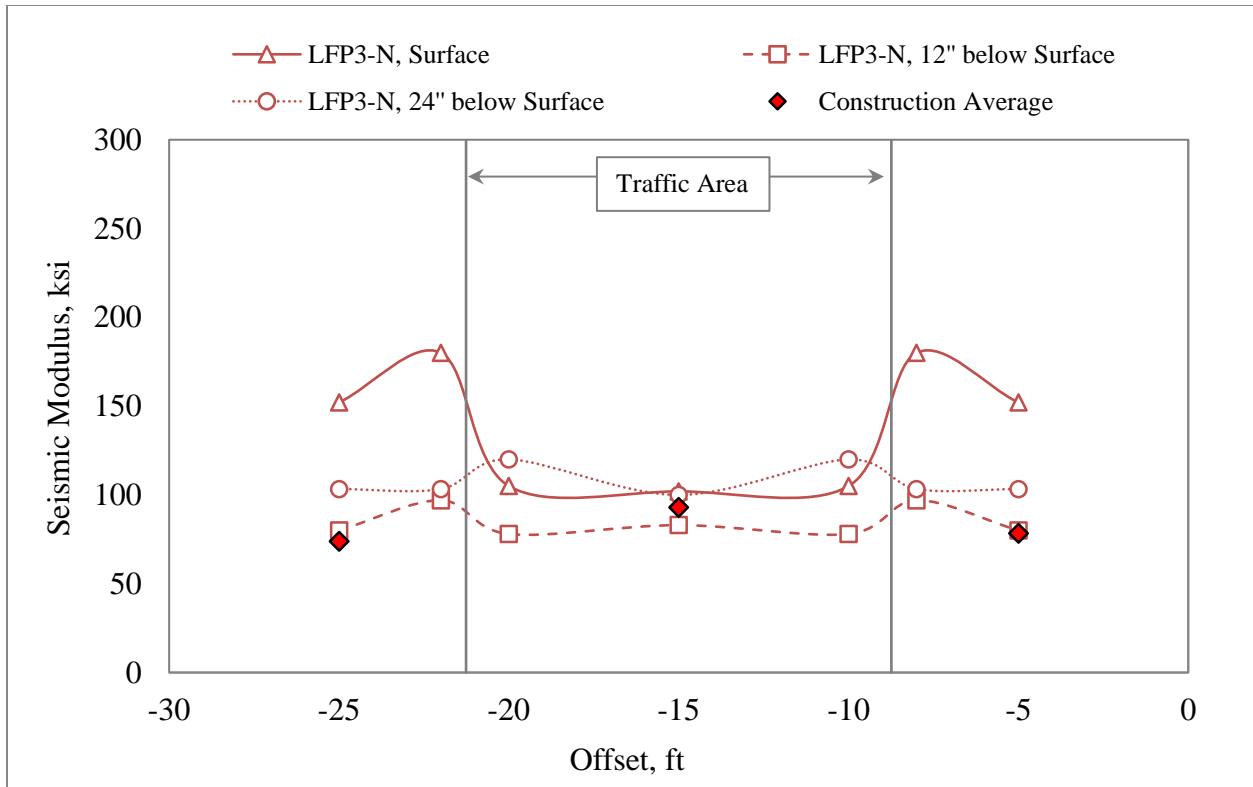


Figure 31. D-PSPA Results on P-154 for LFP3-N (CC7 North Side, transverse direction)

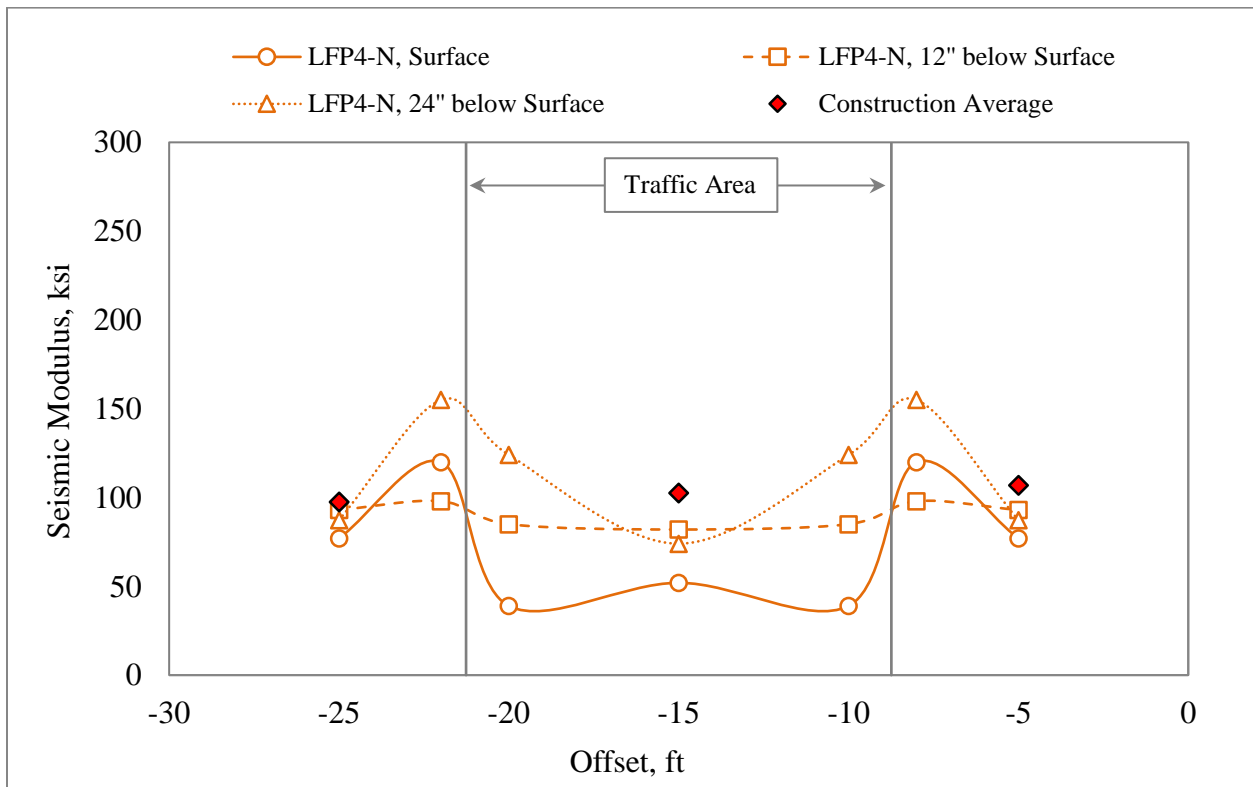


Figure 32. D-PSPA Results on P-154 for LFP4-N (CC7 North Side, longitudinal direction)

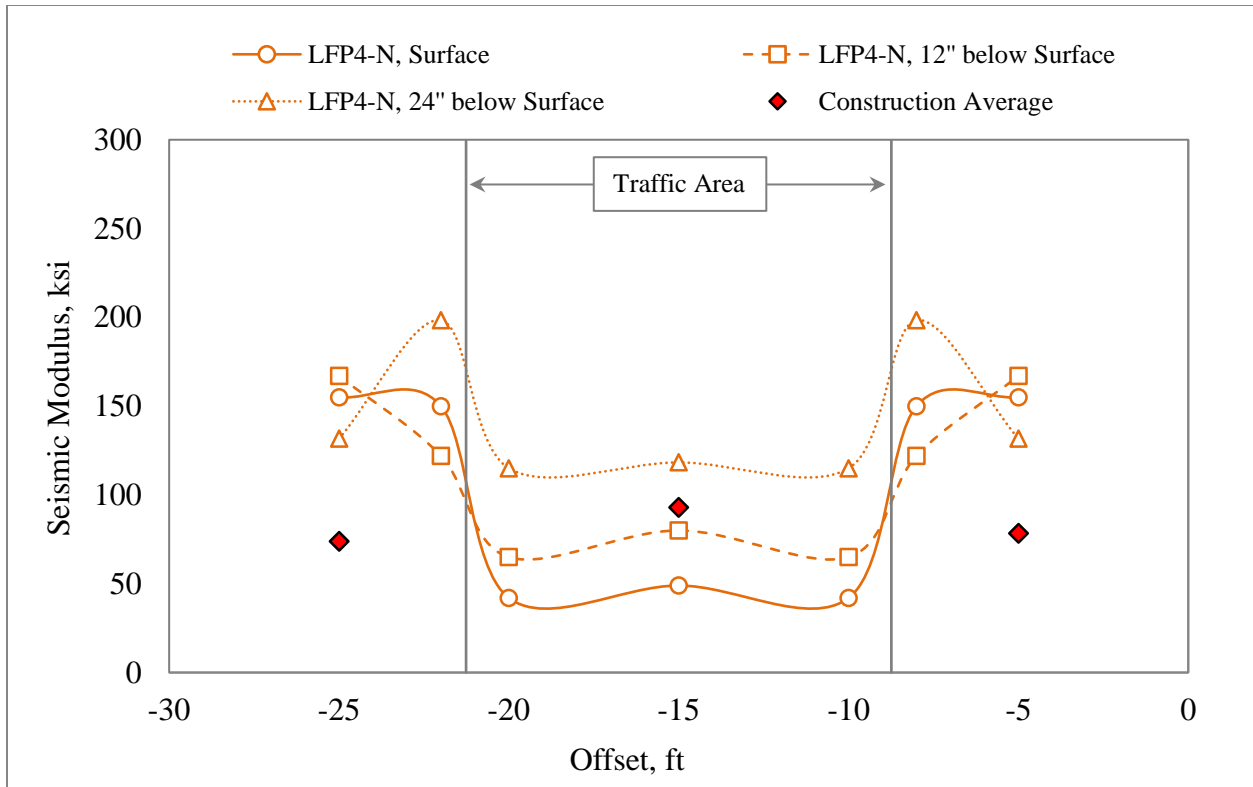
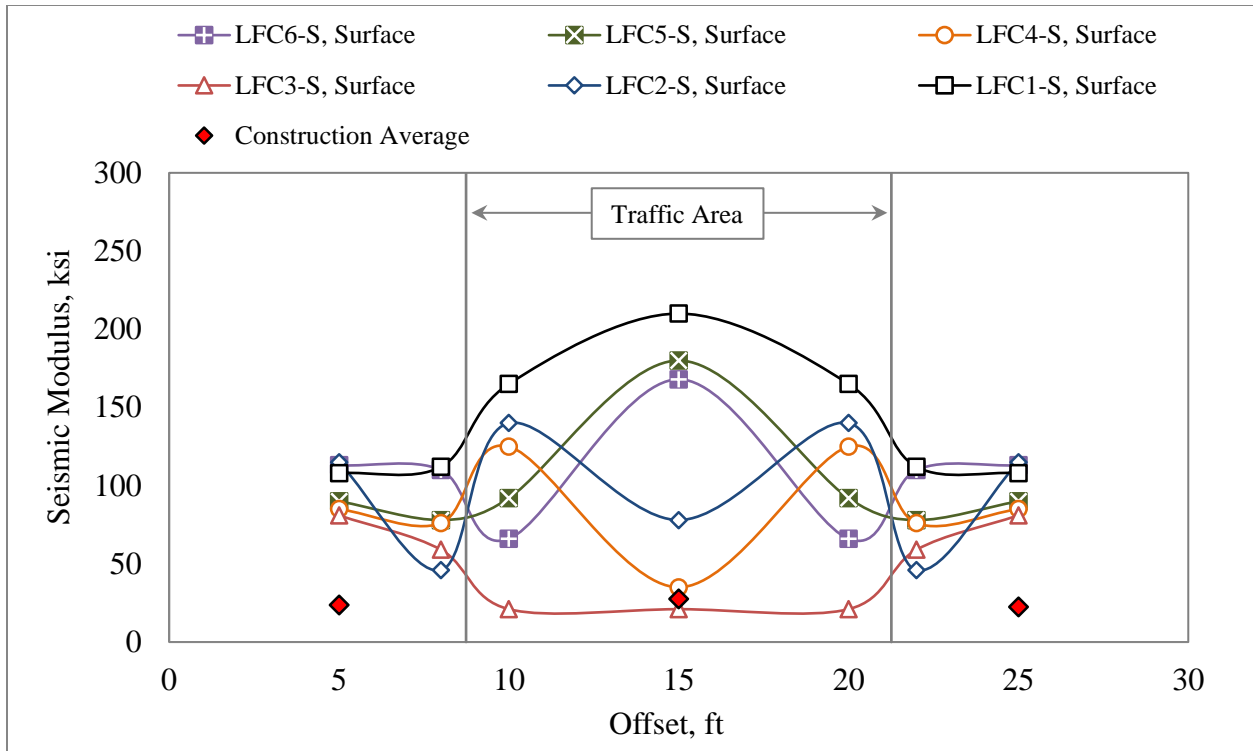
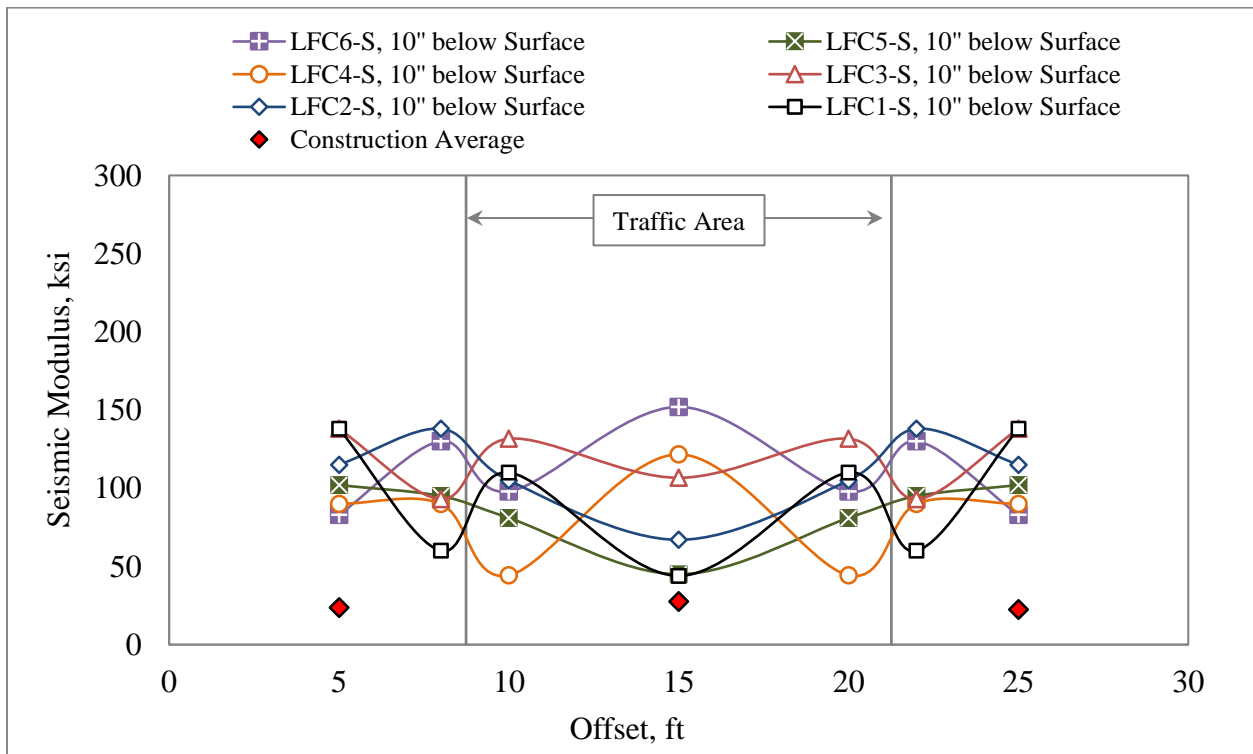


Figure 33. D-PSPA Results on P-154 for LFP4-N (CC7 North Side, transverse direction)

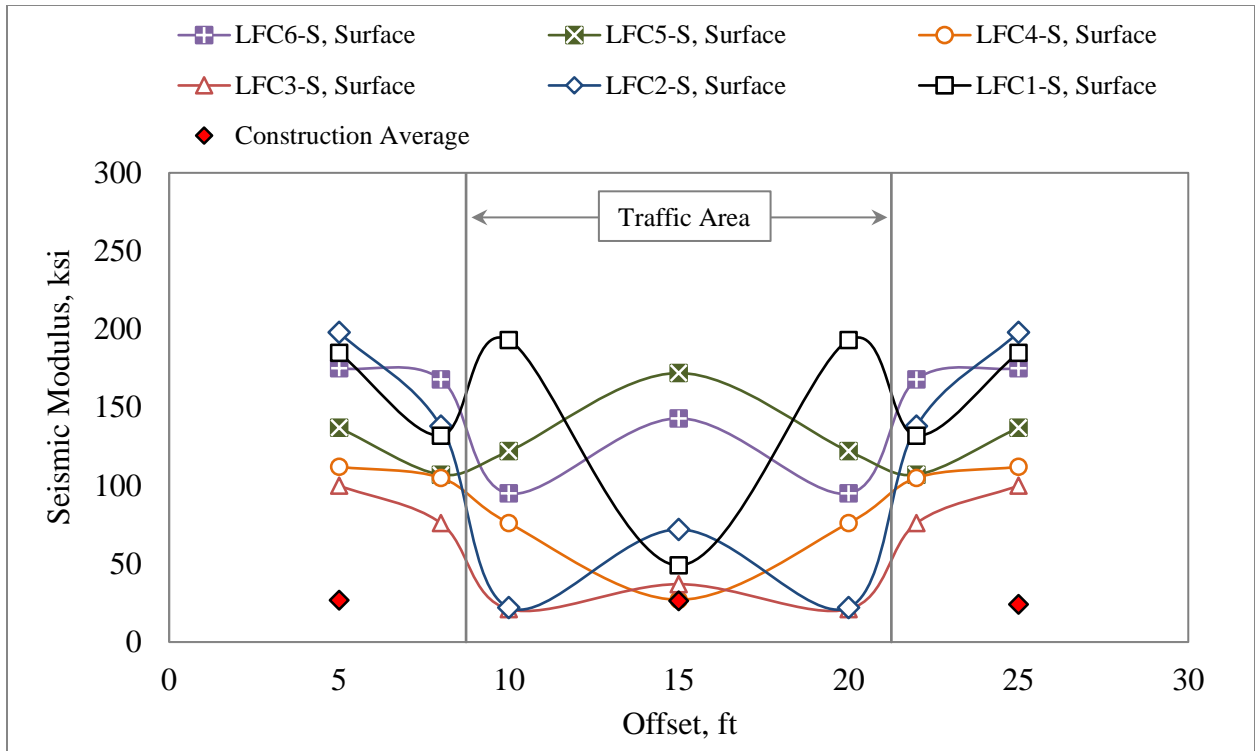


(a)

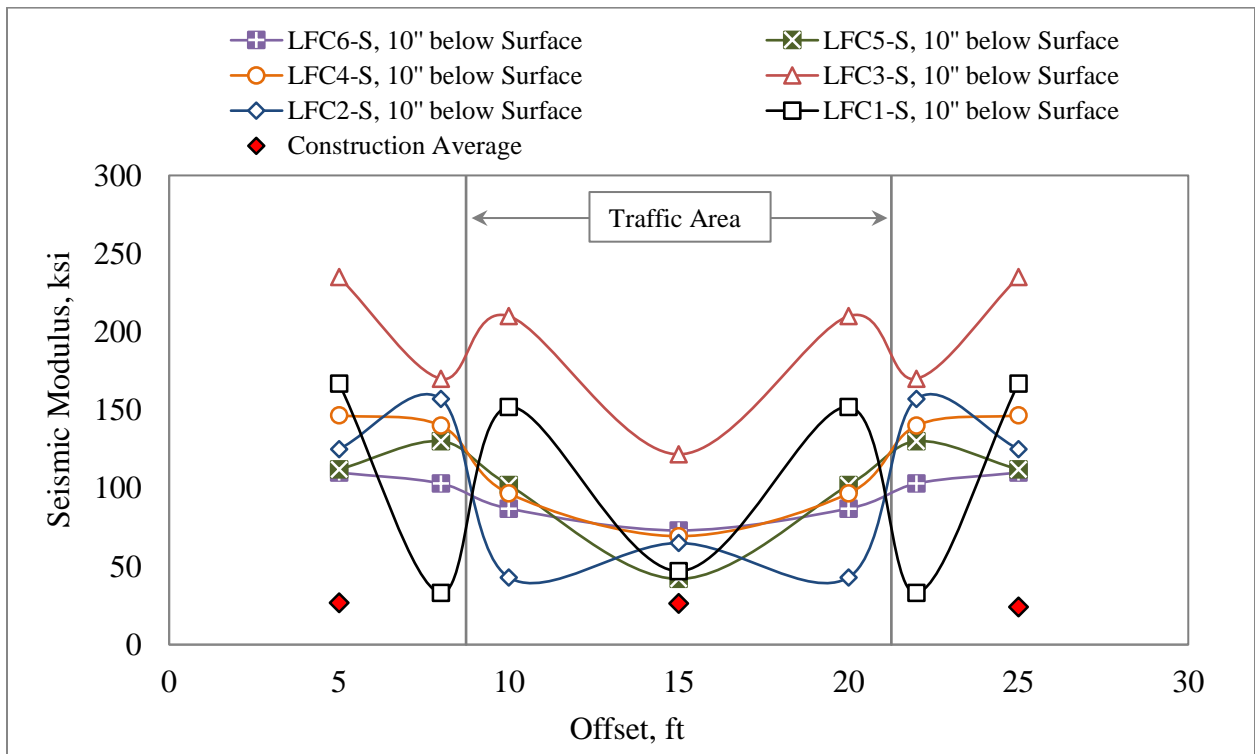


(b)

Figure 34. D-PSPA Results on P-154 (CC7 South Side, longitudinal direction): (a) Layer Surface, (b) 10'' below Surface



(a)



(b)

Figure 35. D-PSPA Results on P-154 (CC7 South Side, transverse direction): (a) Layer Surface, (b) 10'' below Surface

5.2 LWD

LWD tests were conducted at the same locations as D-PSPA. Figures 36-39 summarize the LWD results.

In figures 36 and 37, it can be observed that on the north side, there was no significant difference in LWD modulus between P-154 surface and 12 in. below the surface. In most of the test items, the LWD moduli in traffic areas were higher than non-traffic areas.

Figures 38 and 39 represent the LWD modulus of P-154 on the south side. The LWD modulus of P-154 surface was higher than 12 in. below the surface. The LWD moduli in traffic areas were also higher than non-traffic areas.

The P-401 layers on the north side was thicker than the south side. Therefore, the wheel load was distributed more efficiently on the north side, and traffic-induced stresses on top of the P-154 layer were smaller compared to those on the south side. The P-154 surface on the south side was exposed to higher vertical stresses.

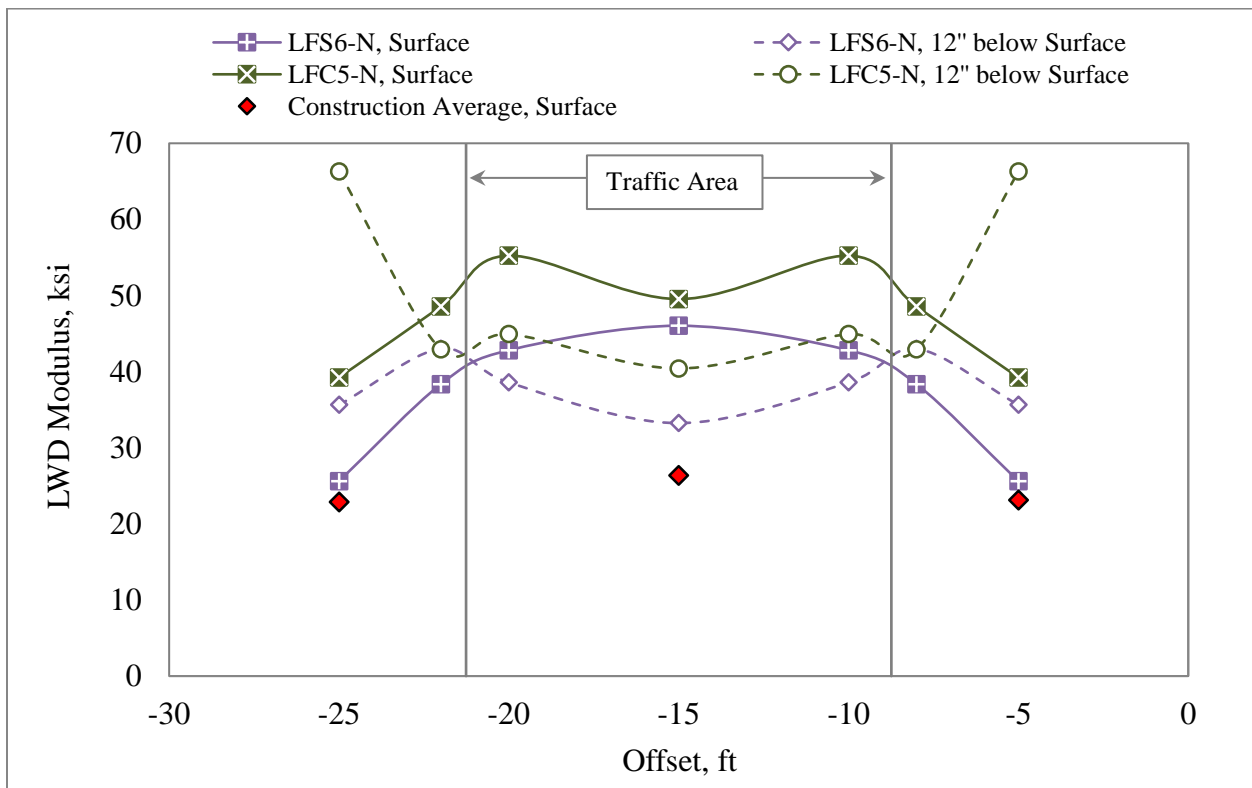
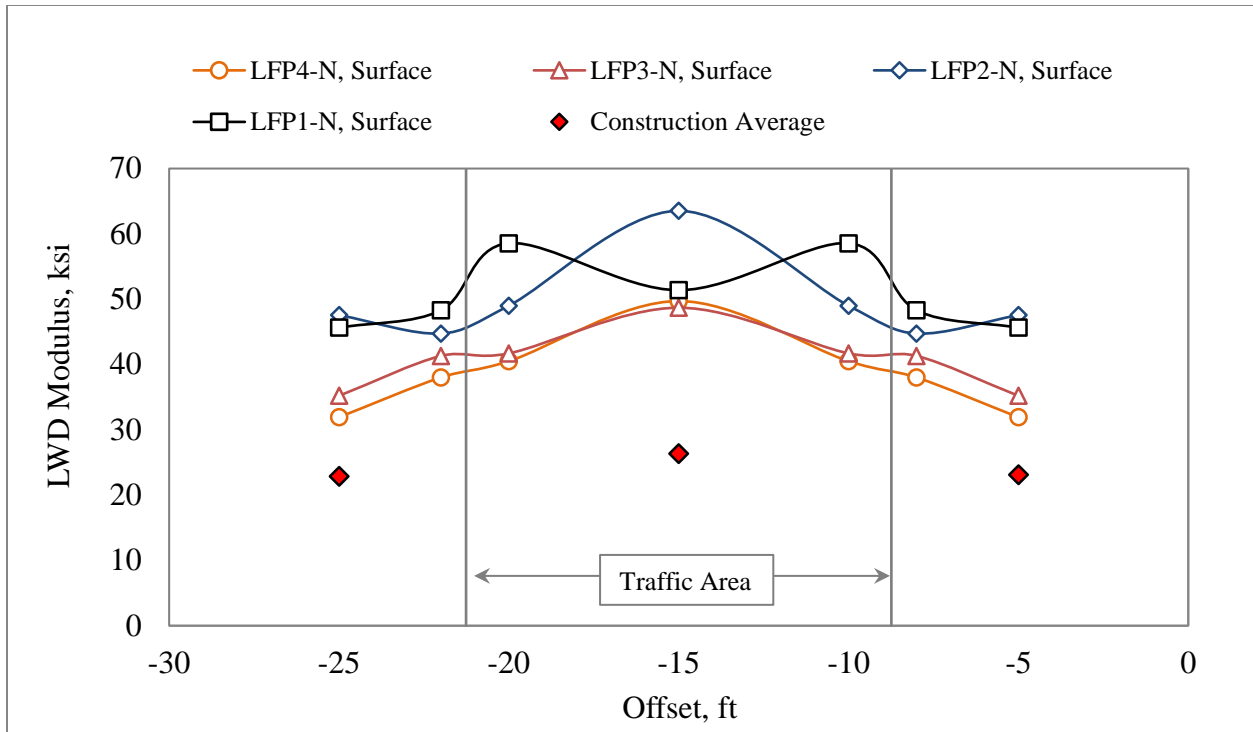
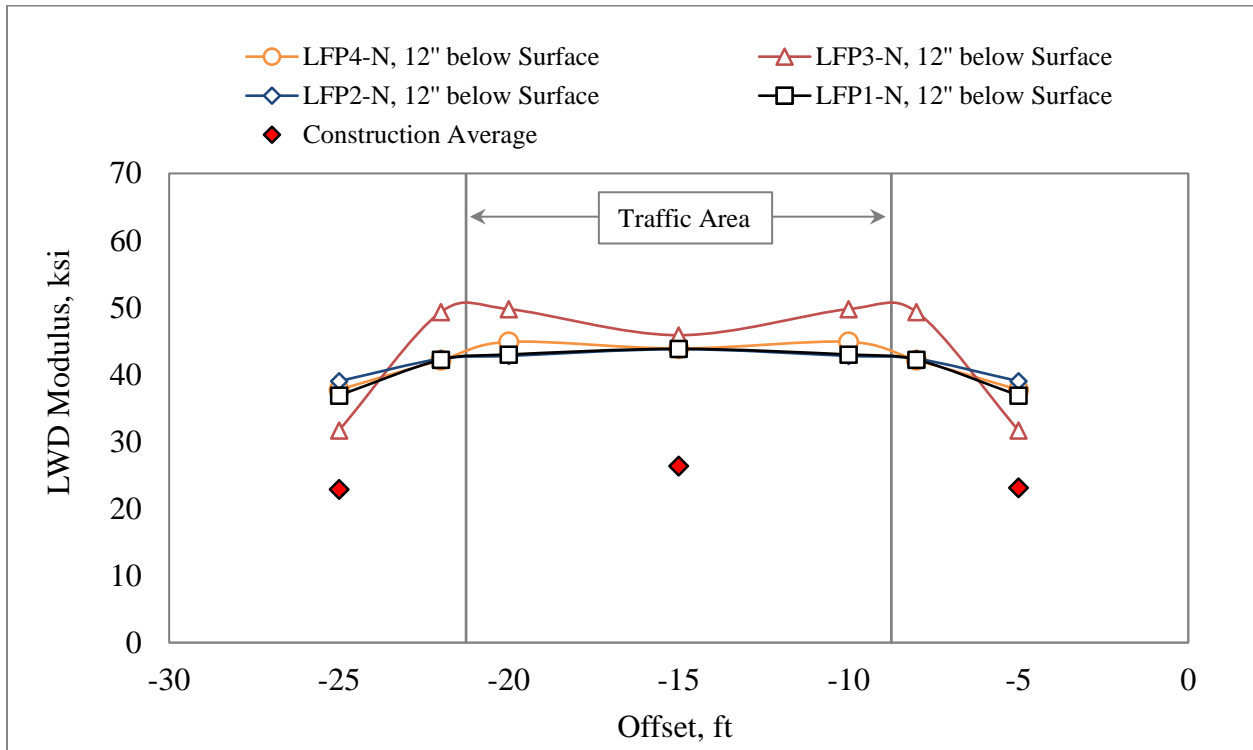


Figure 36. LWD Results on P-154 for LFC5-N and LFS6-N (CC7 North Side)



(a)



(b)

Figure 37. LWD results on P-154 for LFP1-N to LFP4-N (CC7 North Side): (a) Layer Surface, (b) 12'' below Surface

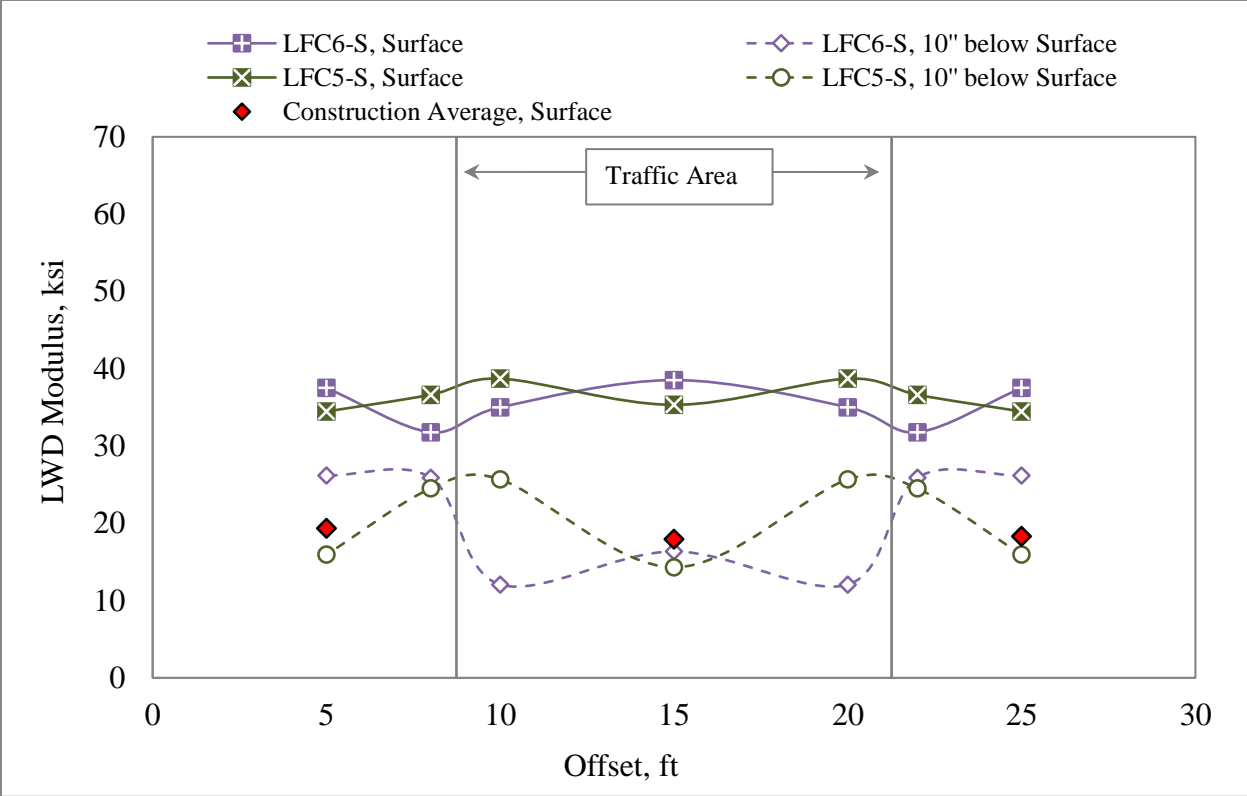
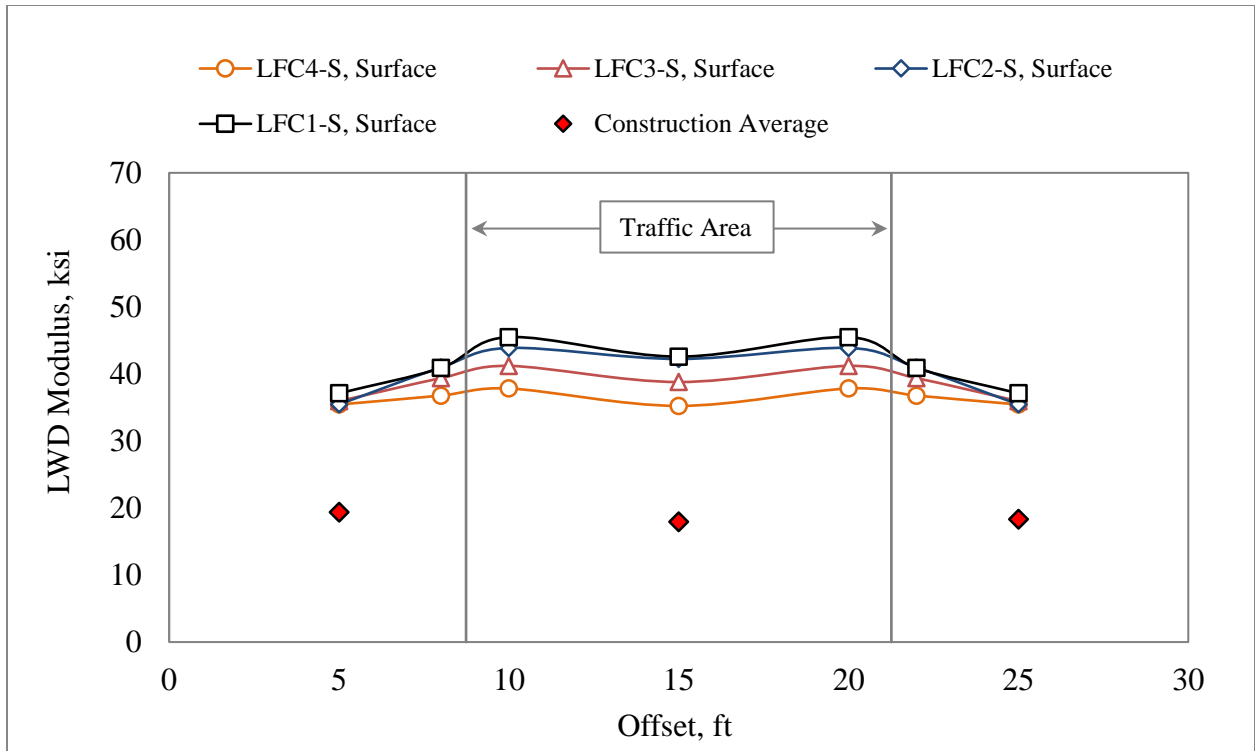
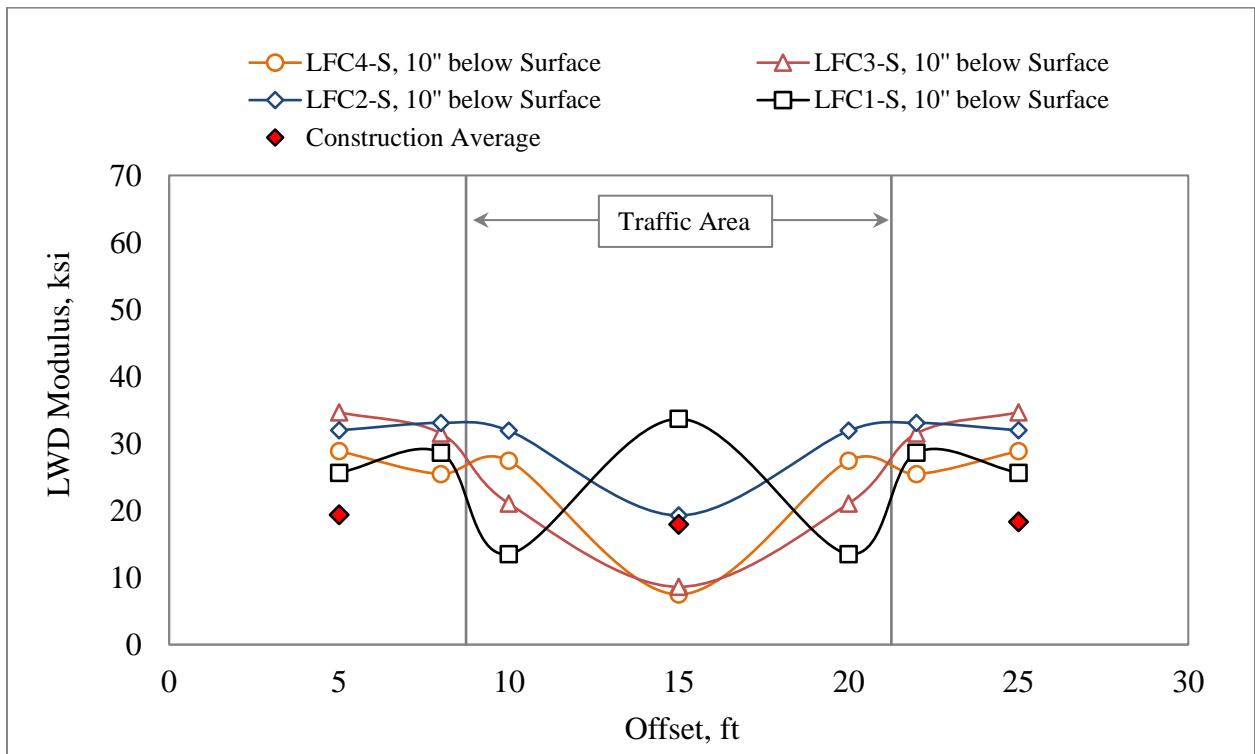


Figure 38. LWD results on P-154 for LFC5-S and LFC6-S (CC7 South Side)



(a)



(b)

Figure 39. LWD results on P-154 for LFC1-S to LFC4-S (CC7 South Side): (a) Layer Surface, (b) 10'' below Surface

5.3 NUCLEAR GAUGE DENSITY AND SAND CONE

There were 6-in sand cone tests done at offsets -15ft, -10ft, -8ft, -5ft, +5ft, +8ft, +10ft, and +15ft for each trench to determine both the in-situ density and moisture content of the subbase material. Nuclear density gauge tests were performed at offsets -25ft, -22ft, -20ft, -15ft, -10ft, -8ft, -5ft, +5ft, +8ft, +10ft, +15ft, +20ft, +22ft, and +25ft for each trench to determine both the in-situ density and moisture content of the subbase material. Tests were conducted on top of the P-154 layer as well as at additional depths.

The average moisture content measured by sand cone tests was 2.2%. The average moisture content determined by nuclear density tests was 3.9%. Sand cone testing performed during construction yielded an average moisture content of 4.1%.

The sand cone results are summarized in figures 40-43. Figures 44-47 show the nuclear density results. Figures 40 and 44 indicate that in test items LFC5-N and LFS6-N, the density at the top of the P-154 layer was higher than 12 in. below the top. The density at the top of the P-154 layer in the south side was higher than 10 in below the top. On the south side, the density in the traffic areas was higher than non-traffic areas. Figures 48-50 show the P-154 gradations. Figures 49 and 50 show the gradation of the P-154 materials collected in traffic area, non-traffic area and pre-construction. The difference between gradations seemed insignificant.

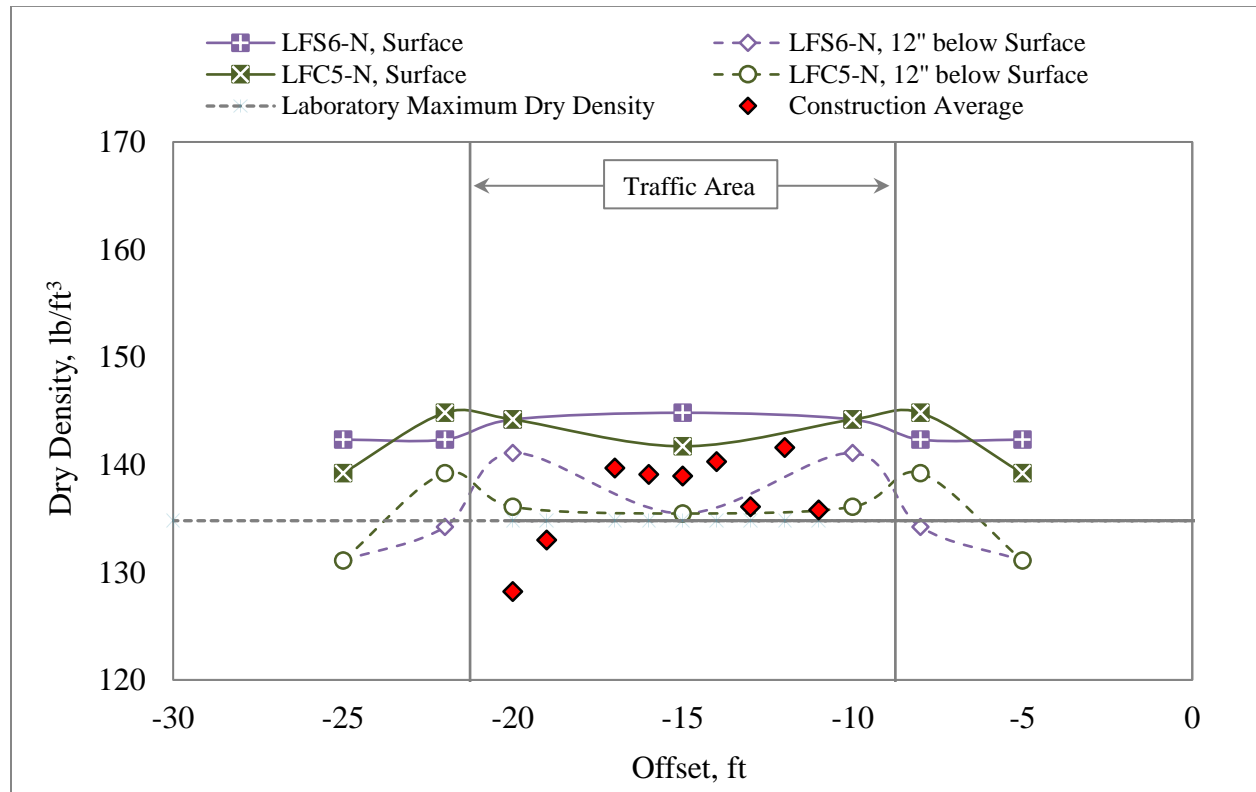
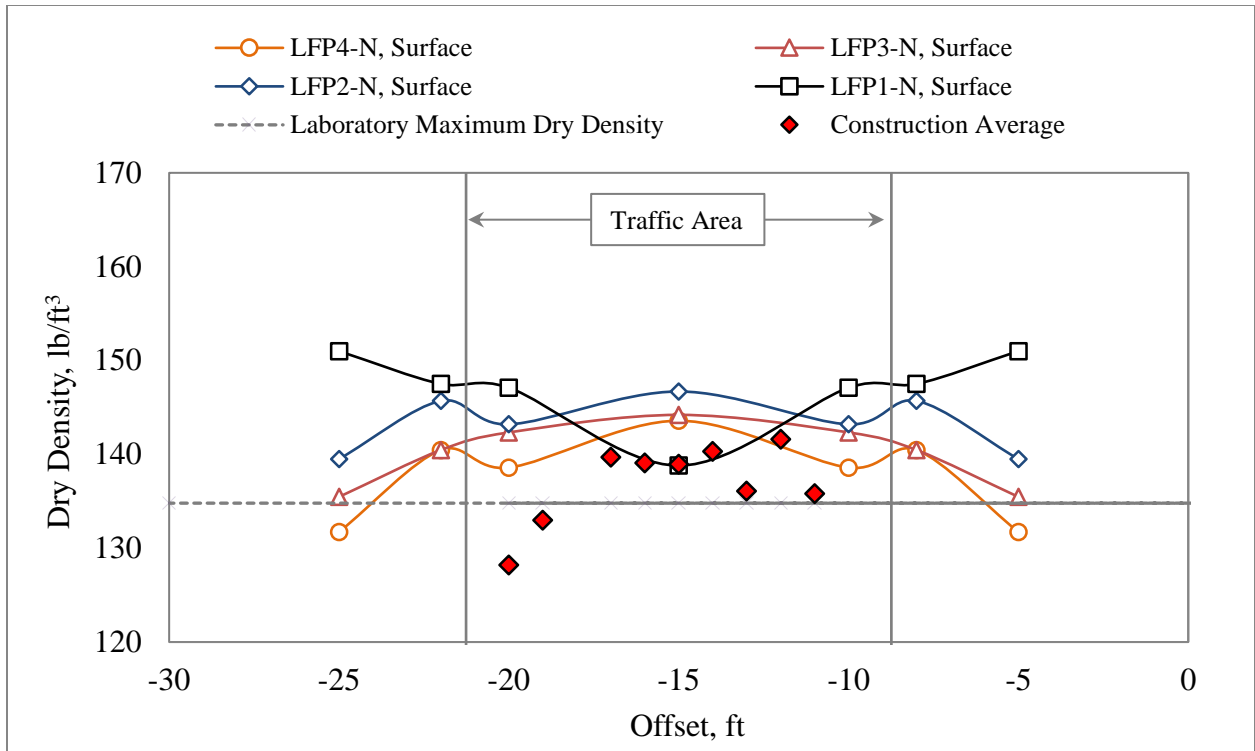
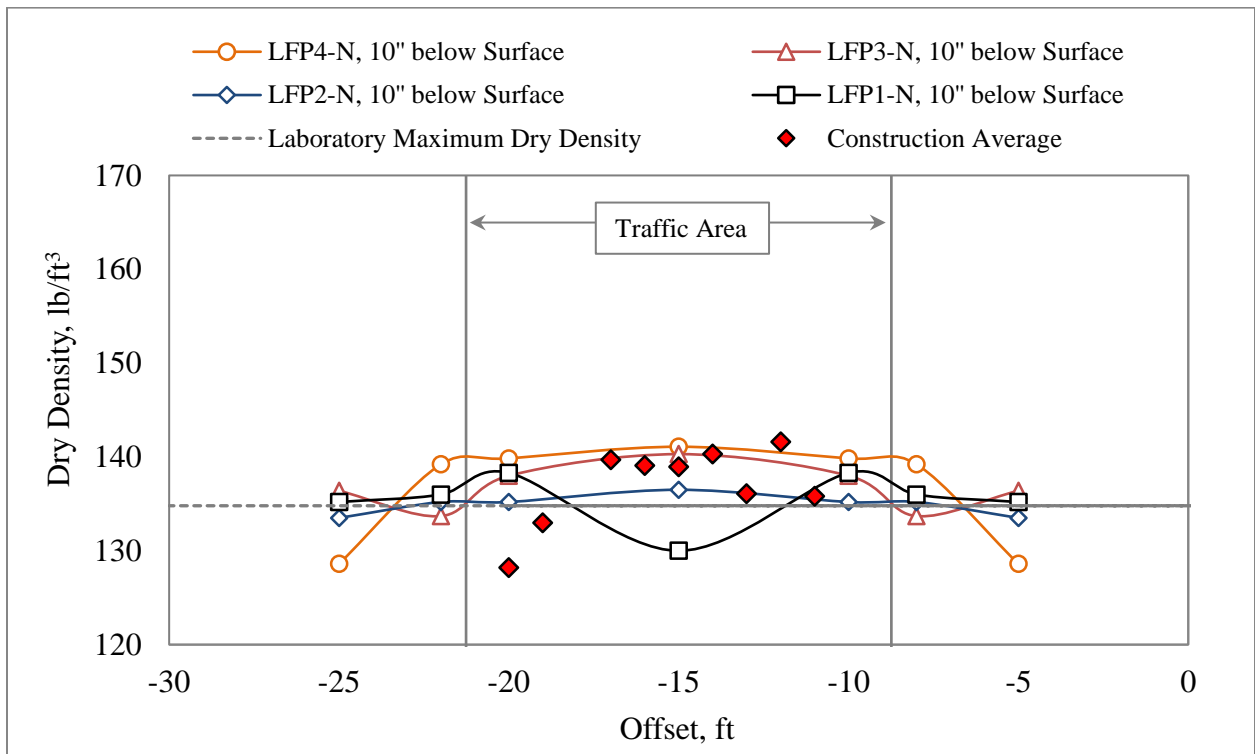


Figure 40. Sand Cone Results on P-154 for LFC5-N and LFS6-N (CC7 North Side)



(a)



(b)

Figure 41. Sand Cone Results on P-154 for LFP1-N to LFP4-N (CC7 North Side): (a) Layer Surface, (b) 10" below Surface

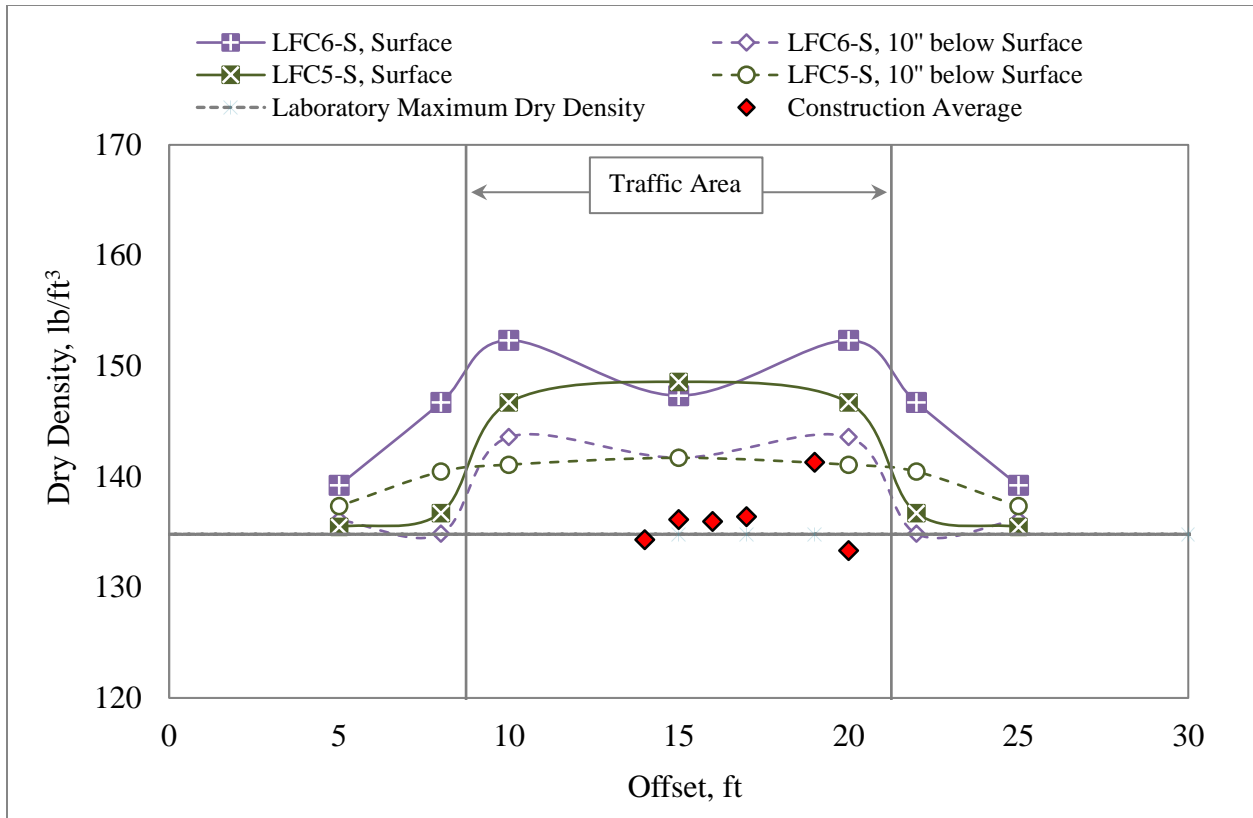
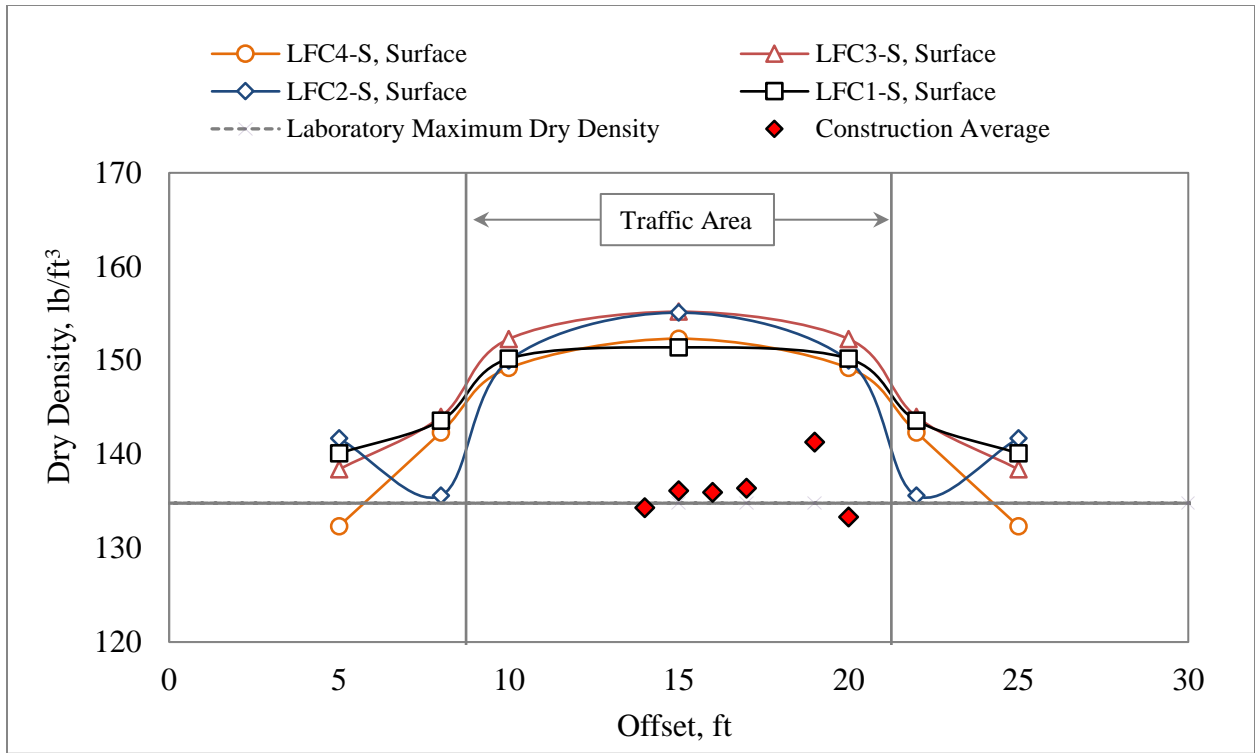
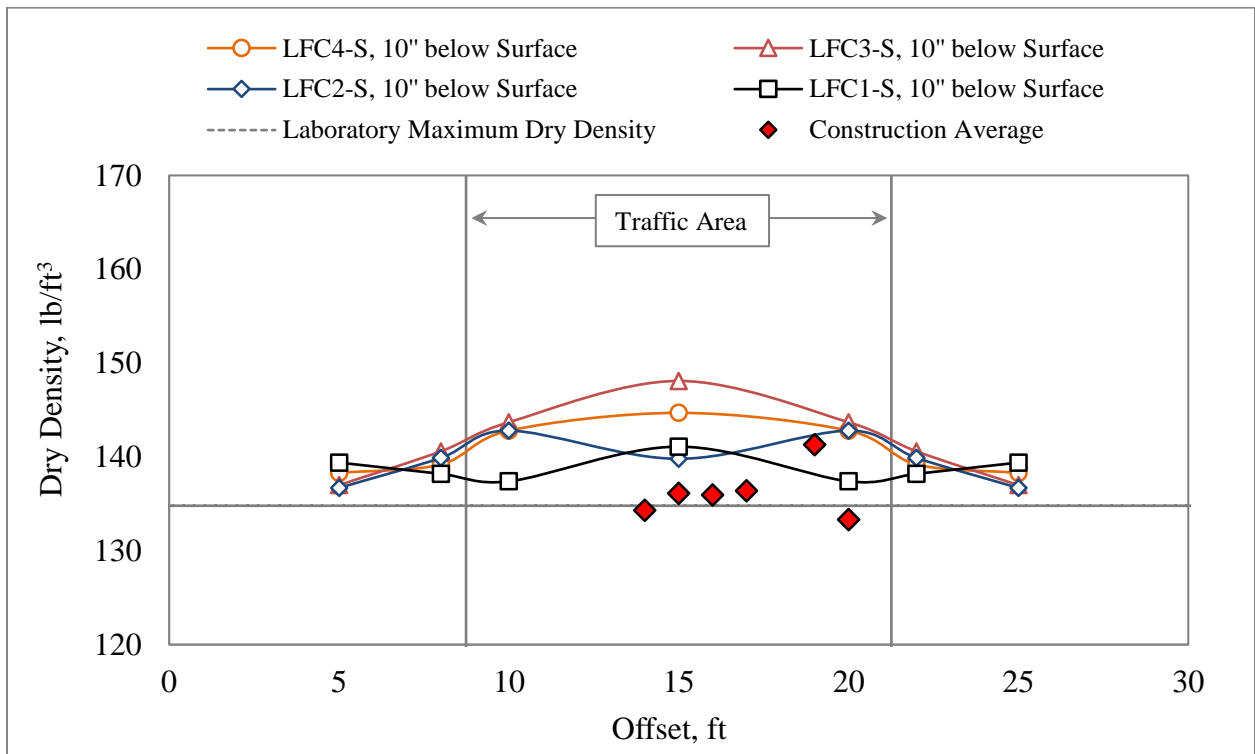


Figure 42. Sand Cone Results on P-154 for LFC5-S and LFC6-S (CC7 South Side)



(a)



(b)

Figure 43. Sand Cone Results on P-154 for LFC1-S to LFC4-S (CC7 South Side): (a) Layer Surface, (b) 10" below Surface

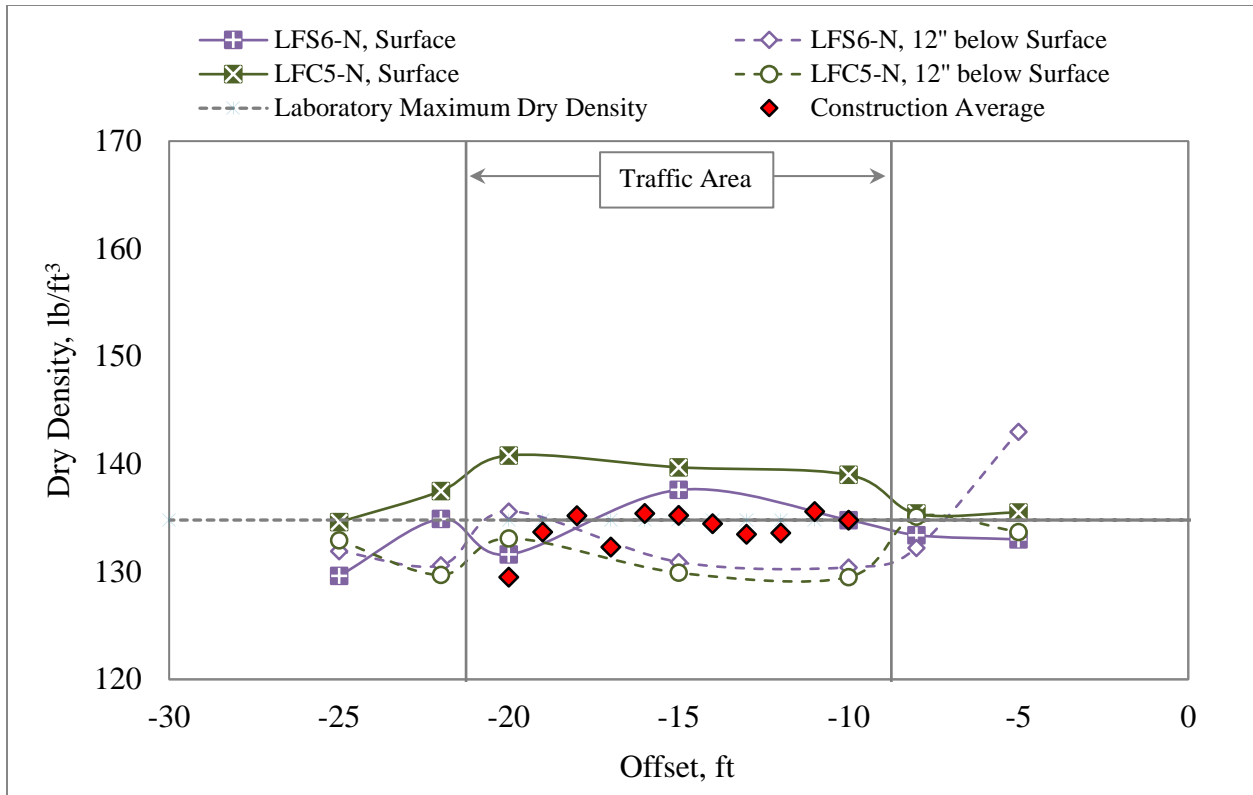
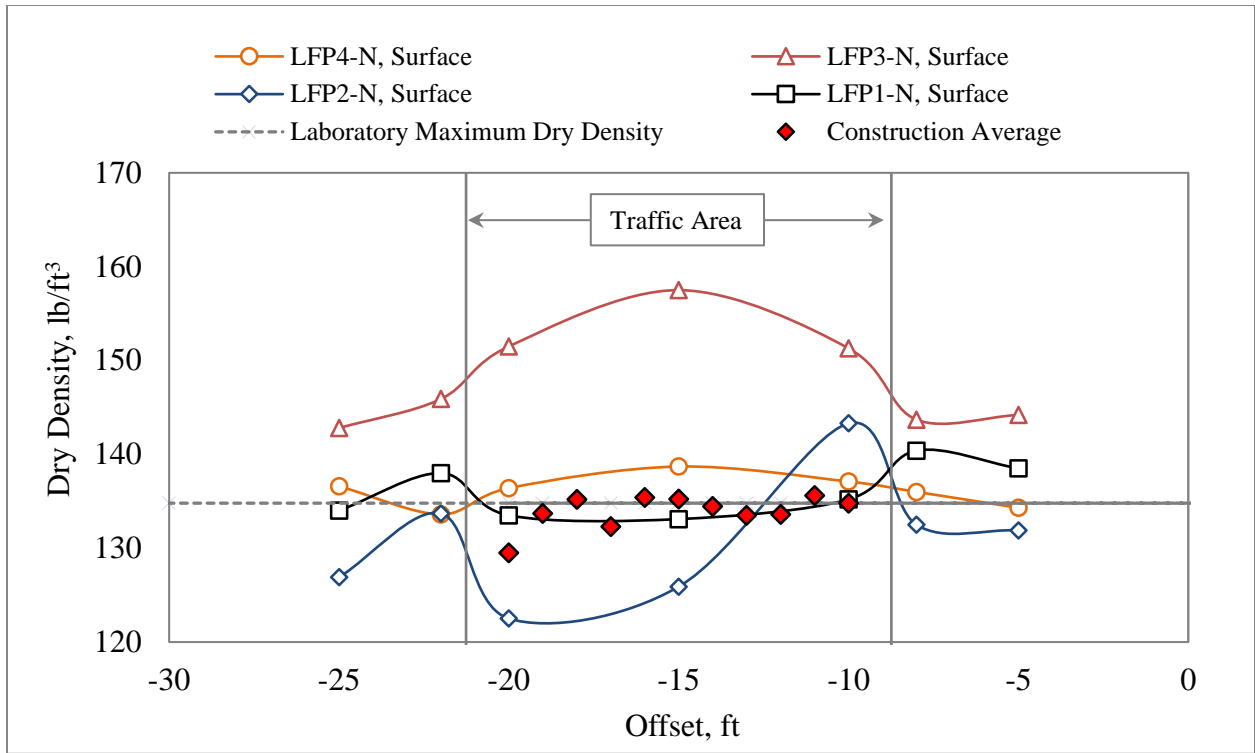
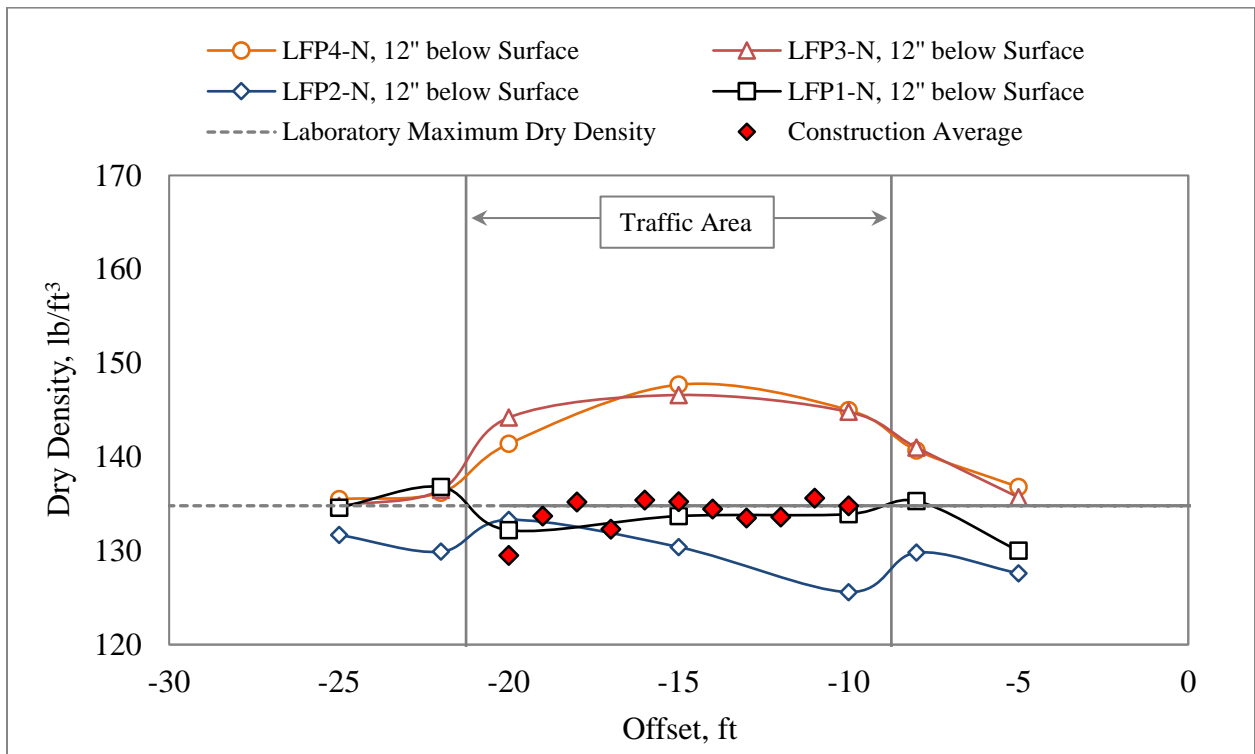


Figure 44. Nuclear Density Results on P-154 for LFC5-N and LFS6-N (CC7 North Side)



(a)



(b)

Figure 45. Nuclear Density Results on P-154 for LFP1-N to LFP4-N (CC7 North Side):
 (a) Layer Surface, (b) 12'' below Surface

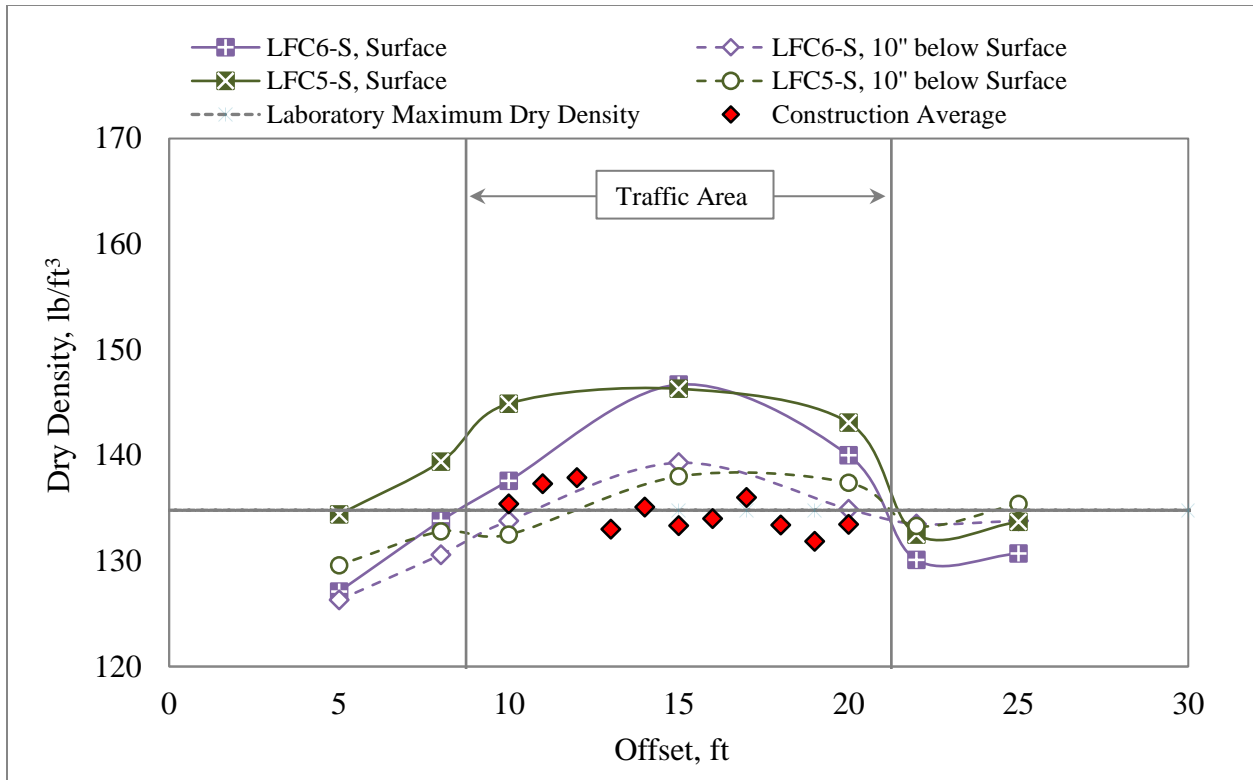
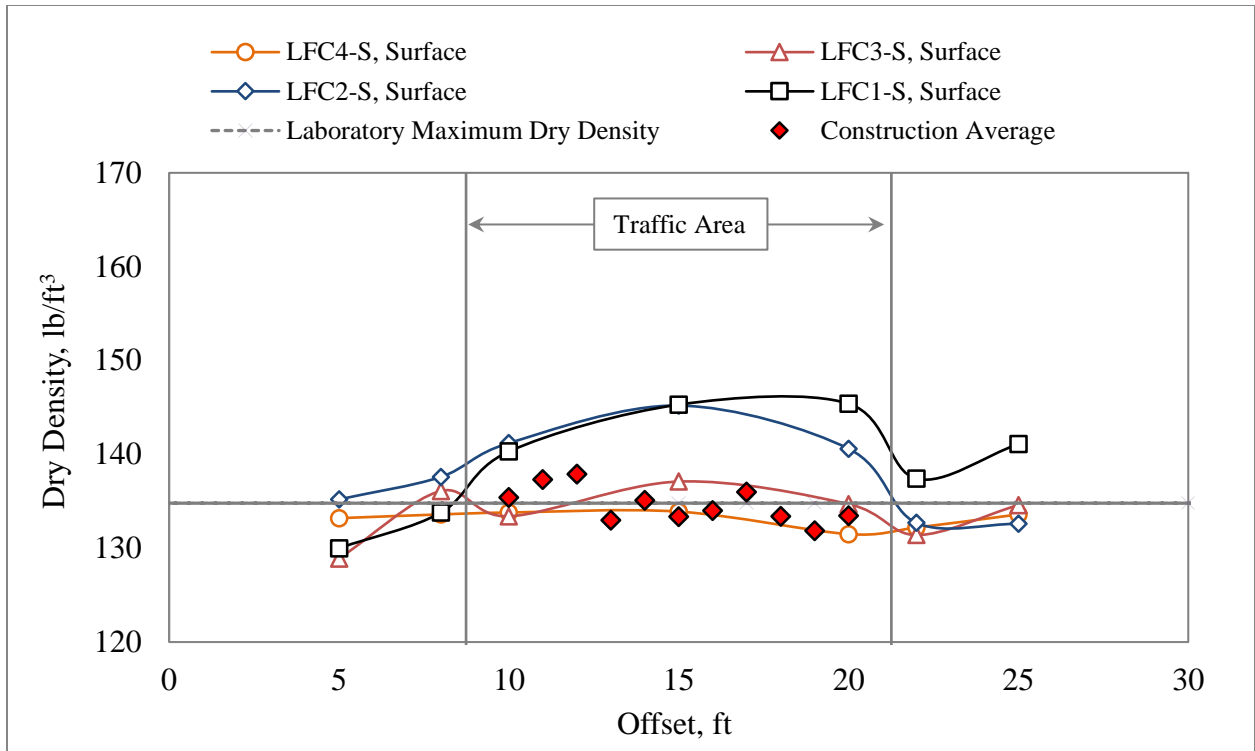
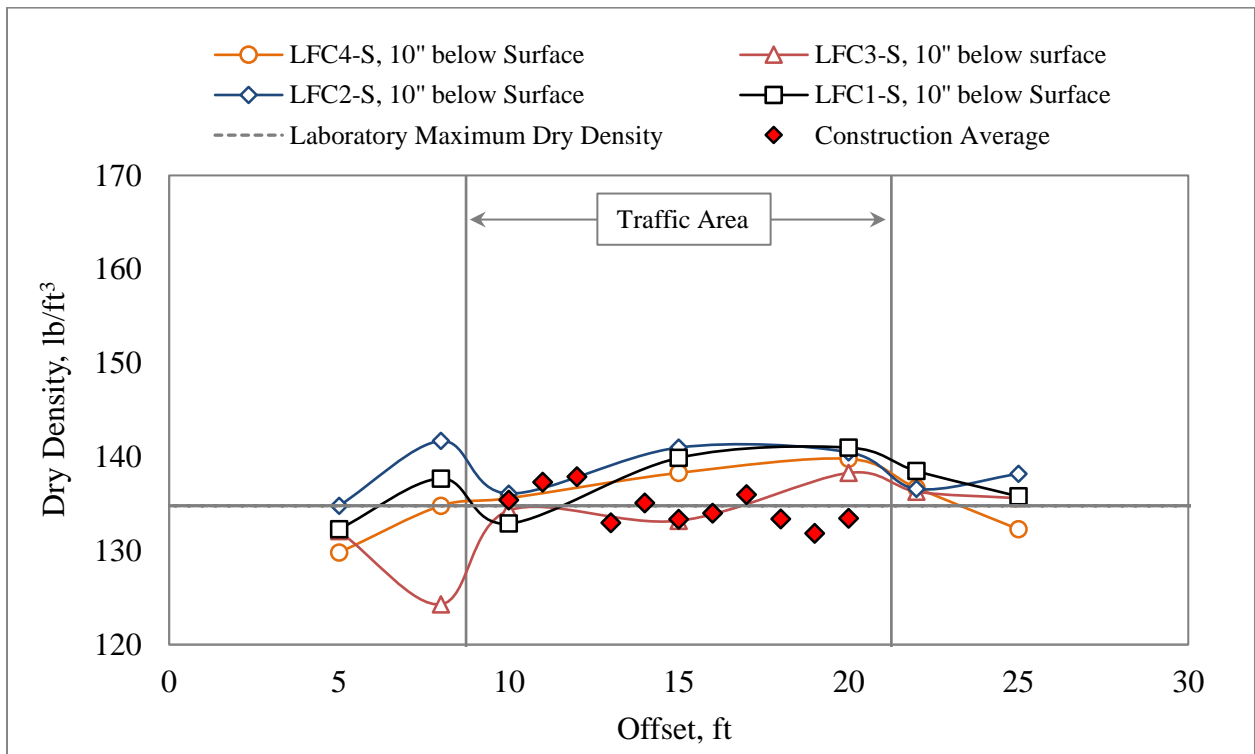


Figure 46. Nuclear Density Results on P-154 for LFC5-S and LFC6-S (CC7 South Side)



(a)



(b)

Figure 47. Nuclear Density Results on P-154 for LFC1-S to LFC4-S (CC7 South Side): (a)Layer Surface, (b)10'' below Surface

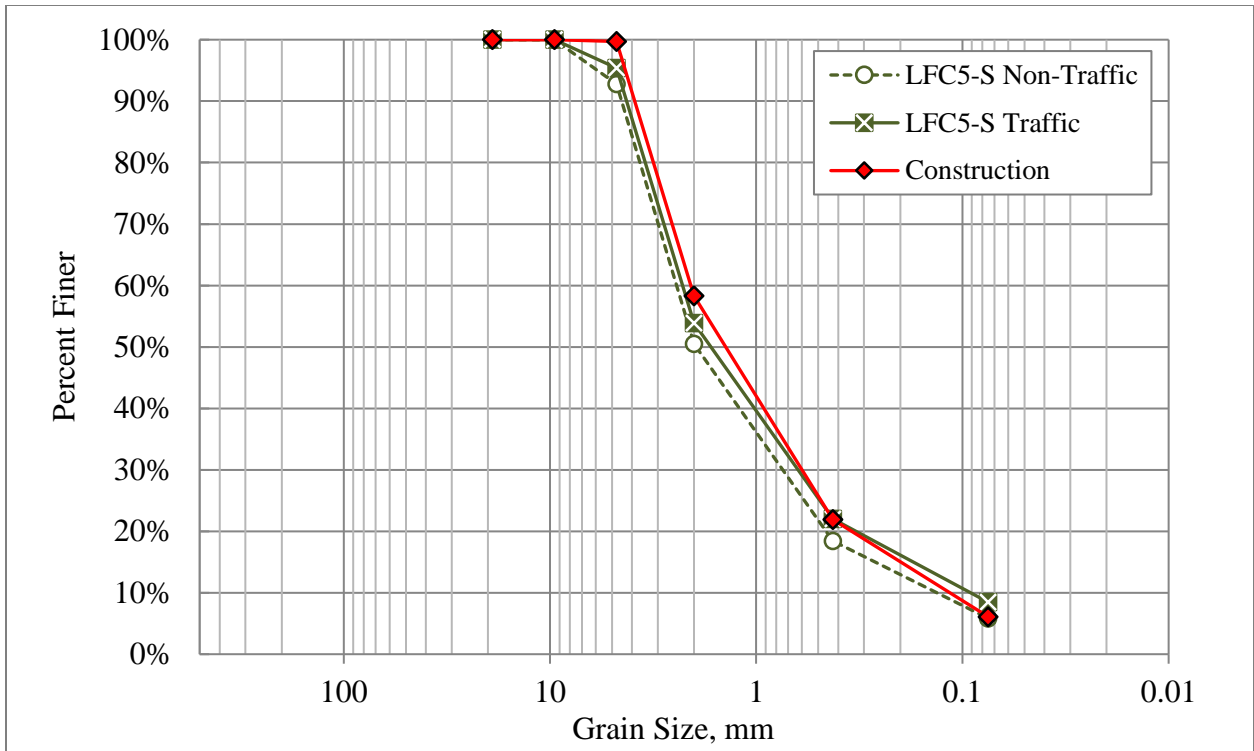


Figure 48. P-154 Gradation LFC5-S

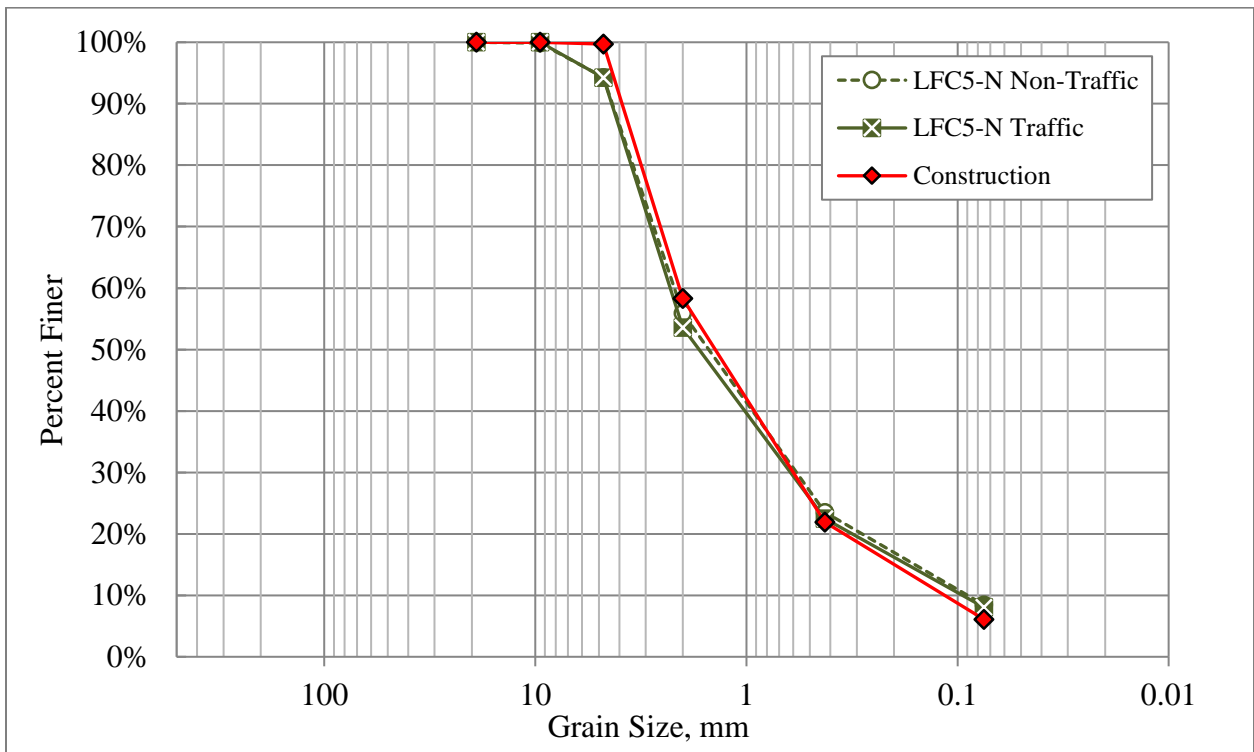


Figure 49. P-154 Gradation LFC5-N

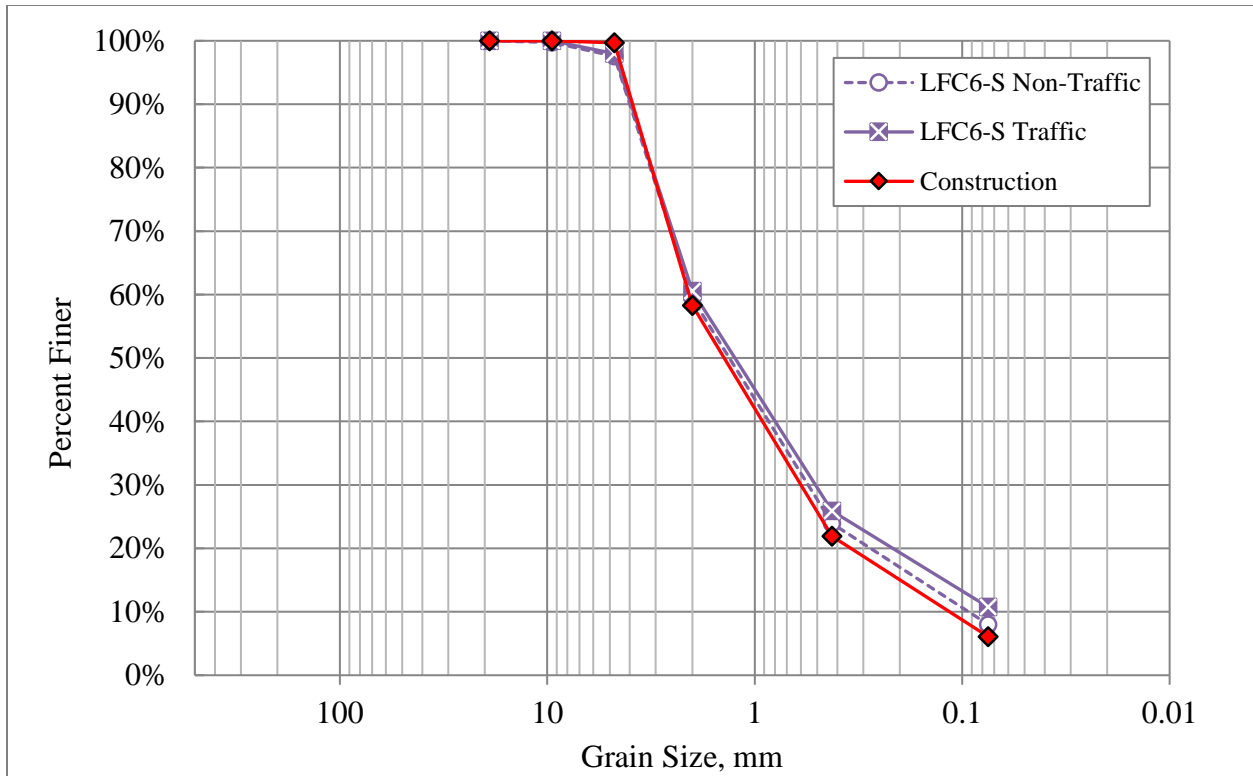


Figure 50. P-154 Gradation LFC6-S

6. P-152 DUPONT CLAY SUBGRADE

The test items were constructed on a low-strength subgrade material with a designed California Bearing Ratio (CBR) between 5 and 6. The subgrade, known as DuPont Clay, was a CH clay of high plasticity as per the Unified Soil Classification System (USCS). Once the P-154 material was removed from the subgrade interface, the interface of the P-154 and the subgrade was documented through notes and photos. The following tests were performed atop of the interface.

6.1 D-PSPA

D-PSPA tests were done at offsets -15ft, -10ft, -8ft, -5ft, +5ft, +8ft, +10ft, and +15ft on P-152 to determine seismic moduli of the subbase material. Figures 51-54 summarize the D-PSPA results.

The figures show that there was no significant differences between traffic area and non-traffic area. The mean value of the post-traffic data was similar to the pre-traffic data.

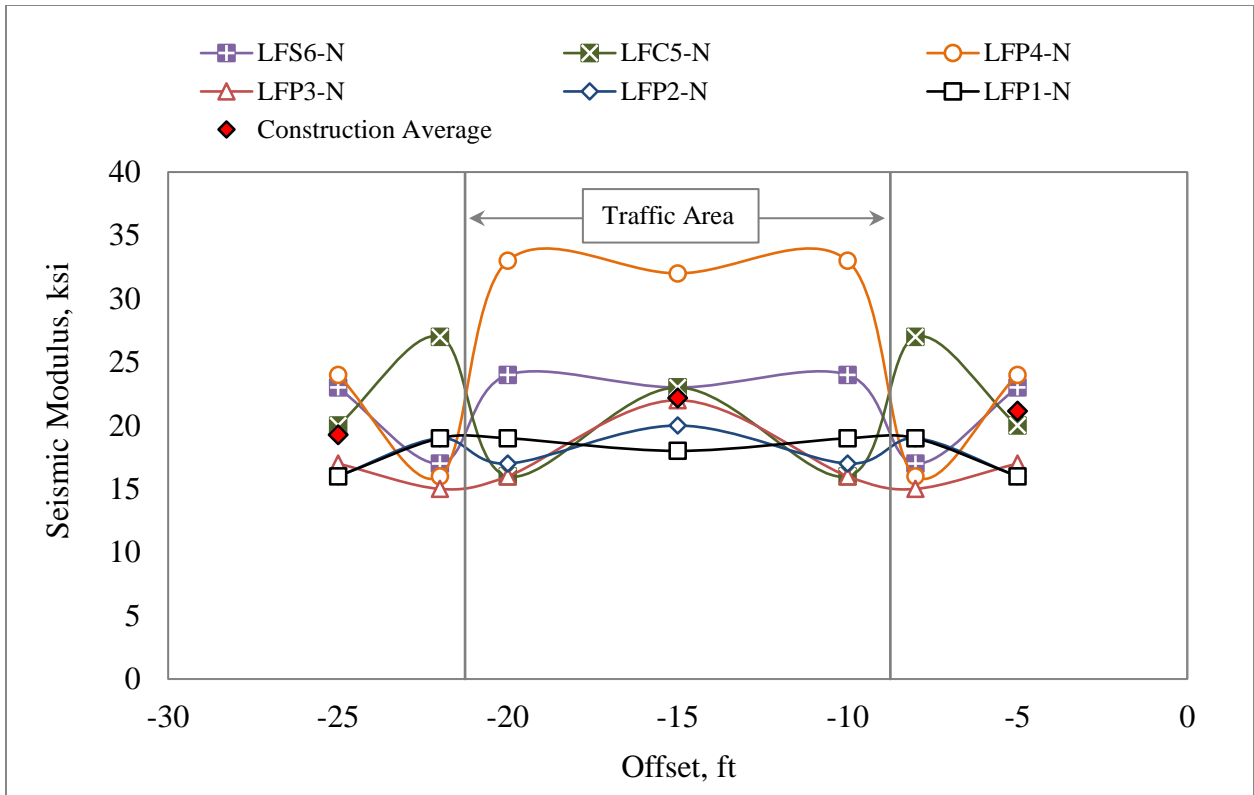


Figure 51. D-PSPA Results on P-152 (CC7 North Side, longitudinal direction)

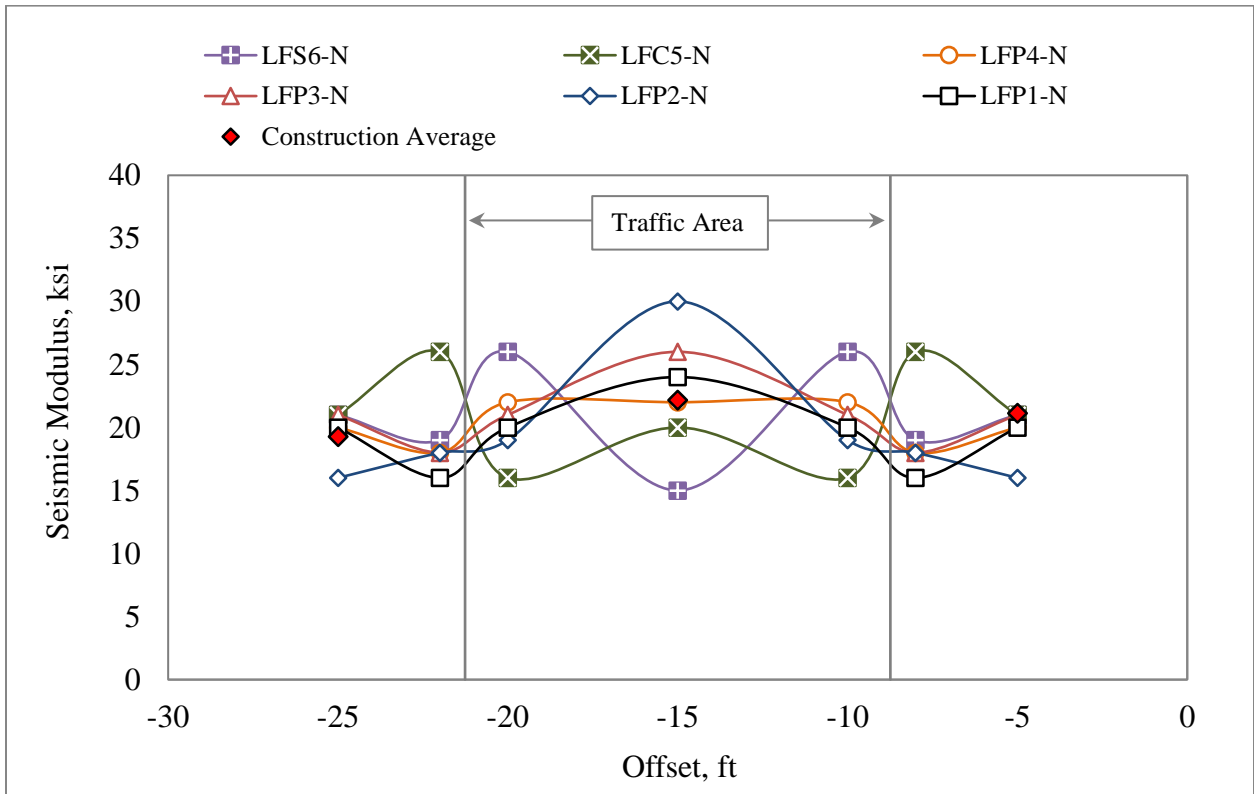


Figure 52. D-PSPA Results on P-152 (CC7 North Side, transverse direction)

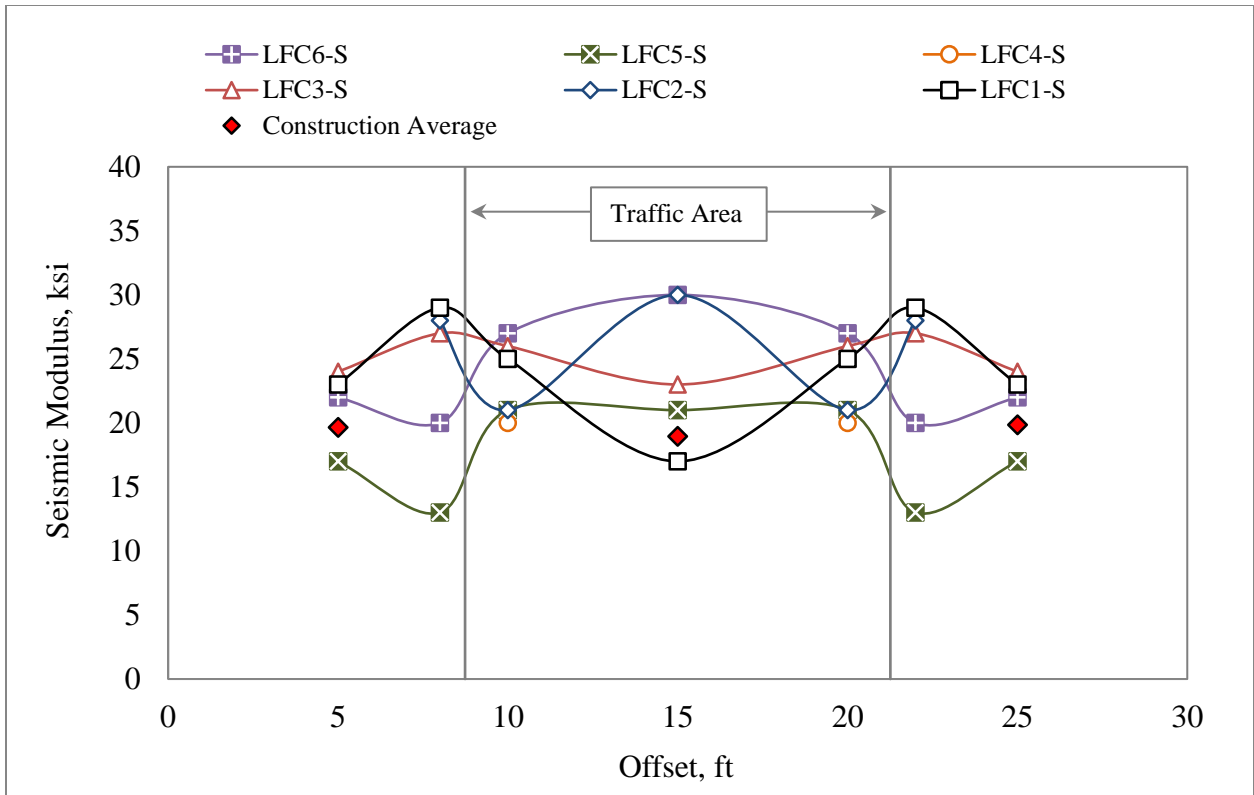


Figure 53. D-PSPA Results on P-152 (CC7 South Side, longitudinal direction)

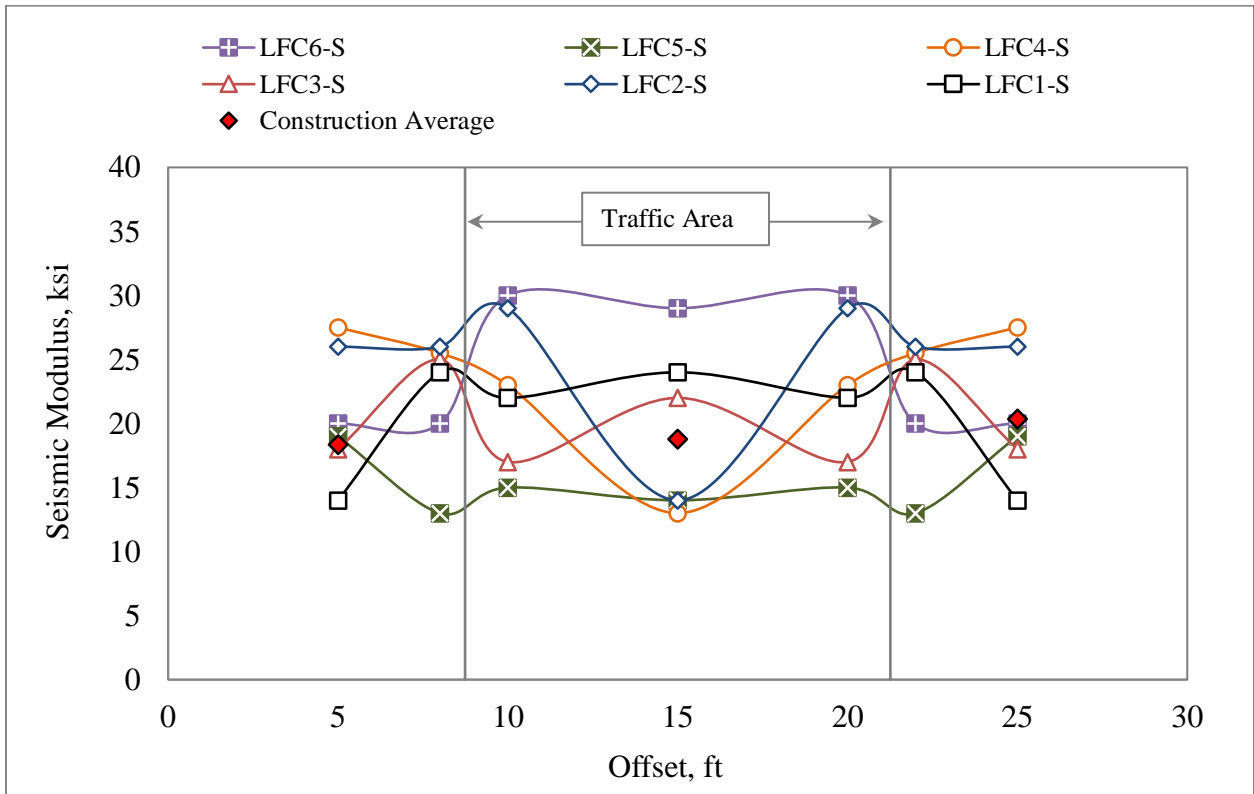


Figure 54. D-PSPA Results on P-152 (CC7 South Side, transverse direction)

6.2 LWD

LWD tests were performed at the same locations as D-PSPA. Figures 55-56 summarize the LWD results.

From figures 55 and 56, we can see that there was no significant difference between traffic area and non-traffic area. On the north side, the LWD moduli were higher than the pre-traffic average values. On the other hand, the LWD moduli on the south side were close to the pre-traffic values.

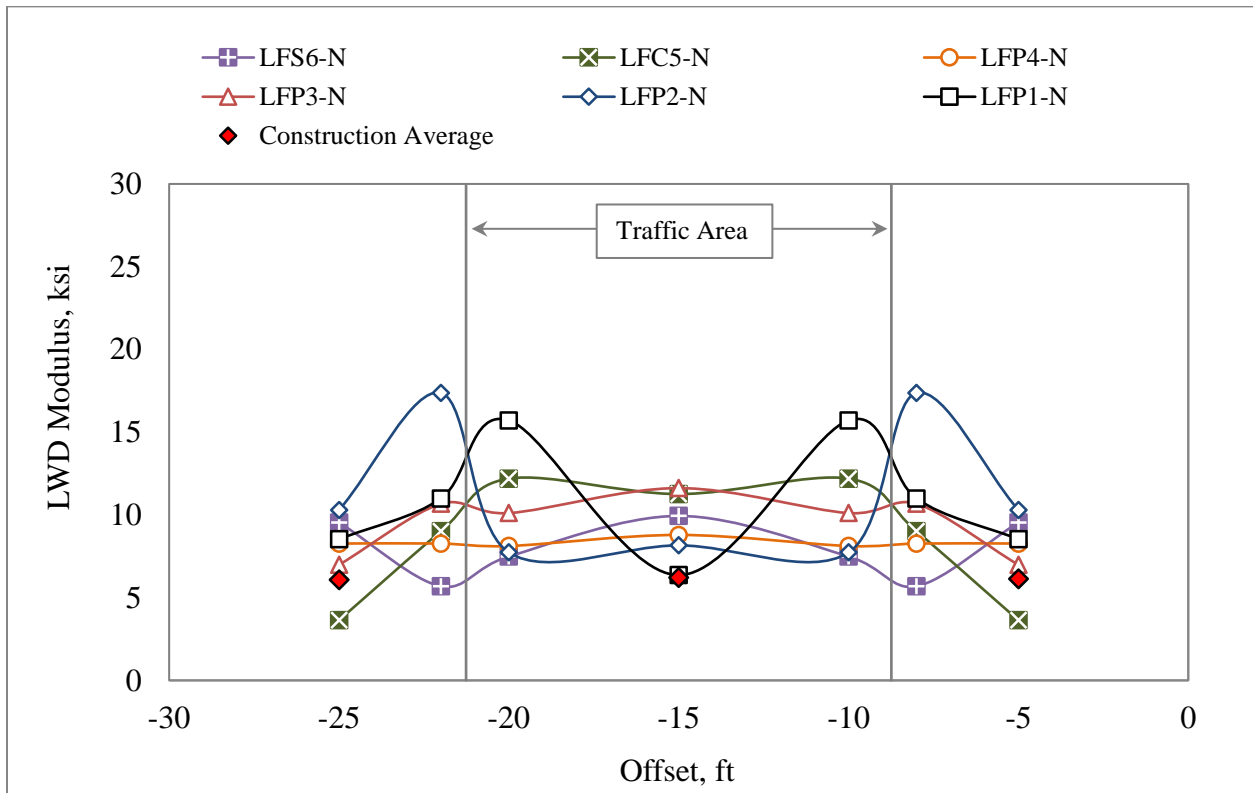


Figure 55. LWD Results on P-152 (CC7 North Side)

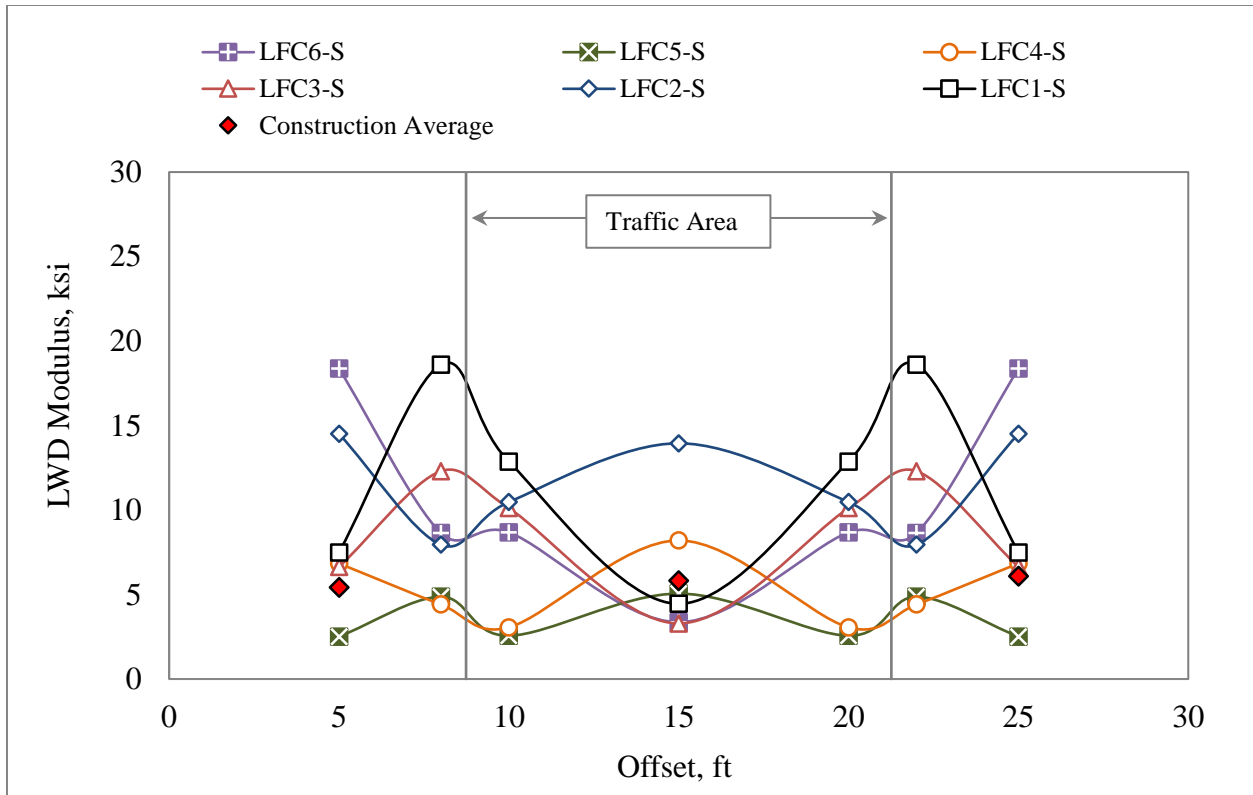
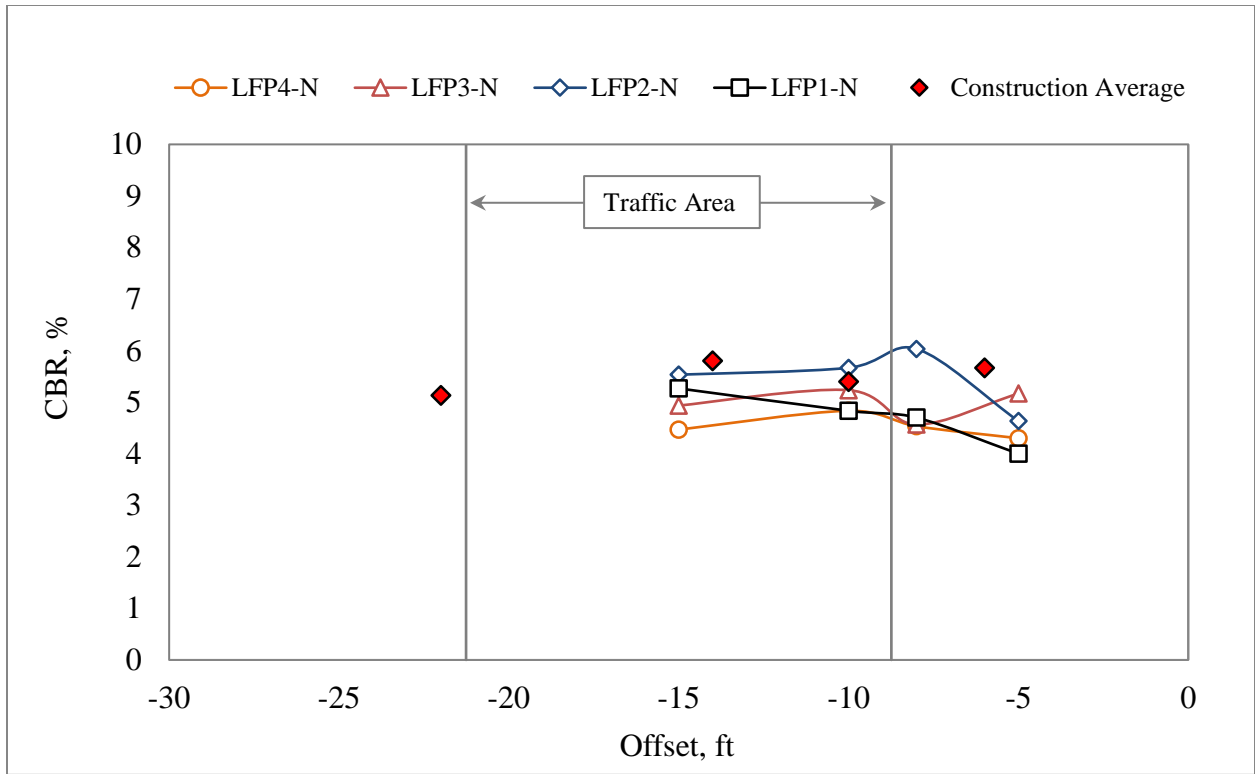


Figure 56. LWD Results on P-152 (CC7 South Side)

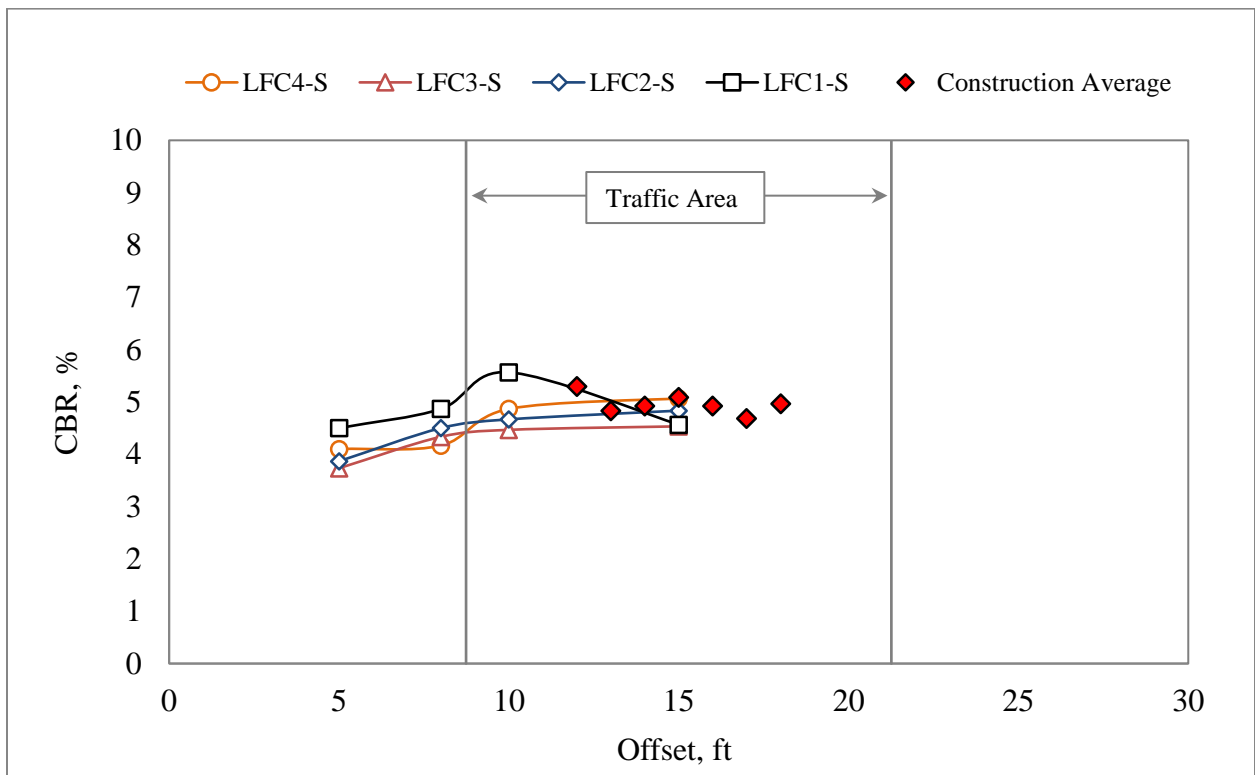
6.3 CBR AND VANE SHEAR

CBR tests were performed at the same locations as LWD tests. Three tests were done at each location. Three vane shear tests were conducted at each CBR location. The CBR and LWD results are summarized in figures 57 and 58. Since the vane shear test equipment was broken when performing tests on Trenches 5 and 6, figure 58 only represents data collected from Trenches 1-4.

In figure 57, it can be observed that most post-traffic CBR values were lower than the pre-traffic values. This is possibly a result of additional water that seeped by gravity during construction of P-154 and P-209 layers. The CBR and Vane Shear values in traffic area were slightly higher than non-traffic area.

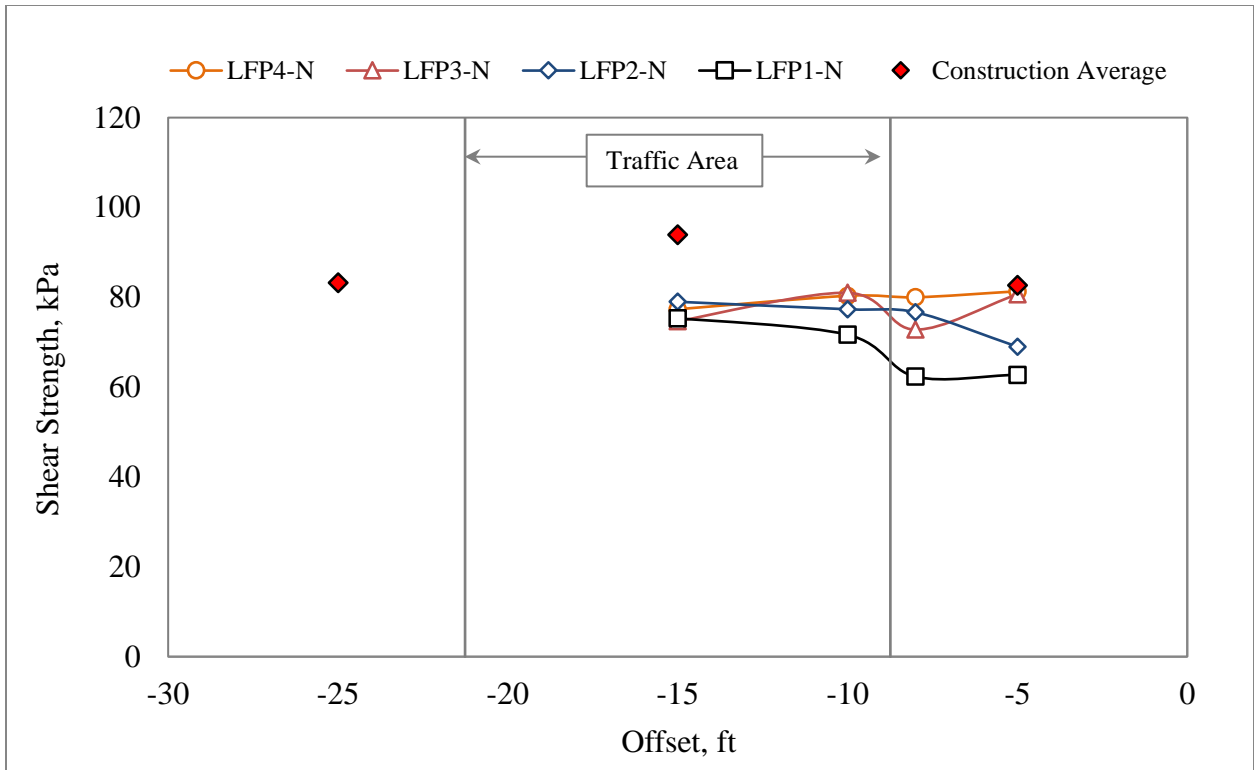


(a)

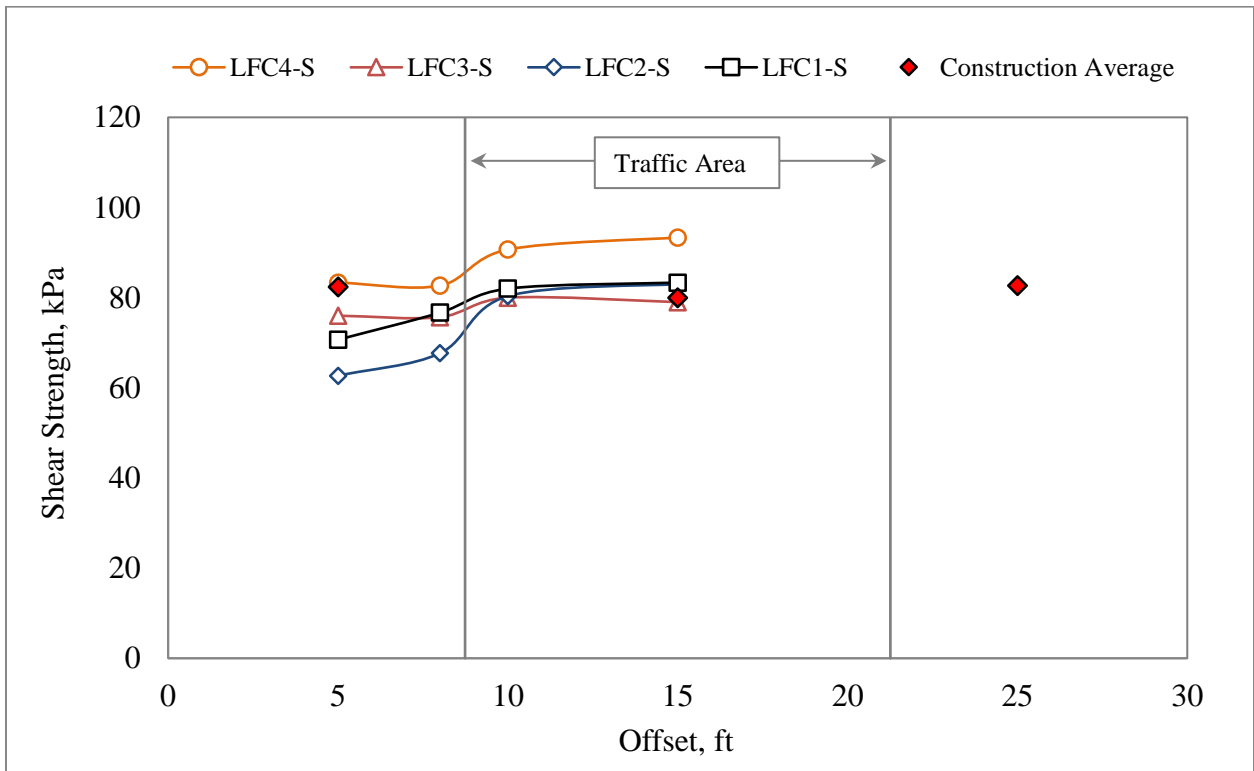


(b)

Figure 57. CBR Results on P-152: (a)North Side, (b)South Side



(a)



(b)

Figure 58. Vane Shear Results on P-152: (a)North Side, (b)South Side

6.4 DRIVE CYLINDER AND NUCLEAR DENSITY

In order to measure the dry density and moisture content, Drive Cylinder and Nuclear Density tests were performed at CBR locations.

The average moisture content in test items LFC5-N and LFS6-N was 27.4%, which was higher than pre-traffic test value of 26.2%. For test items LFP1-N, LFP2-N, LFP3-N, and LFP4-N the average moisture content was 34.5%. This average value was also higher than the construction moisture content of 33.6%. On the south side, the post-traffic moisture content was 27.4%, whereas the pre-traffic moisture content was 26.6%. In general, the post-traffic moisture content was approximately 1% higher than pre-traffic values.

The dry densities determined by Drive Cylinder and Nuclear Density tests are summarized in figures 59-64. The results indicate that there was no significant difference in density between traffic and non-traffic areas. The difference between post-traffic and pre-traffic density values were also negligible.

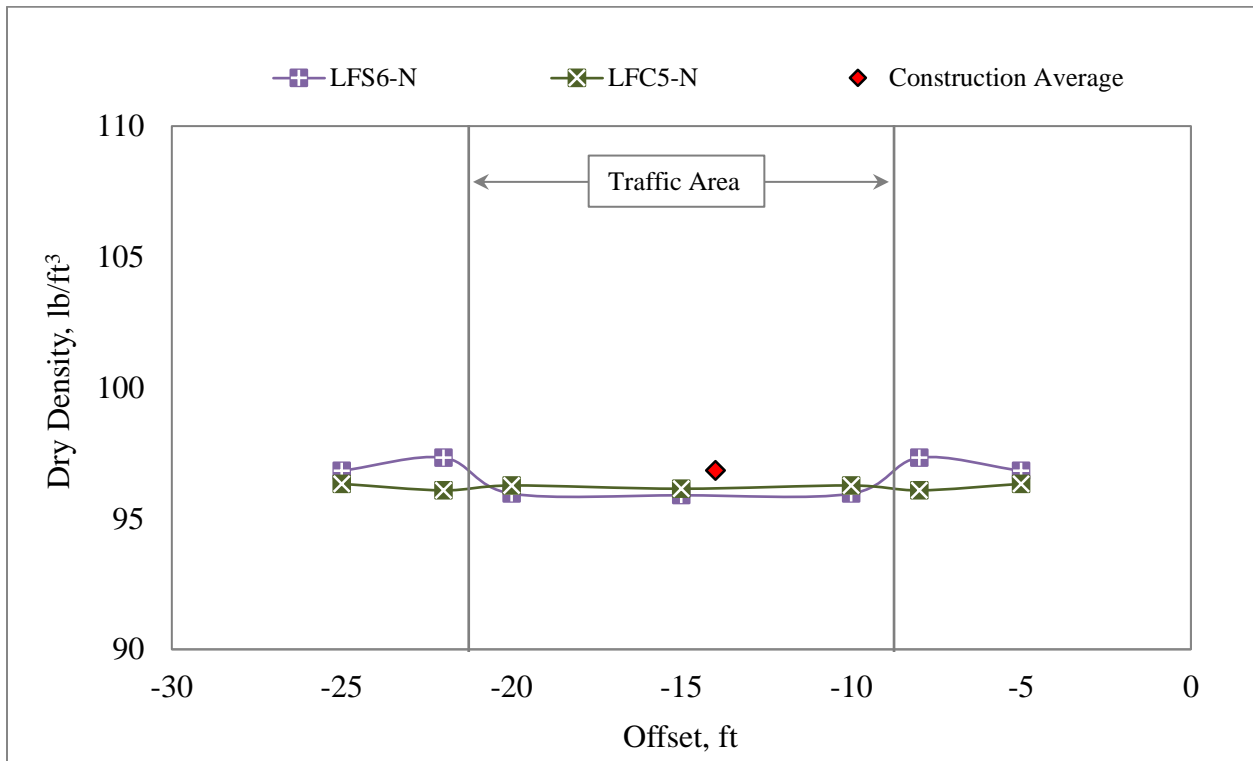


Figure 59. Drive Cylinder Results on P-152 for LFS6-N and LFC5-N (CC7 North Side)

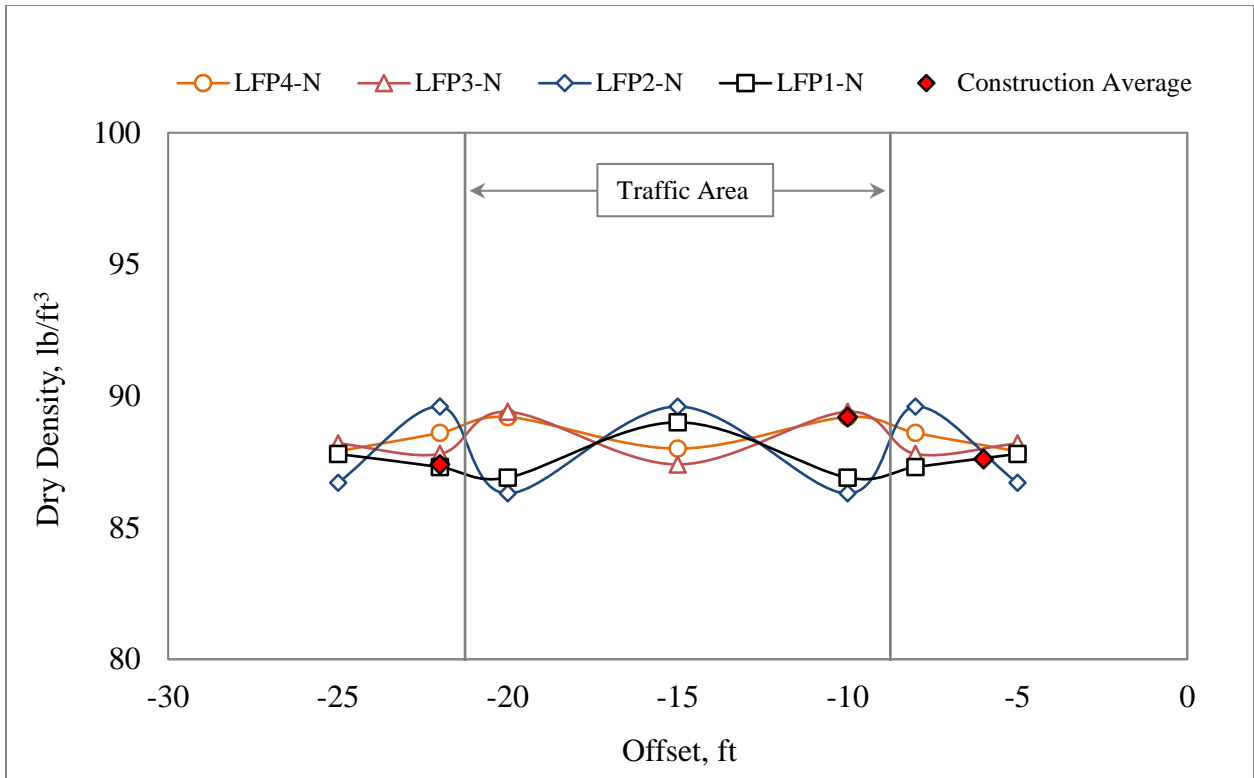


Figure 60. Drive Cylinder Results on P-152 for LFP1-N to LFP4-N (CC7 North Side)

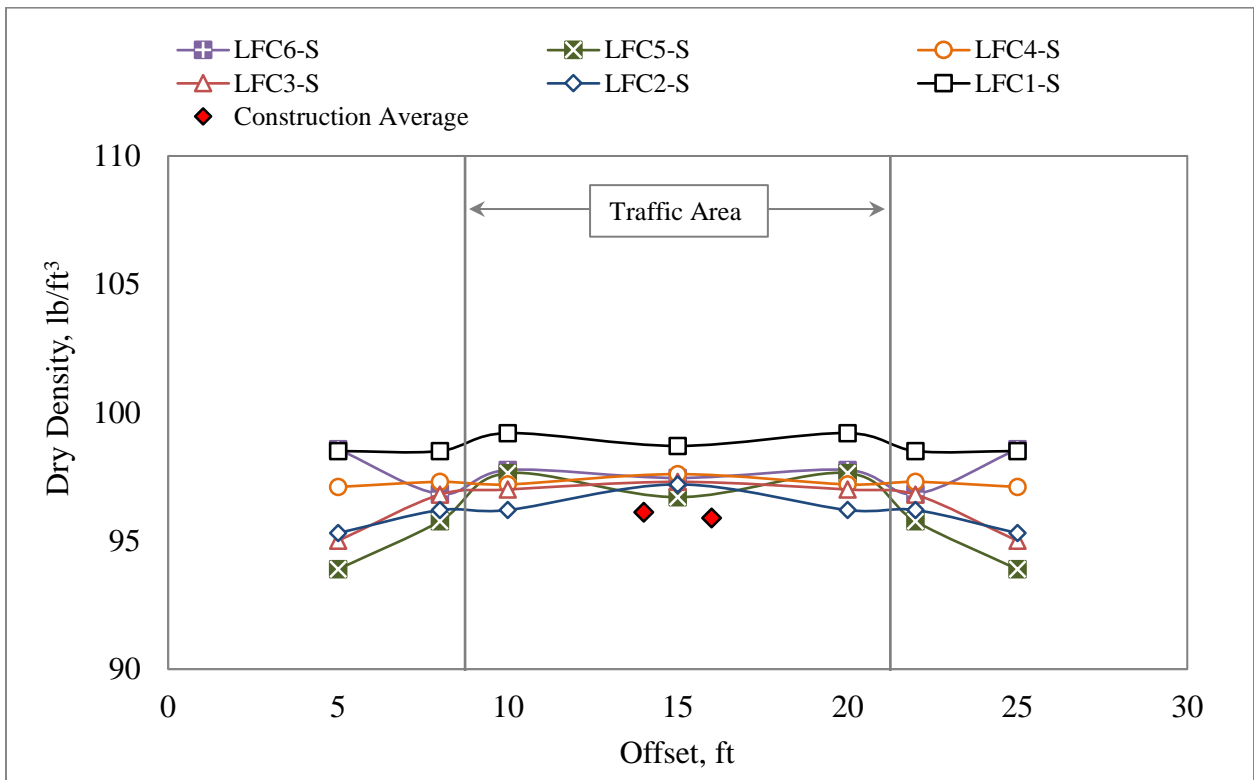


Figure 61. Drive Cylinder Results on P-152 (CC7 South Side)

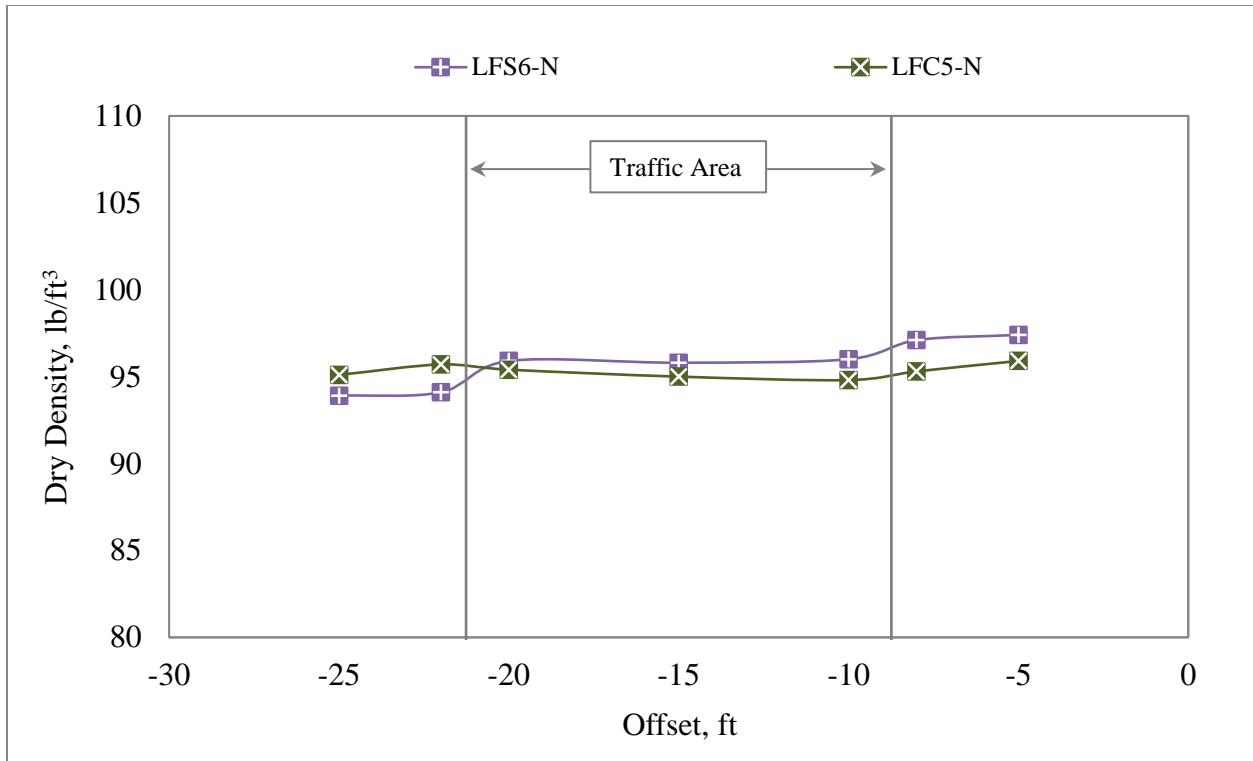


Figure 62. Nuclear Density Results on P-152 for LFS6-N and LFC5-N (CC7 North Side)

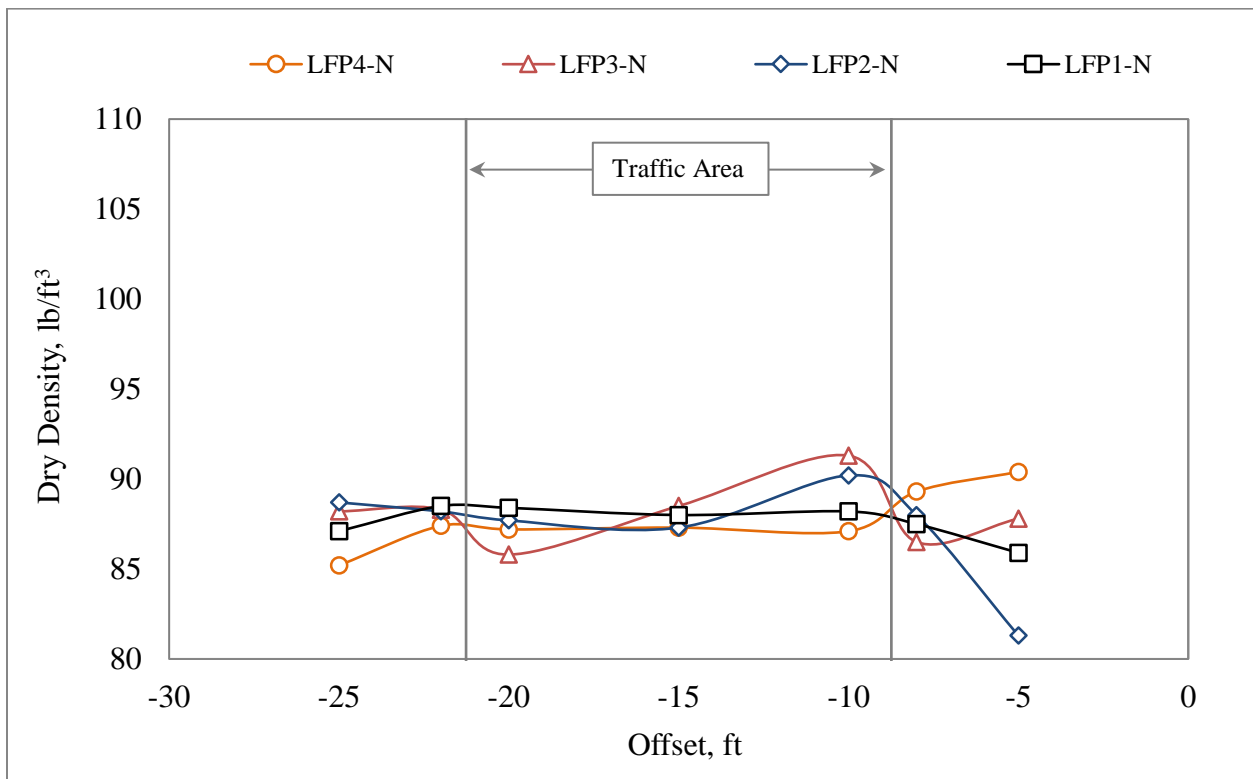


Figure 63. Nuclear Density Results on P-152 for LFP1-N to LFP4-N (CC7 North Side)

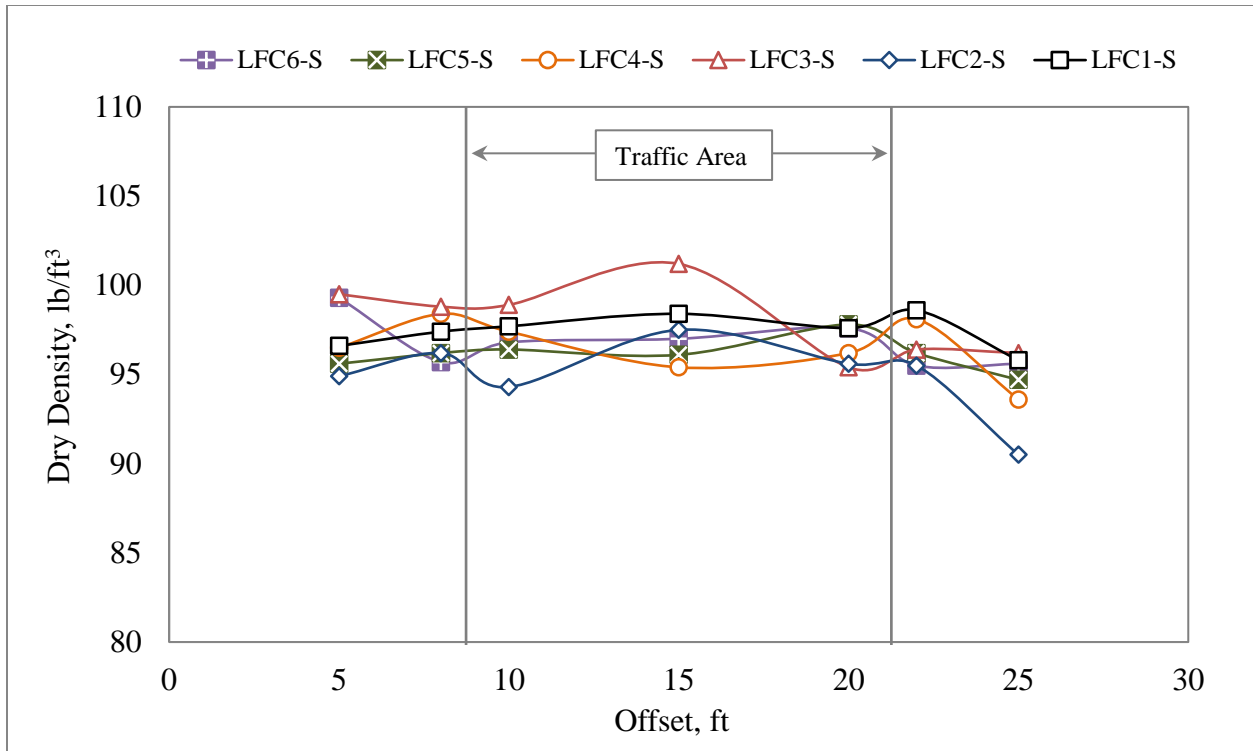


Figure 64. Nuclear Density Results on P-152 (CC7 South Side)

6.5 DCP

The Dynamic Cone Penetrometer (DCP) tests were performed at offsets -15ft, -10ft, -8ft, -5ft, +5ft, +8ft, +10ft, and +15ft on P-152 to measure the strength of compacted material of subgrade layers.

DCP test result consists of number of blow counts versus penetration depth. DCP Index (DCPI) can be determined using the equation below,

$$DCPI = \frac{\Delta D}{\Delta BC}$$

Where,

DCPI: DCP Index;

ΔD : Penetration Depth;

ΔBC : Blow Counts corresponding to penetration depth ΔD .

The CBR was calculated using the equation below for CH soils,

$$CBR = \frac{1}{(0.072923 \times DCPI)}$$

Where,

CBR: California Bearing Ratio;

DCPI: DCP Index.

The CBR values were plotted versus penetration depth as shown in figures 65 to 76. The DCP results indicate that the CBR values are increasing with depth. On the south side, the CBR values range from 2% to 23%. On the north side, the CBR values vary from 2% to 14%.

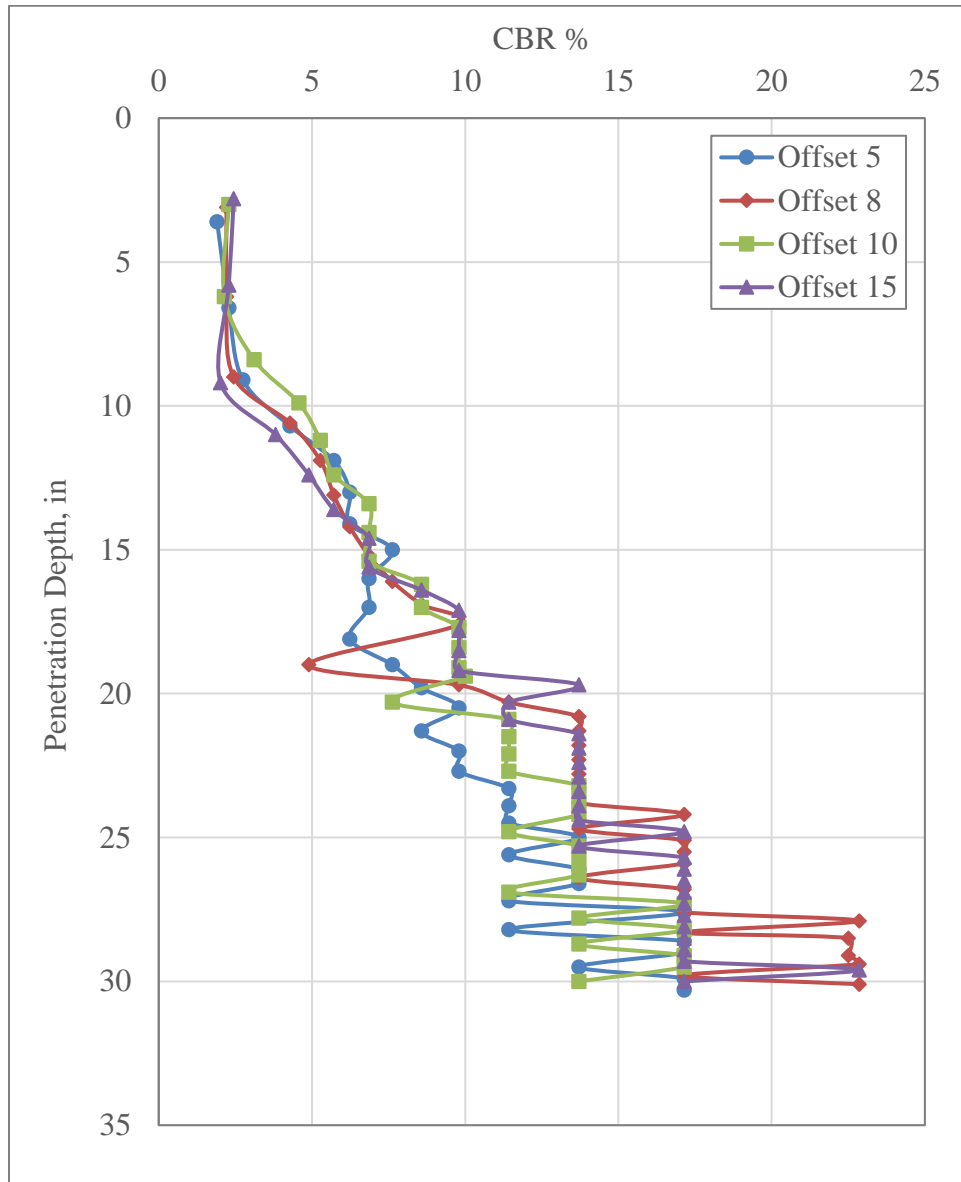


Figure 65. DCP Results for LFC1-S

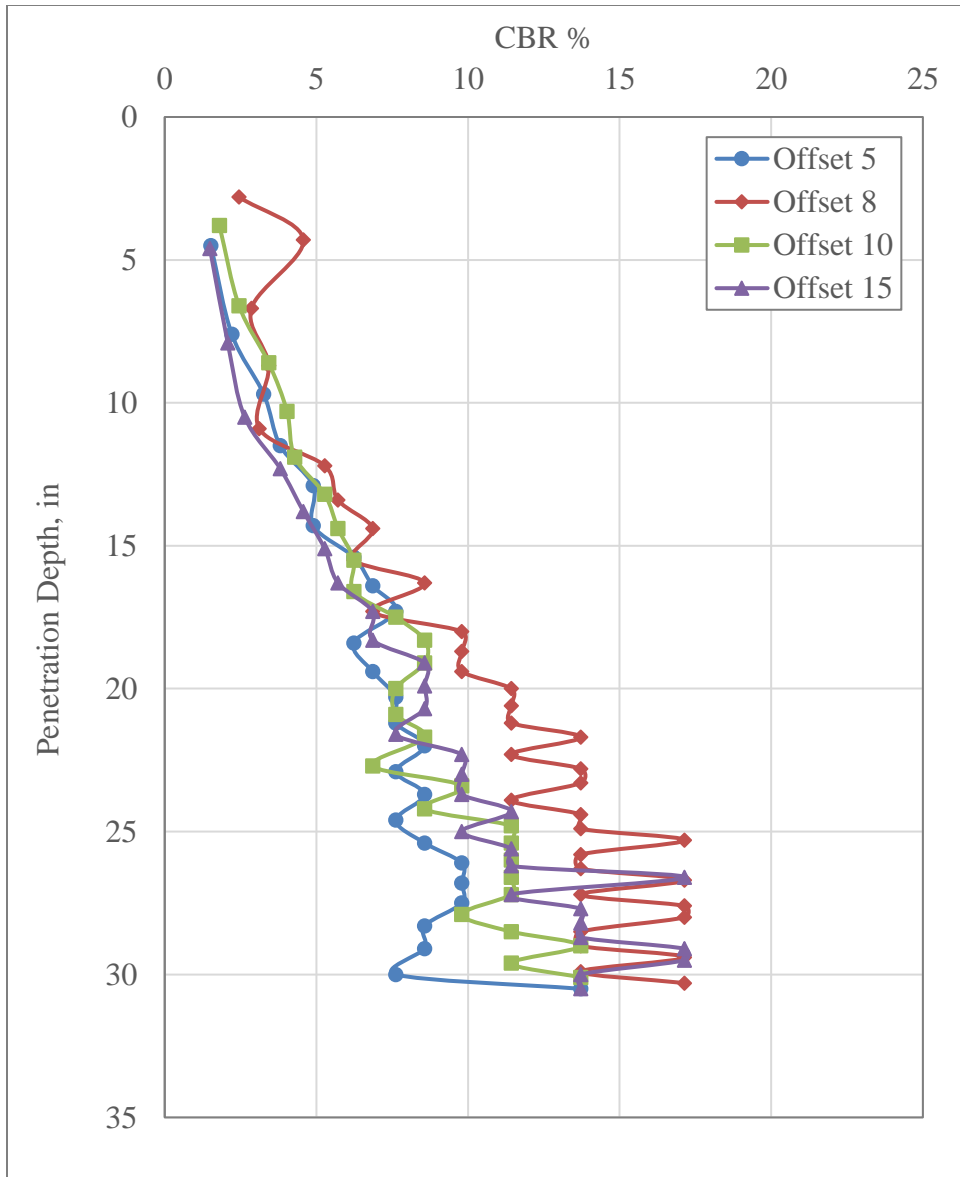


Figure 66. DCP Results for LFC2-S

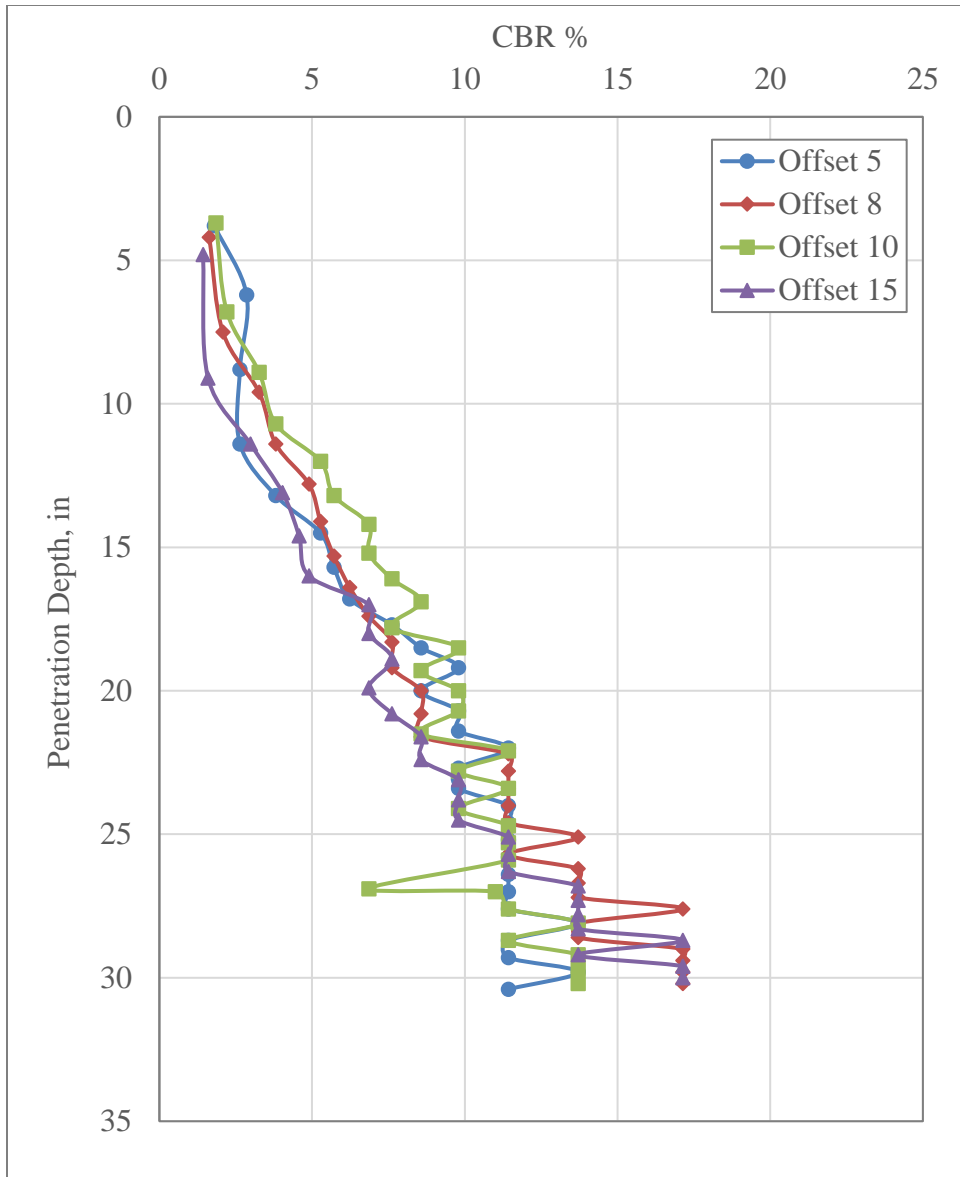


Figure 67. DCP Results for LFC3-S

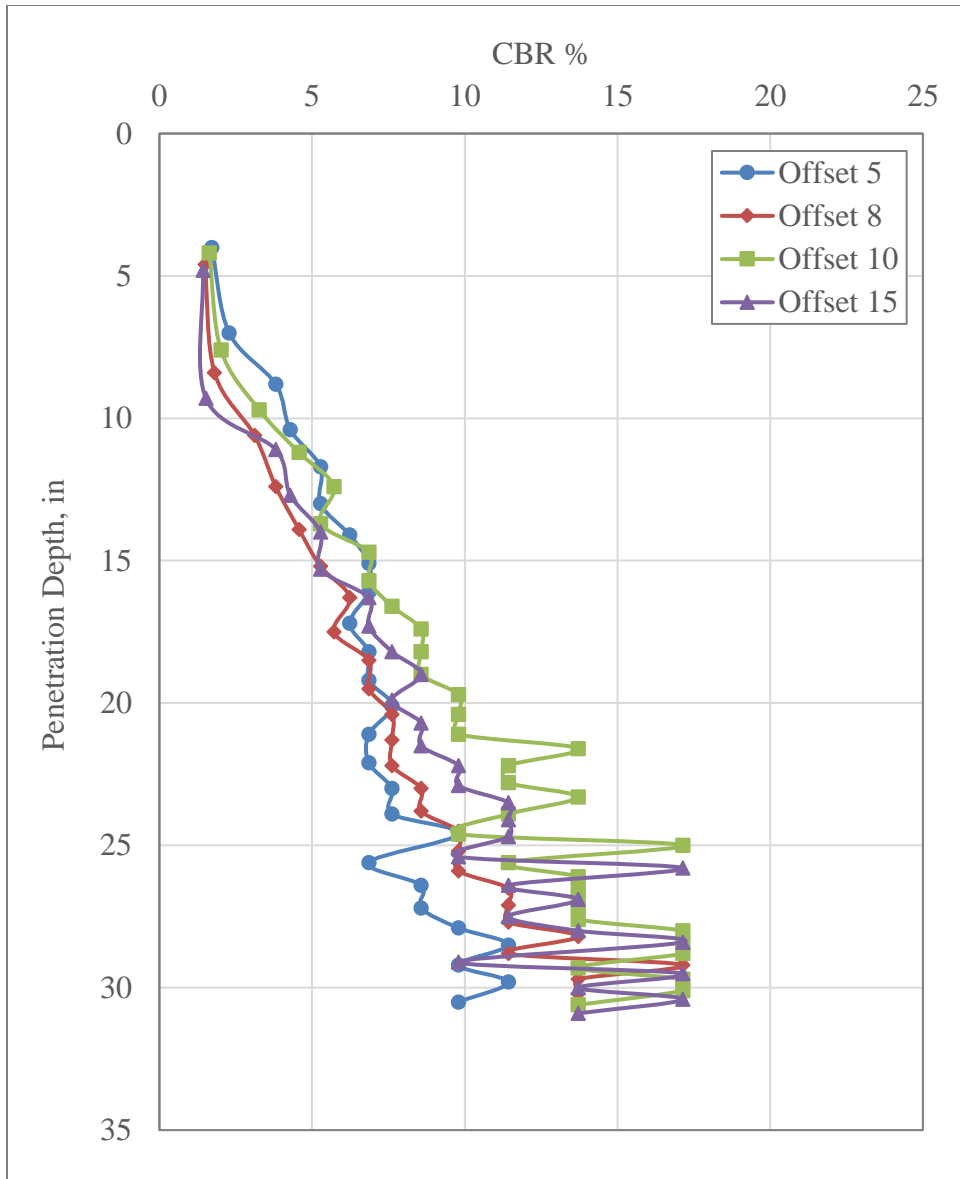


Figure 68. DCP Results for LFC4-S

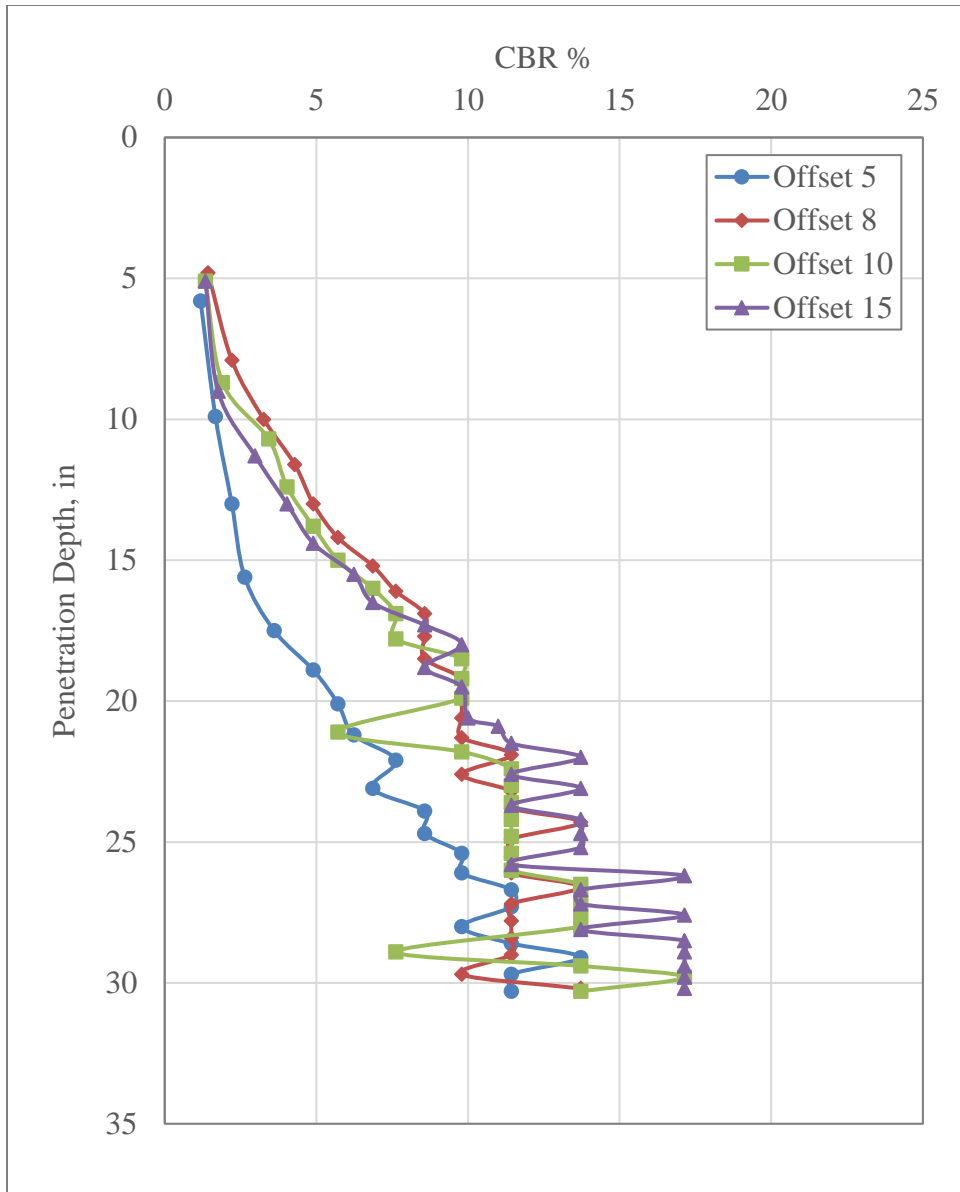


Figure 69. DCP Results for LFC5-S

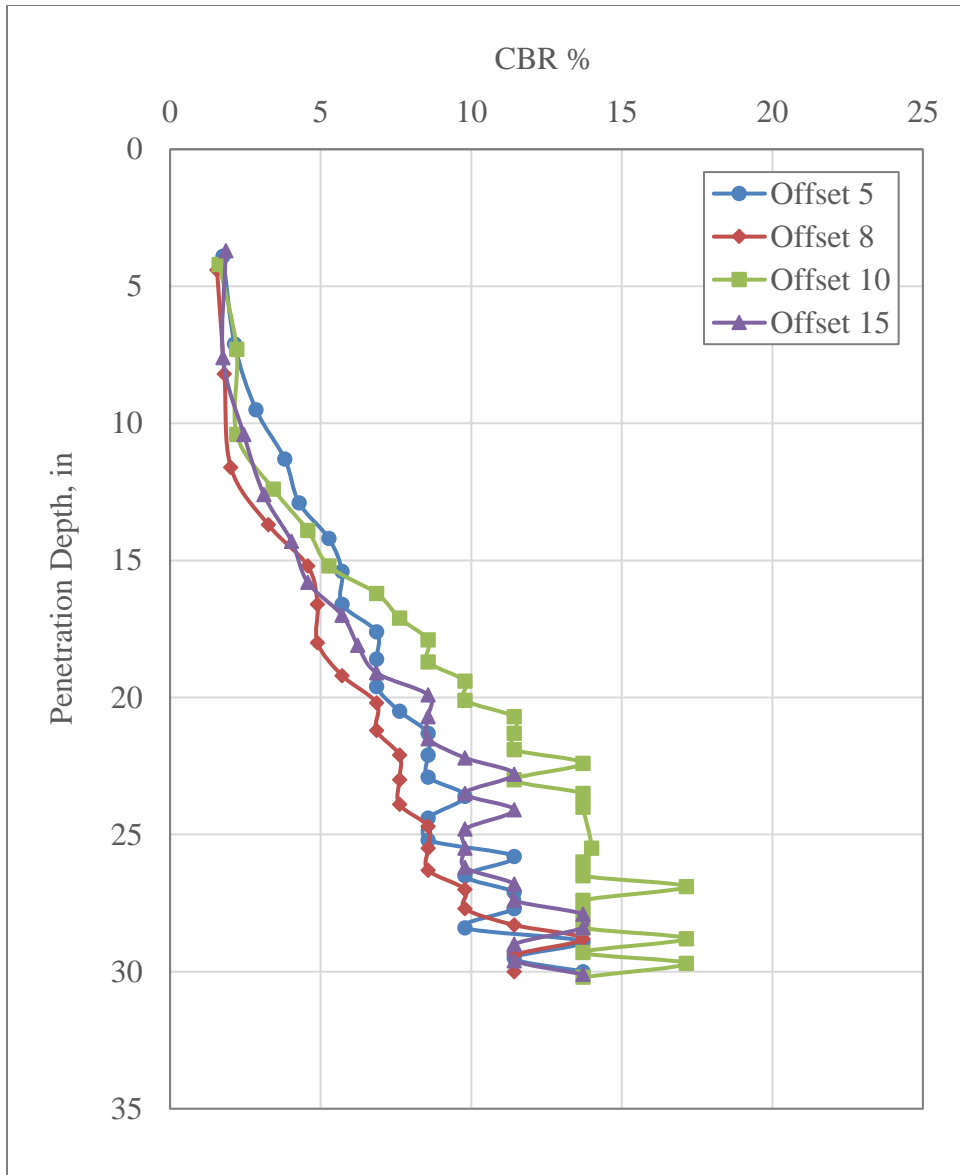


Figure 70. DCP Results for LFC6-S

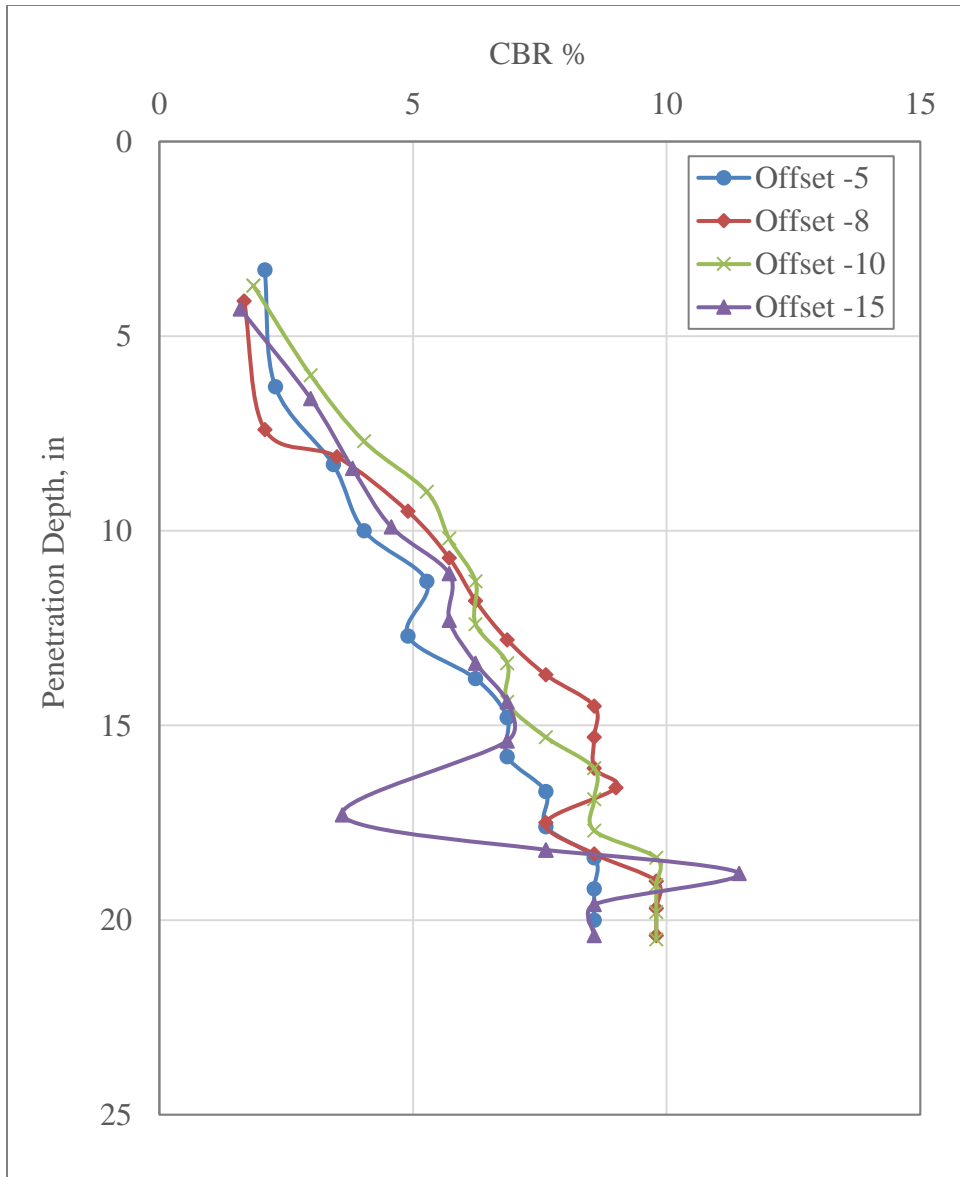


Figure 71. DCP Results for LFP1-N

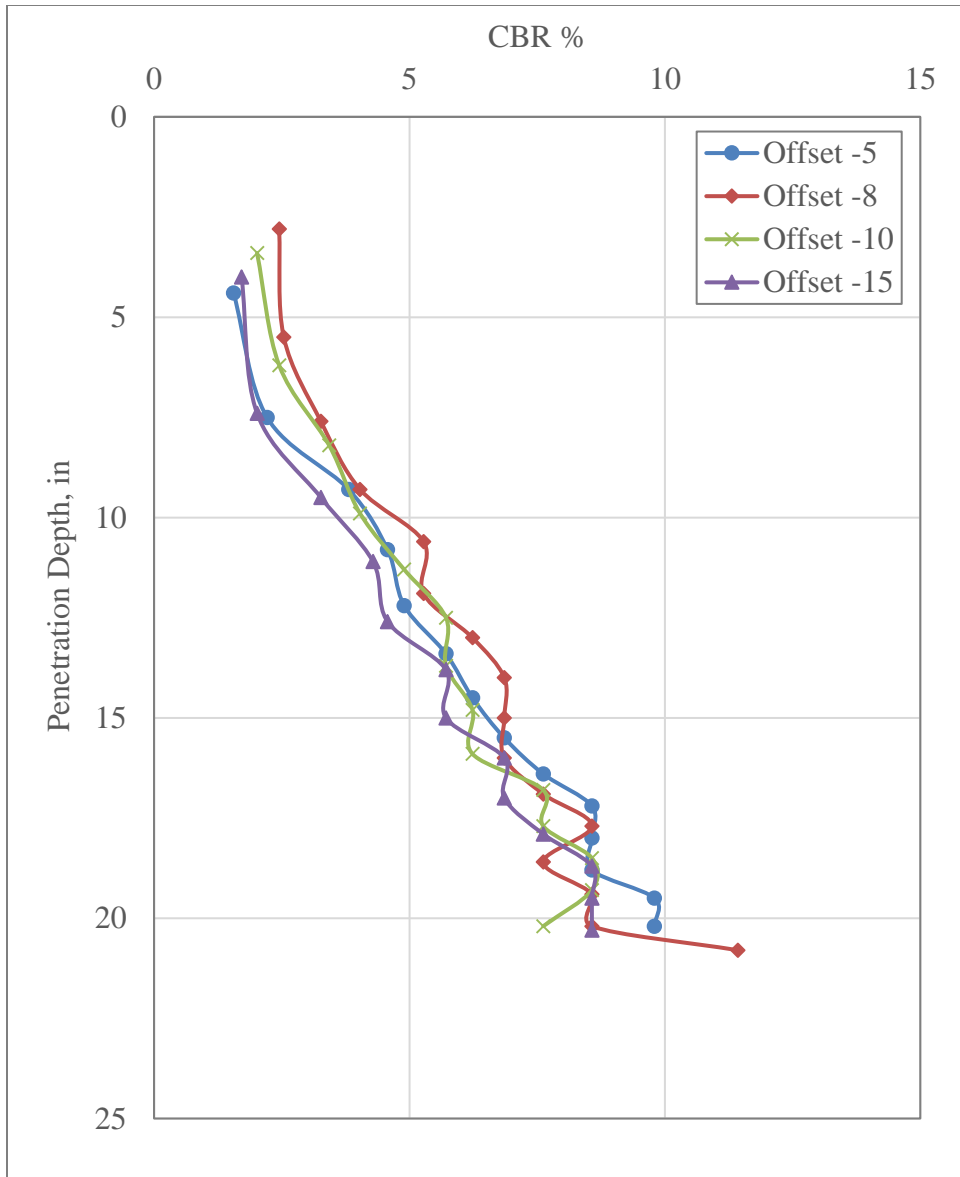


Figure 72. DCP Results for LFP2-N

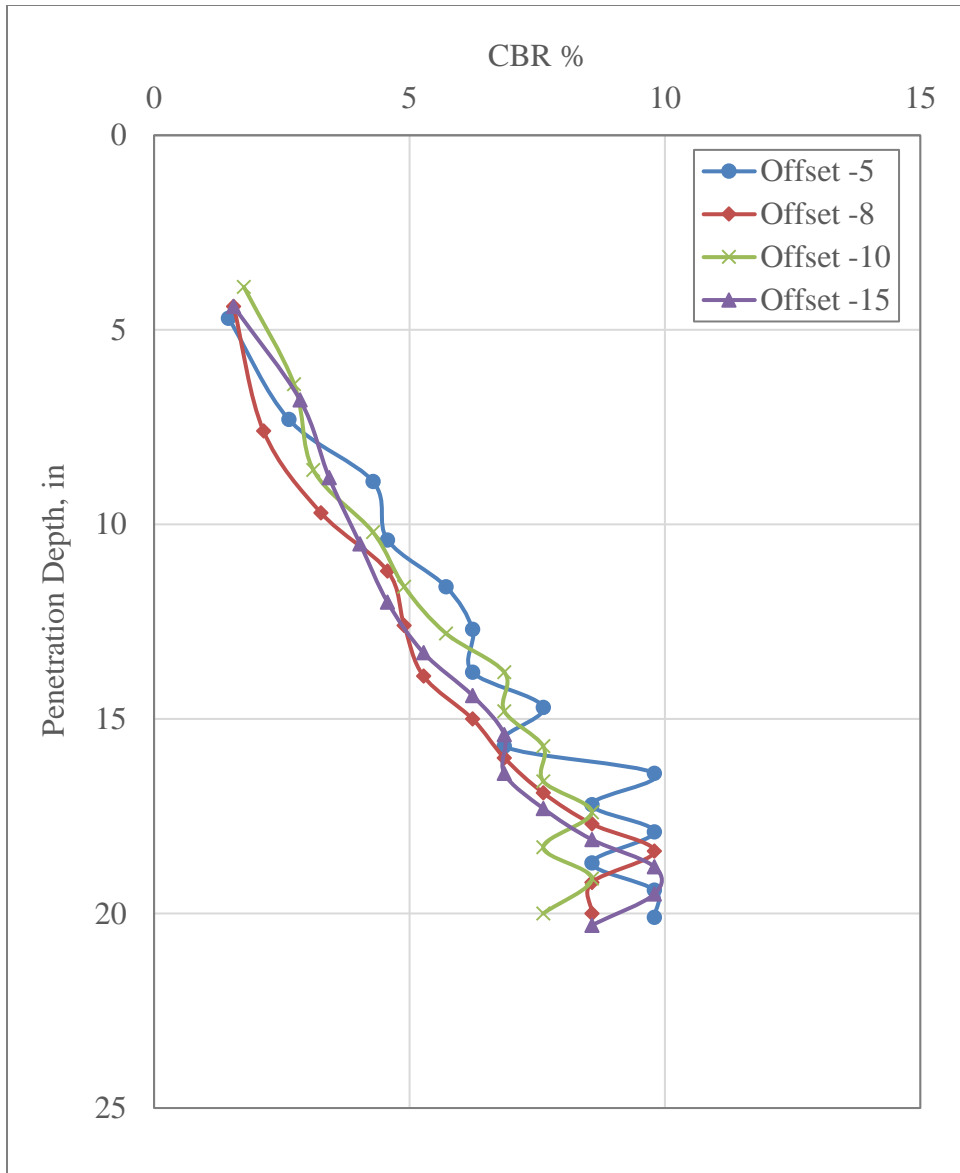


Figure 73. DCP Results for LFP3-N

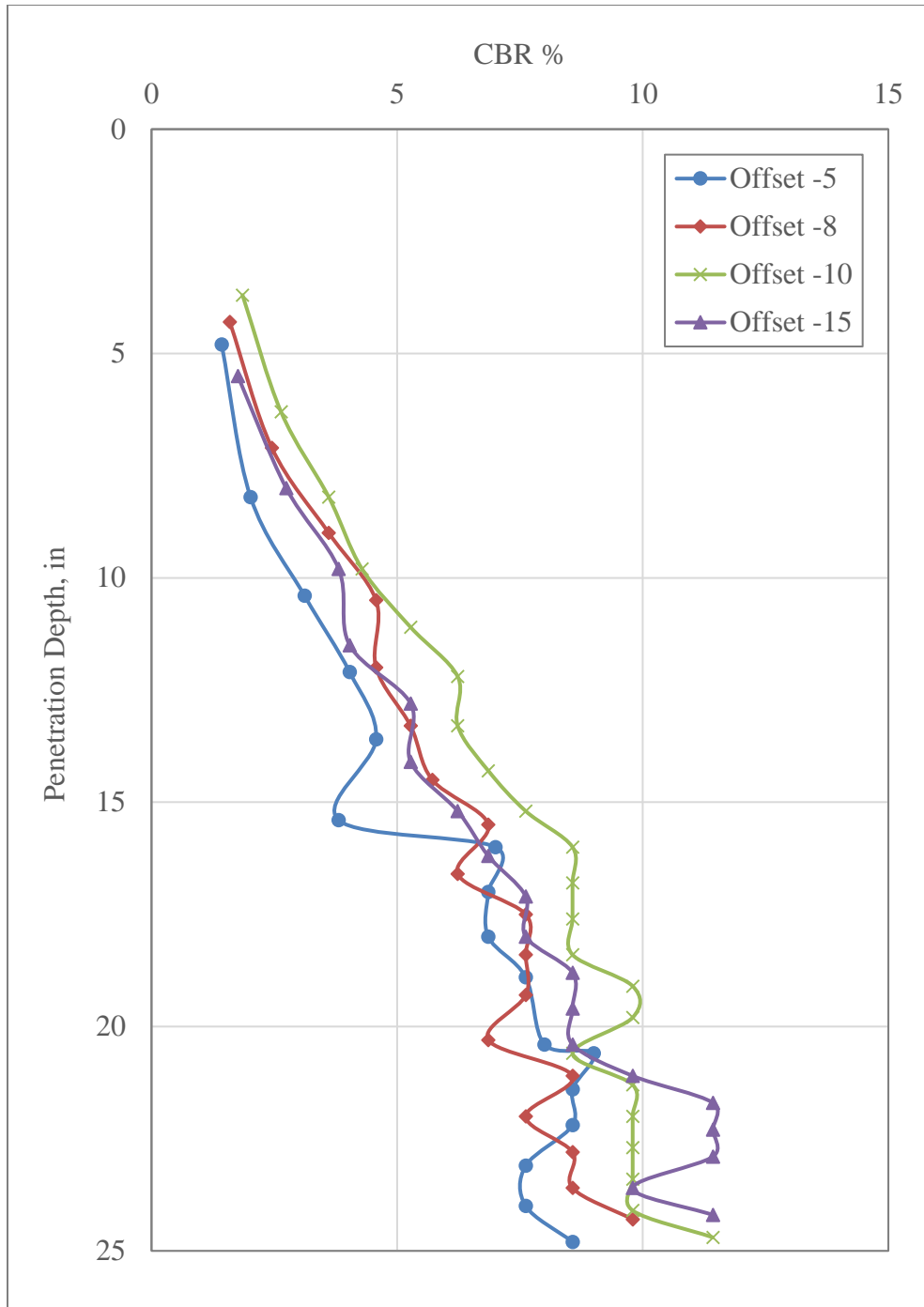


Figure 74. DCP Results for LFP4-N

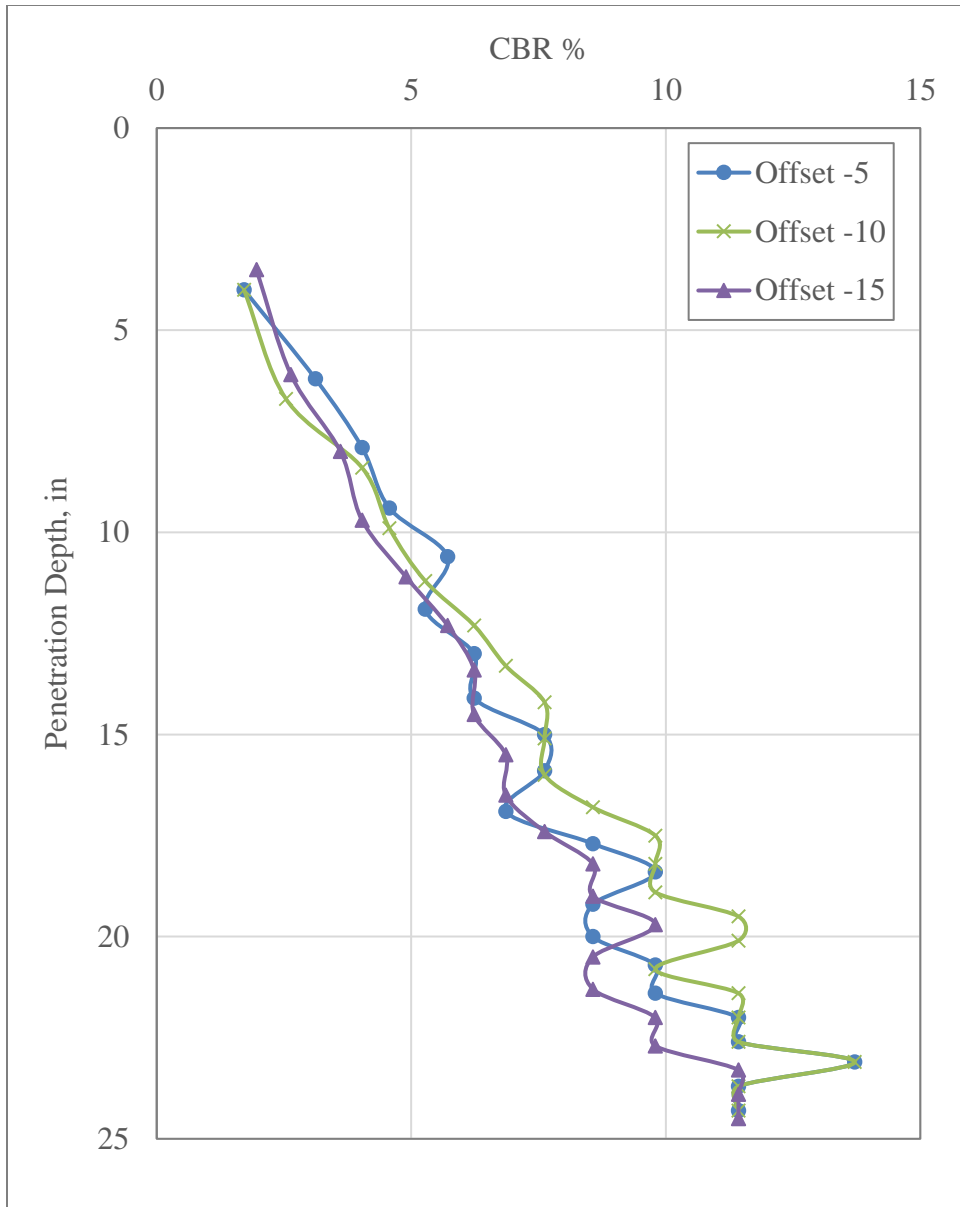


Figure 75. DCP Results for LFC5-N

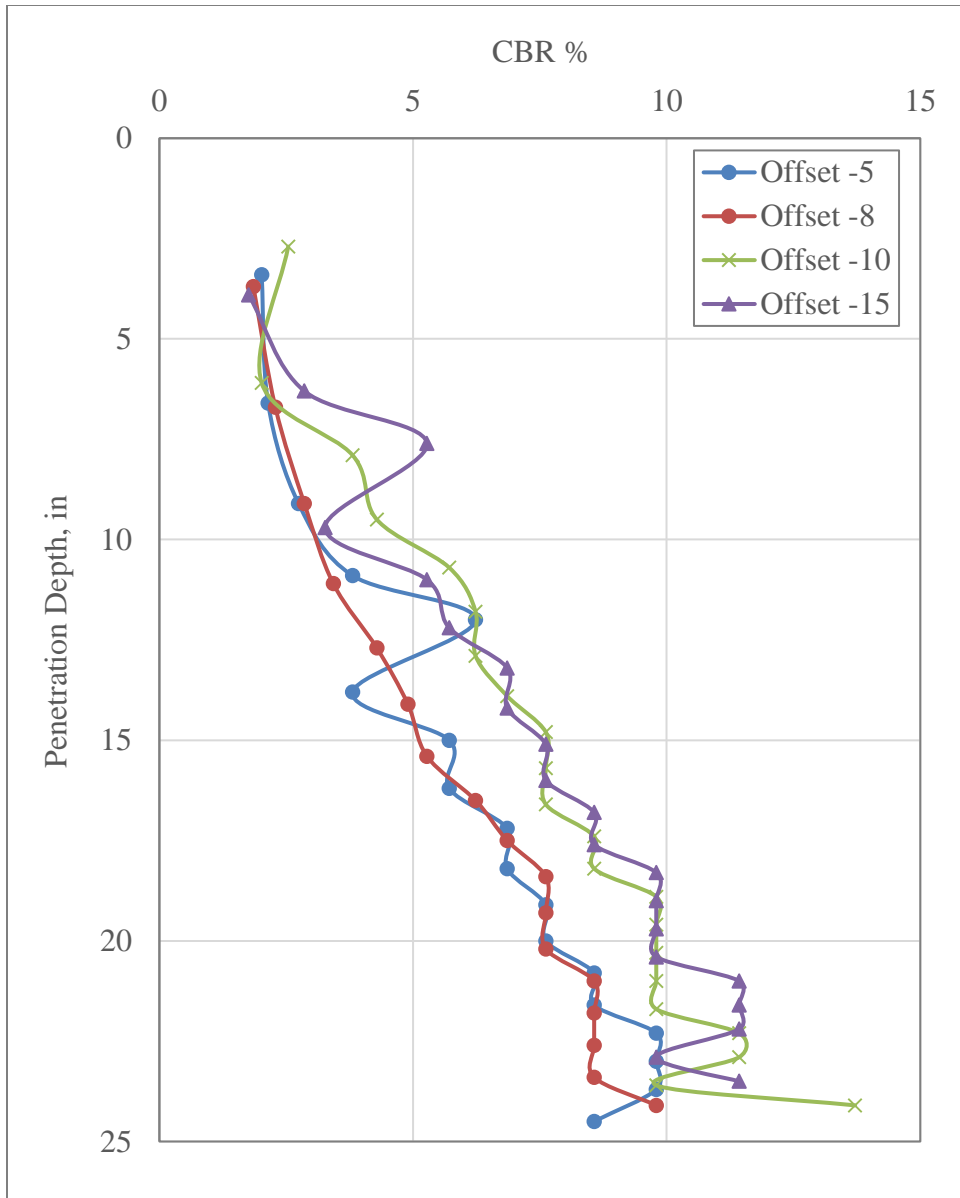


Figure 76. DCP Results for LFS6-N

7. PROFILE

Trenching provides a viable option to examine failed test items and confirmation of the contribution of each pavement layer to the total rutting. Once the field tests were completed, the trench walls were cleaned to clearly expose the layer interfaces. Using a laser straight line, the face of each trench was measured to get the profile of each layer of the pavement.

In figures 77 to 88, the pavement layer profile measurements on the west and east trench walls are presented along with as built pavement profiles. Figures 89-91 show the percent contribution of each layer to the maximum rut depths. The layer thickness measurements were made at 5 ft. intervals during the construction (as-built thickness), whereas in the trench, measurements were made at 1 ft. intervals outside the wheel paths, and at 6 in. intervals inside the wheel path.

Trench profiles show that for all the test items, the majority of the observed rutting was contributed by the subbase P-154 layer. The P-154 layer thickness reduction contributed 70% to 100% of the total rutting. The P-154 layer thickness reduction in LFC5-N was higher than LFS6-N. It is speculated that the ATDB material may distribute the traffic load more effectively than P-209 material. Consequently, under the same traffic load, the vertical stress on top of the P-154 surface in test item LFC5-N was higher than LFS6-N.

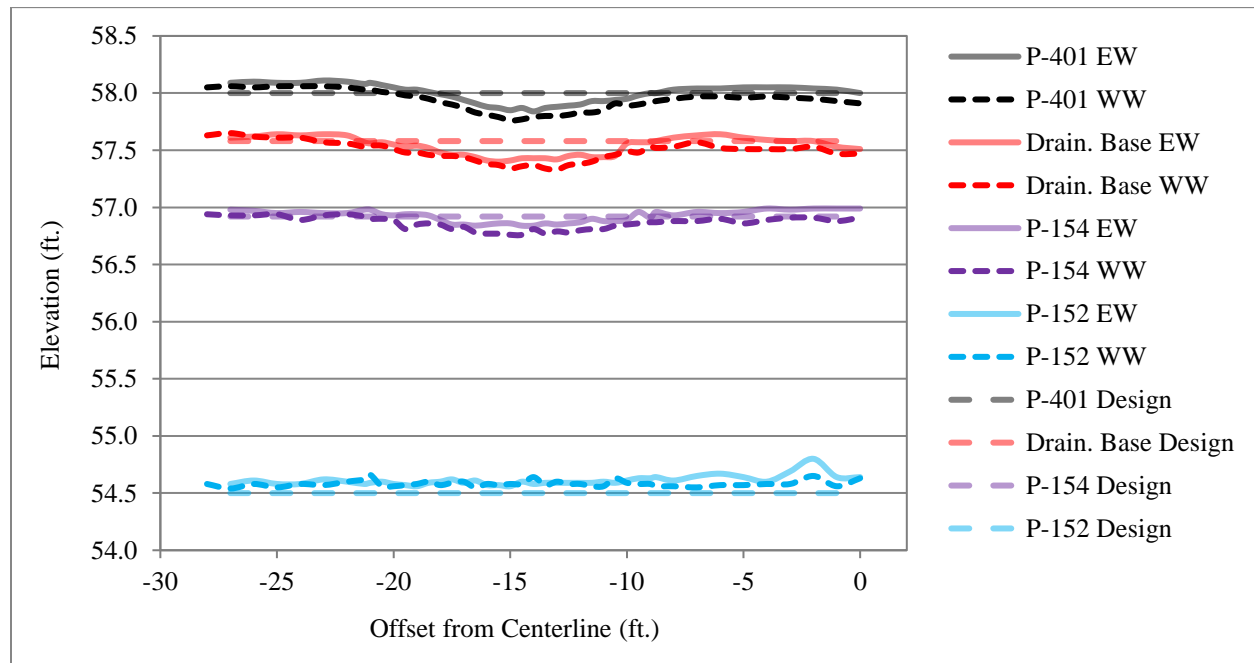


Figure 77. Pavement Layer Profiles, LFS6-N

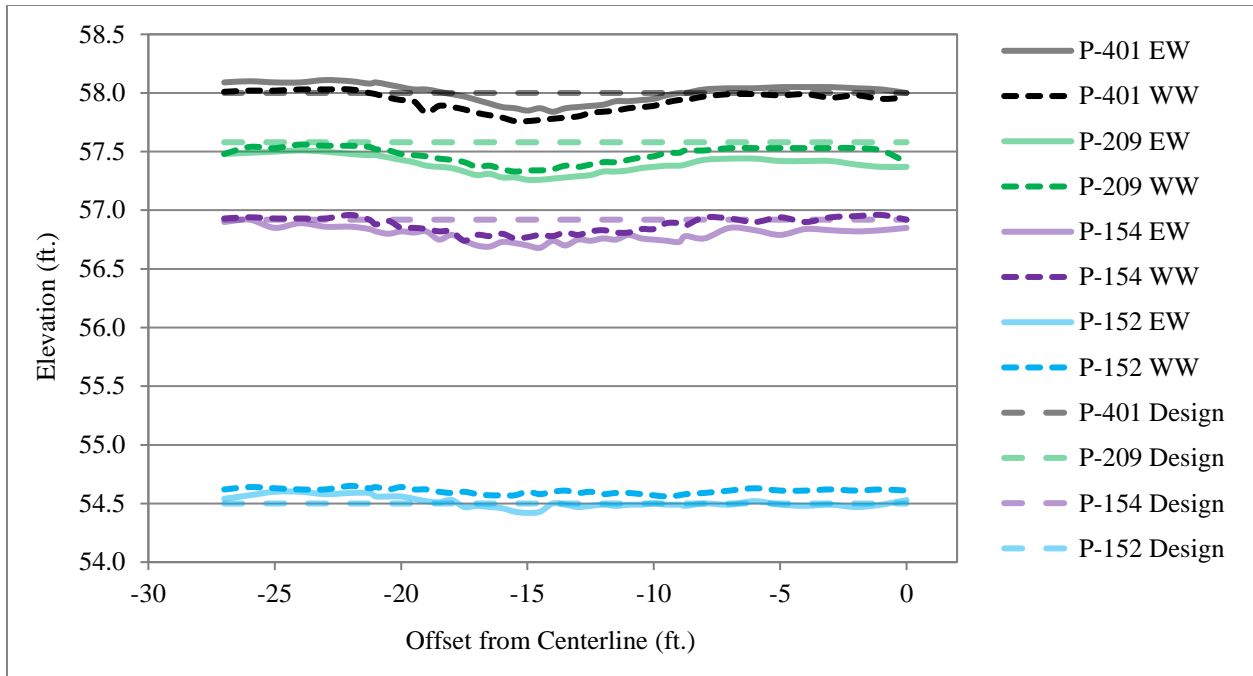


Figure 78. Pavement Layer Profiles, LFC5-N

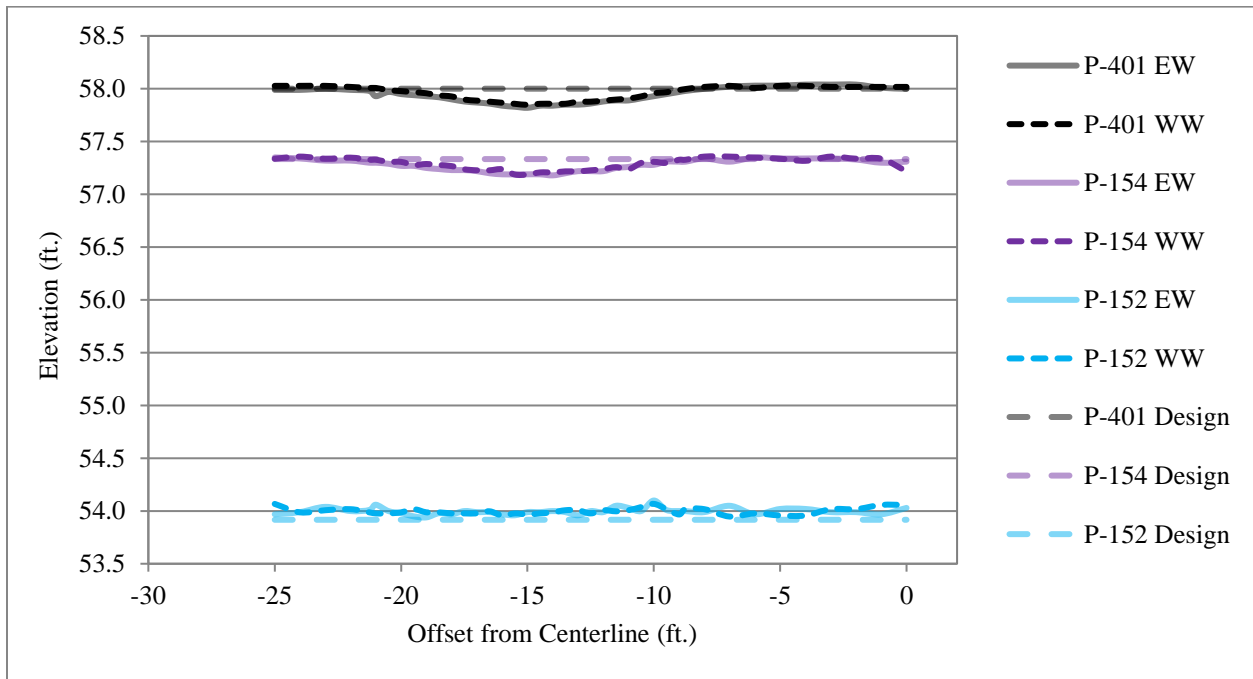


Figure 79. Pavement Layer Profiles, LFP4-N

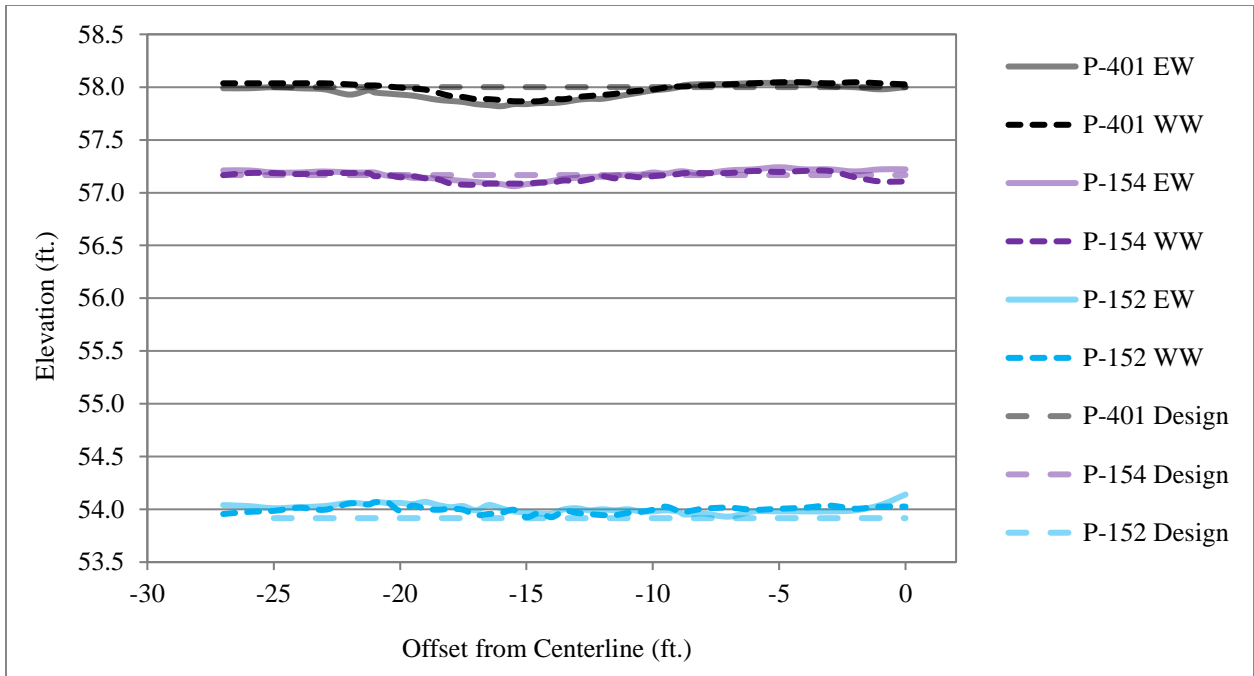


Figure 80. Pavement Layer Profiles, LFP3-N

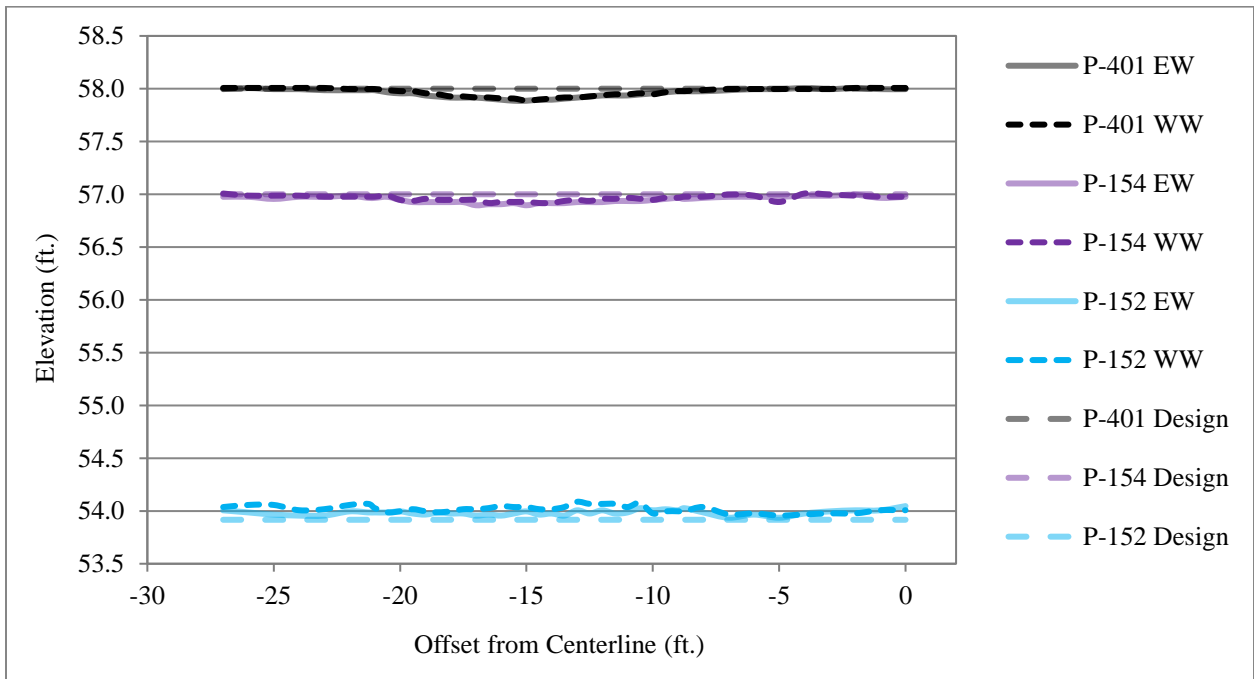


Figure 81. Pavement Layer Profiles, LFP2-N

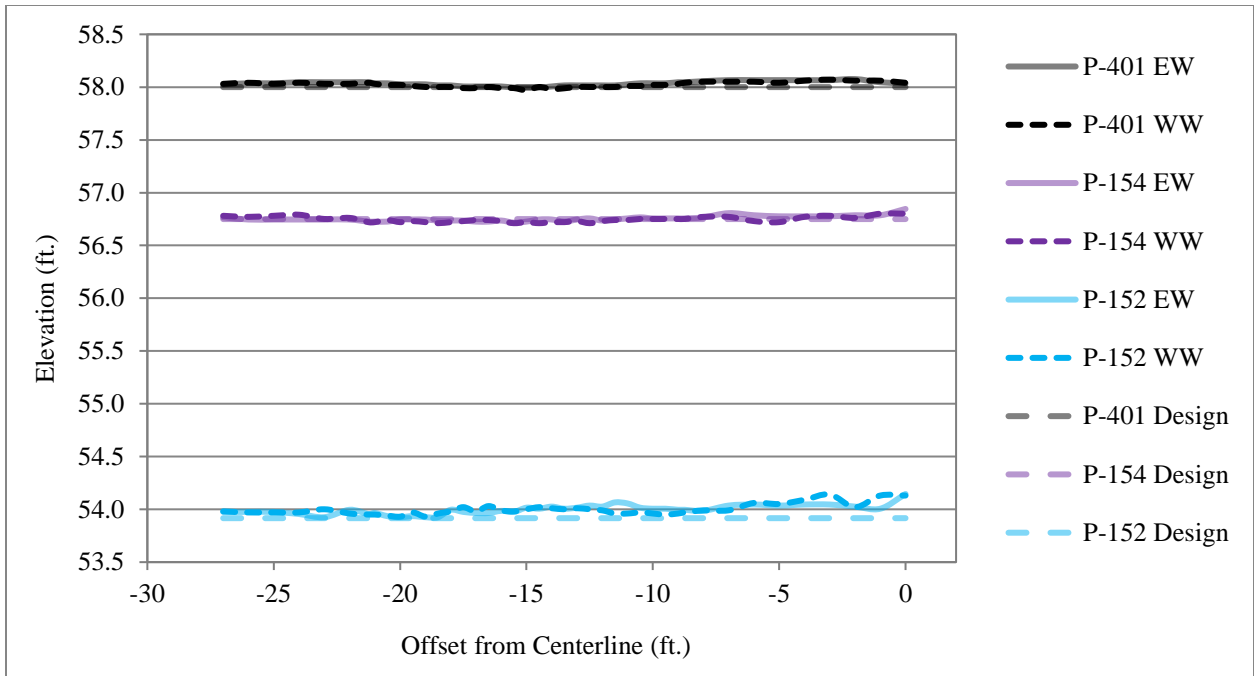


Figure 82. Pavement Layer Profiles, LFP1-N

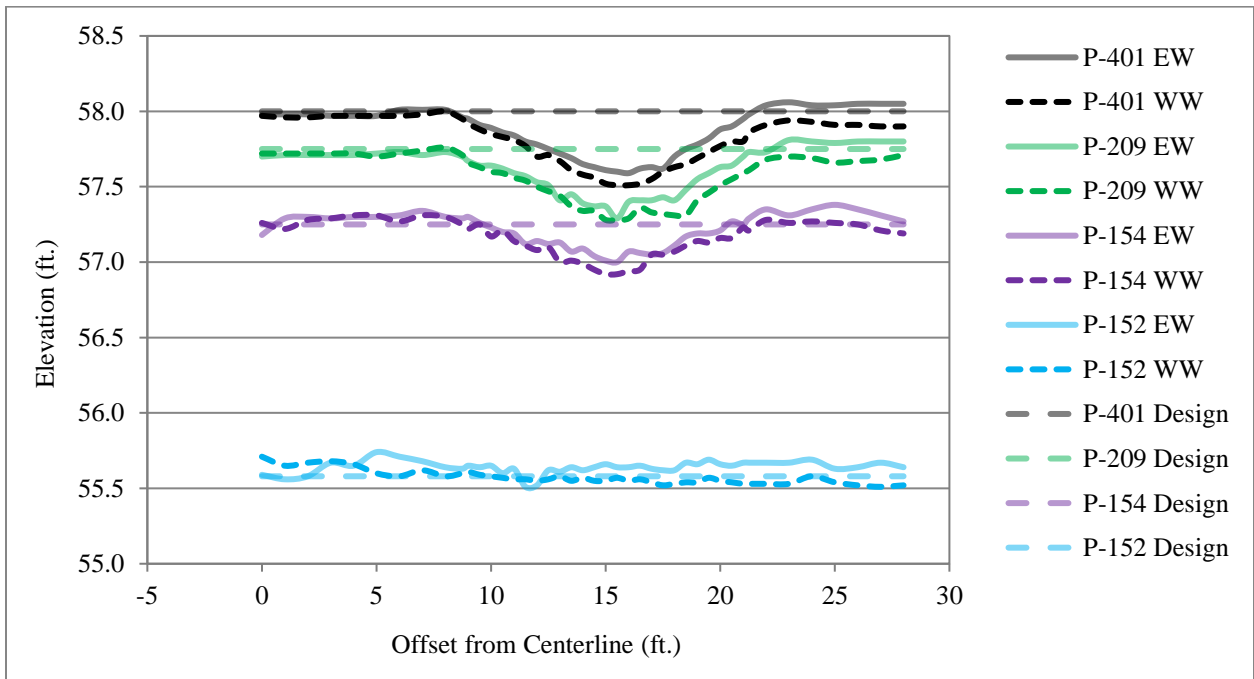


Figure 83. Pavement Layer Profiles, LFC6-S

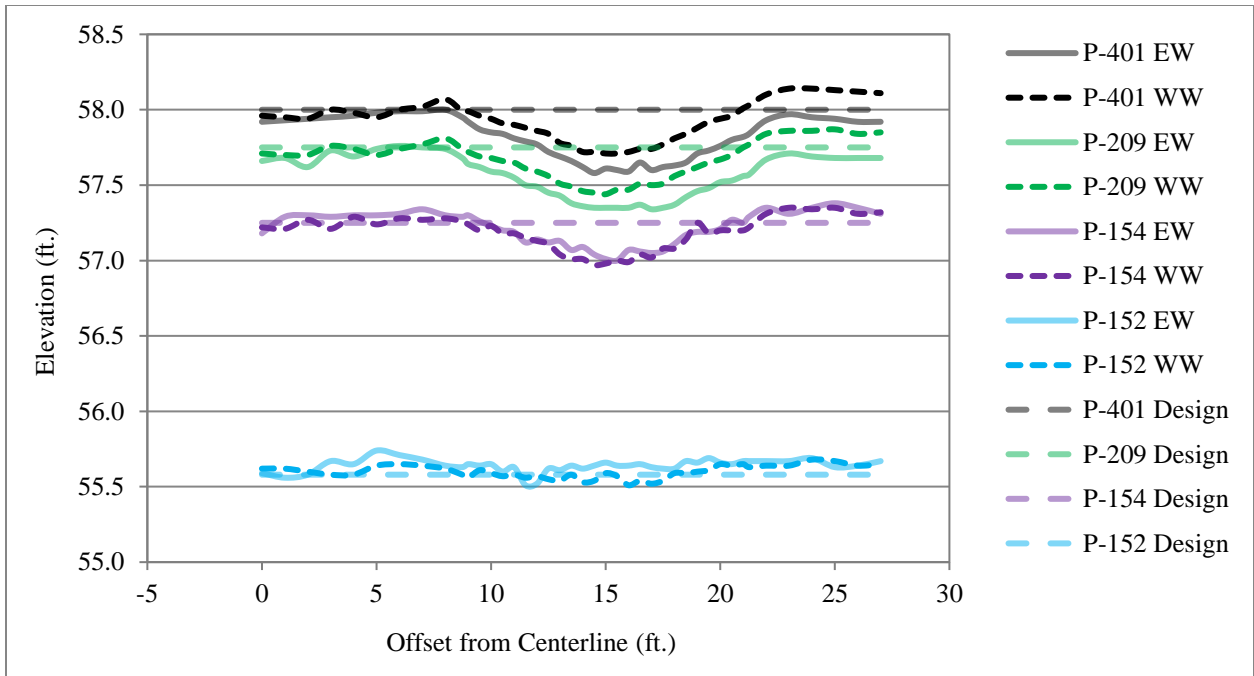


Figure 84. Pavement Layer Profiles, LFC5-S

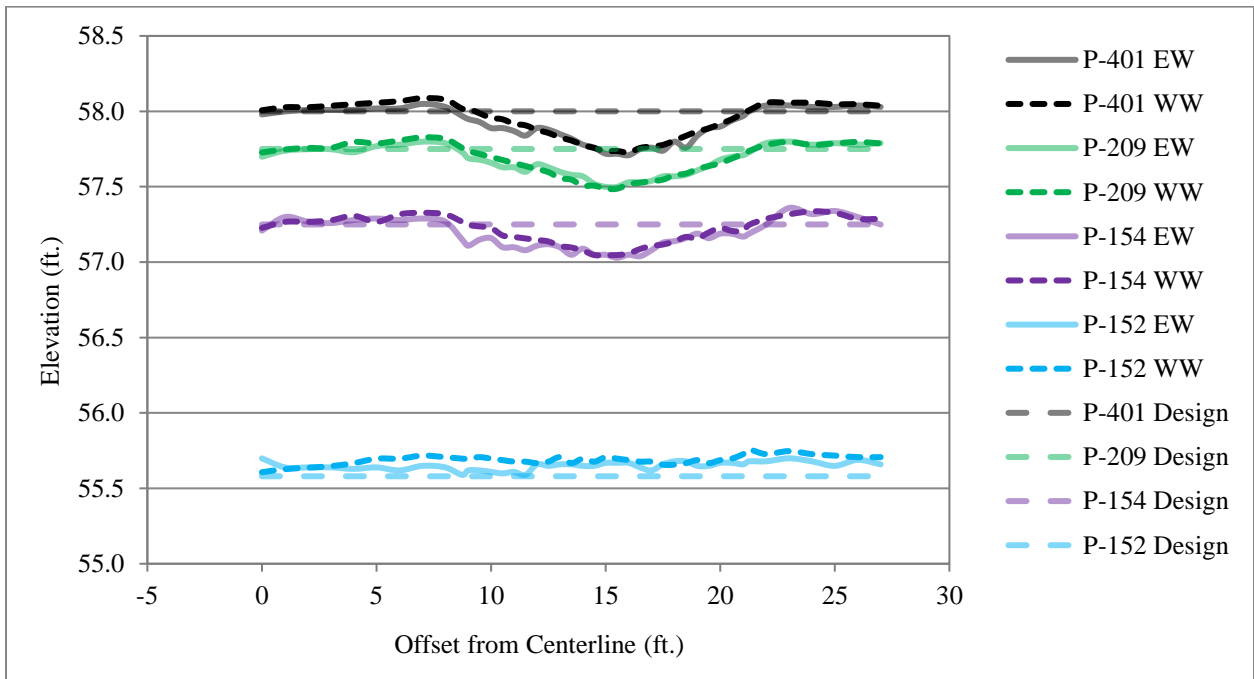


Figure 85. Pavement Layer Profiles, LFC4-S

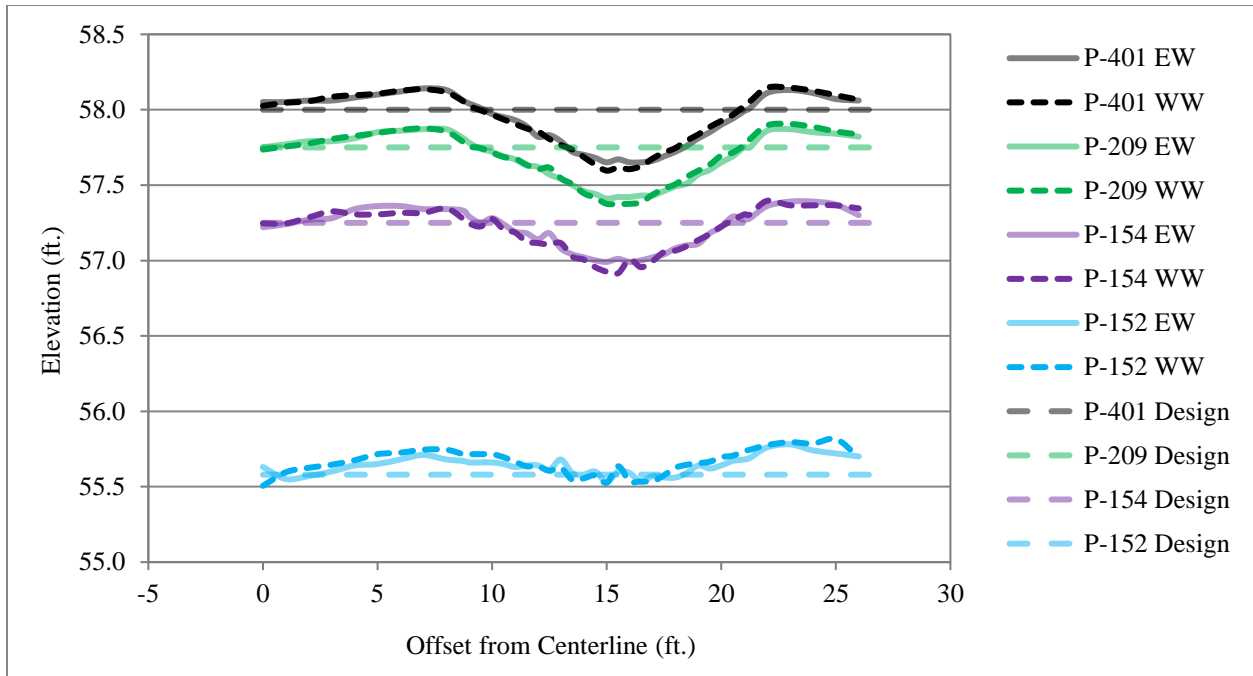


Figure 86. Pavement Layer Profiles, LFC3-S

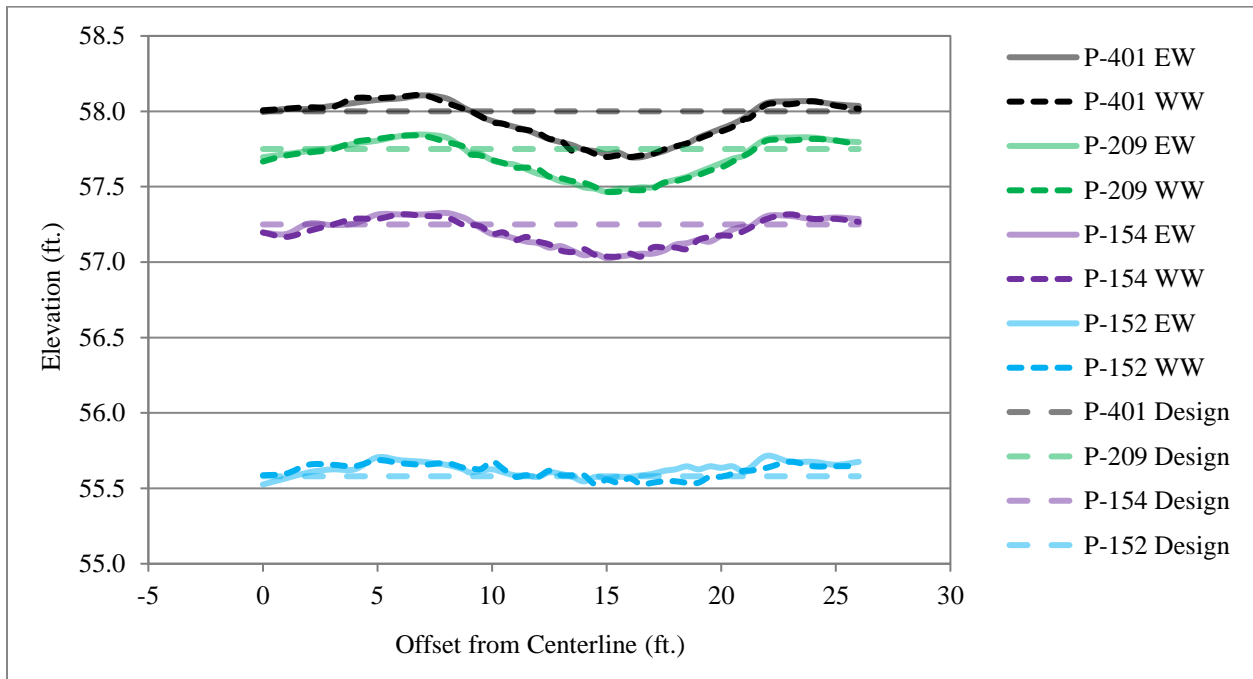


Figure 87. Pavement Layer Profiles, LFC2-S

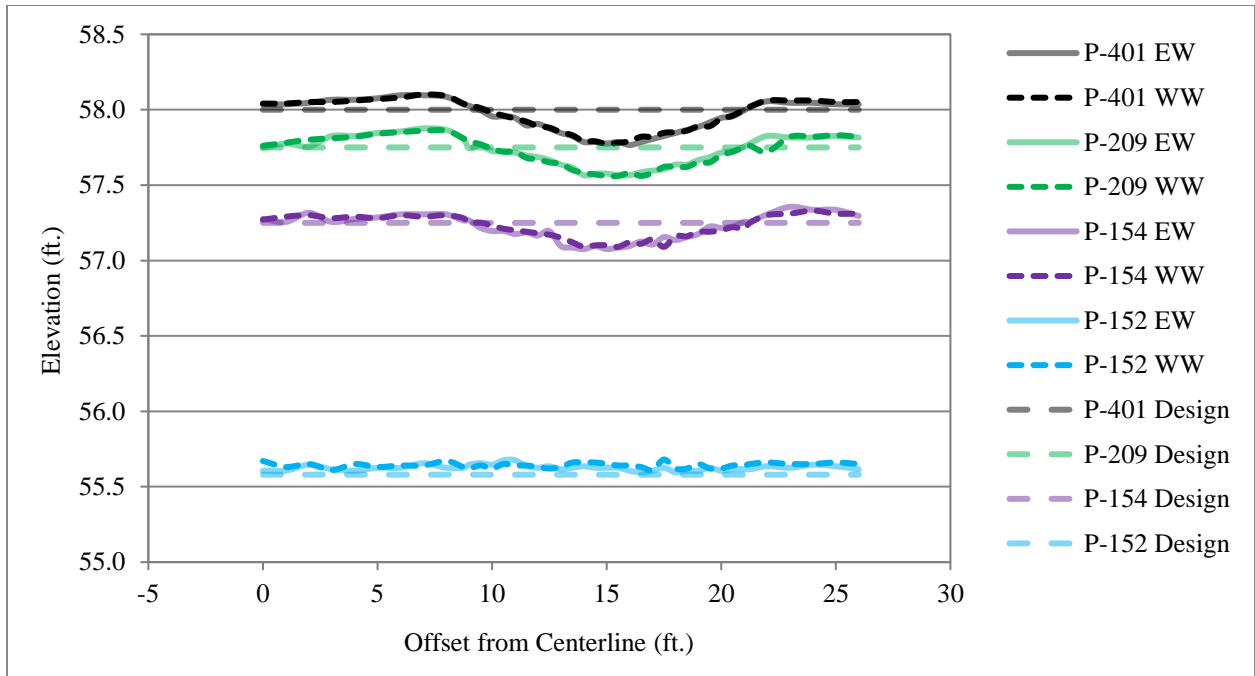


Figure 88. Pavement Layer Profiles, LFC1-S

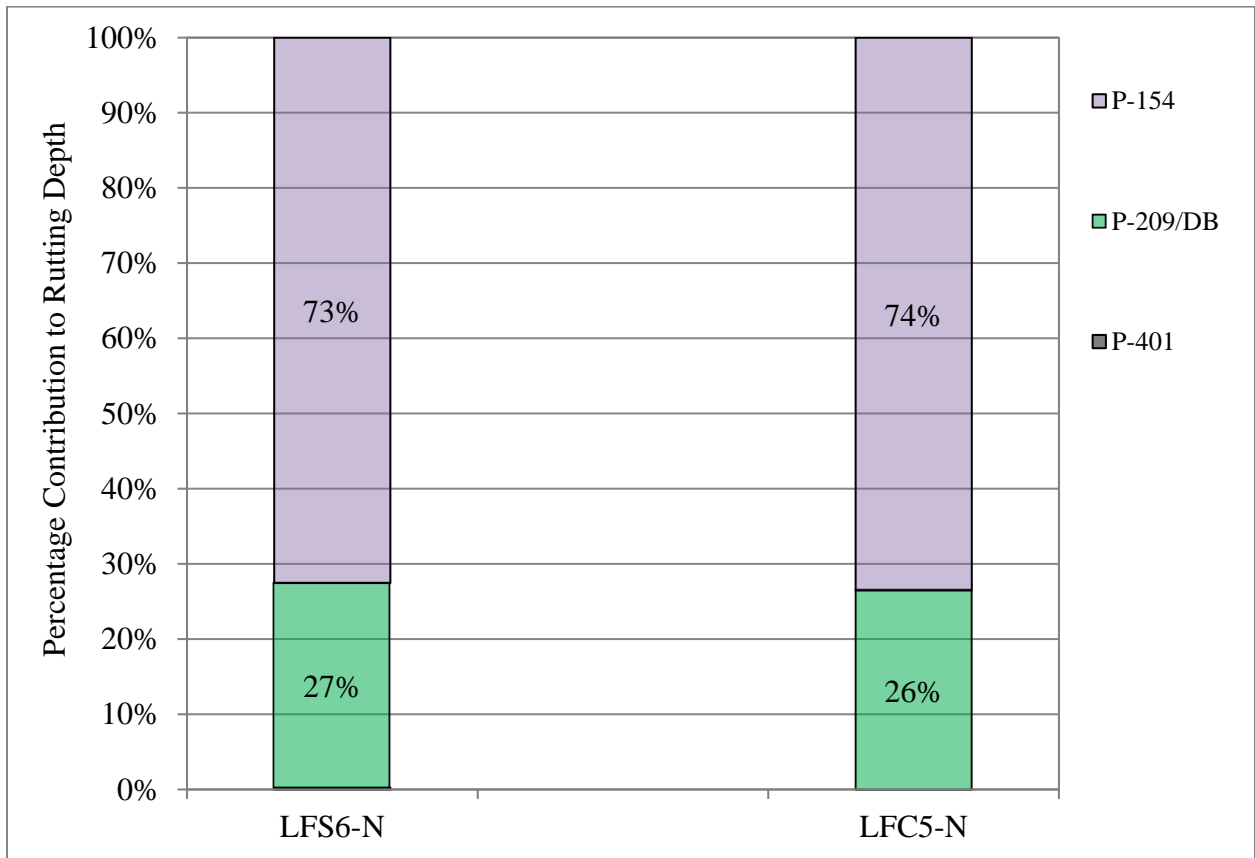


Figure 89. Percent Contribution to Rut Depth (LFS6-N LFC5-N)

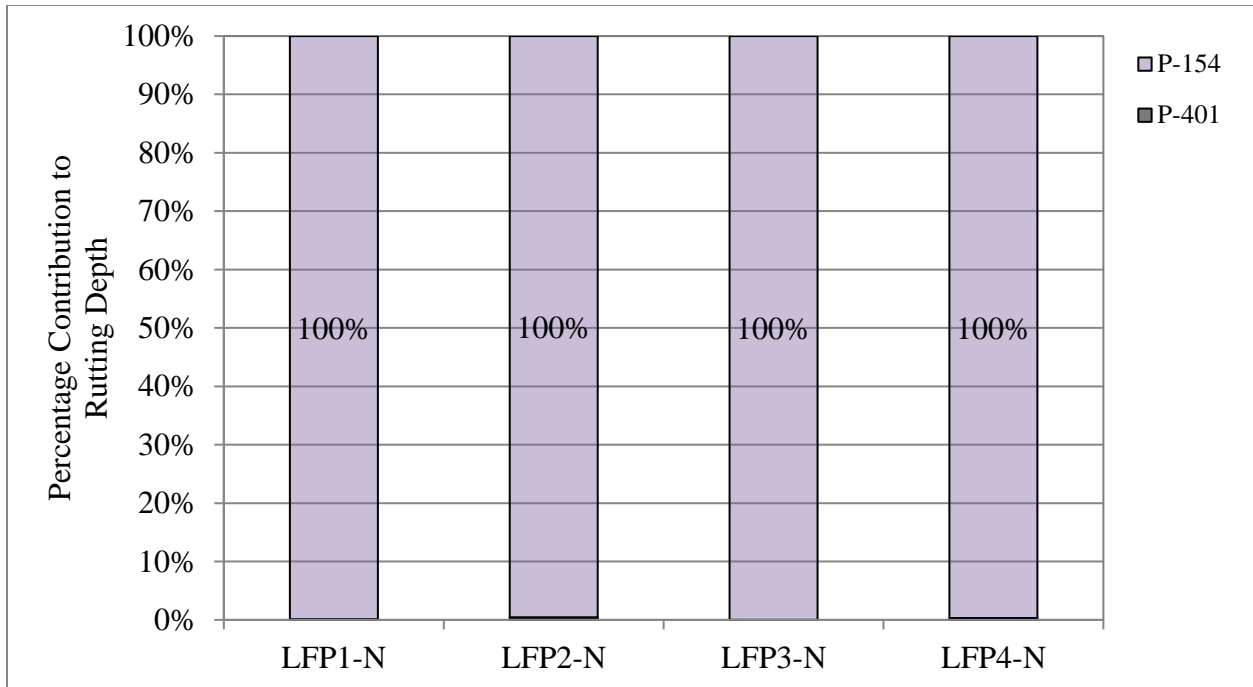


Figure 90. Percent Contribution to Rut Depth (LFP1-N to LFP4-N)

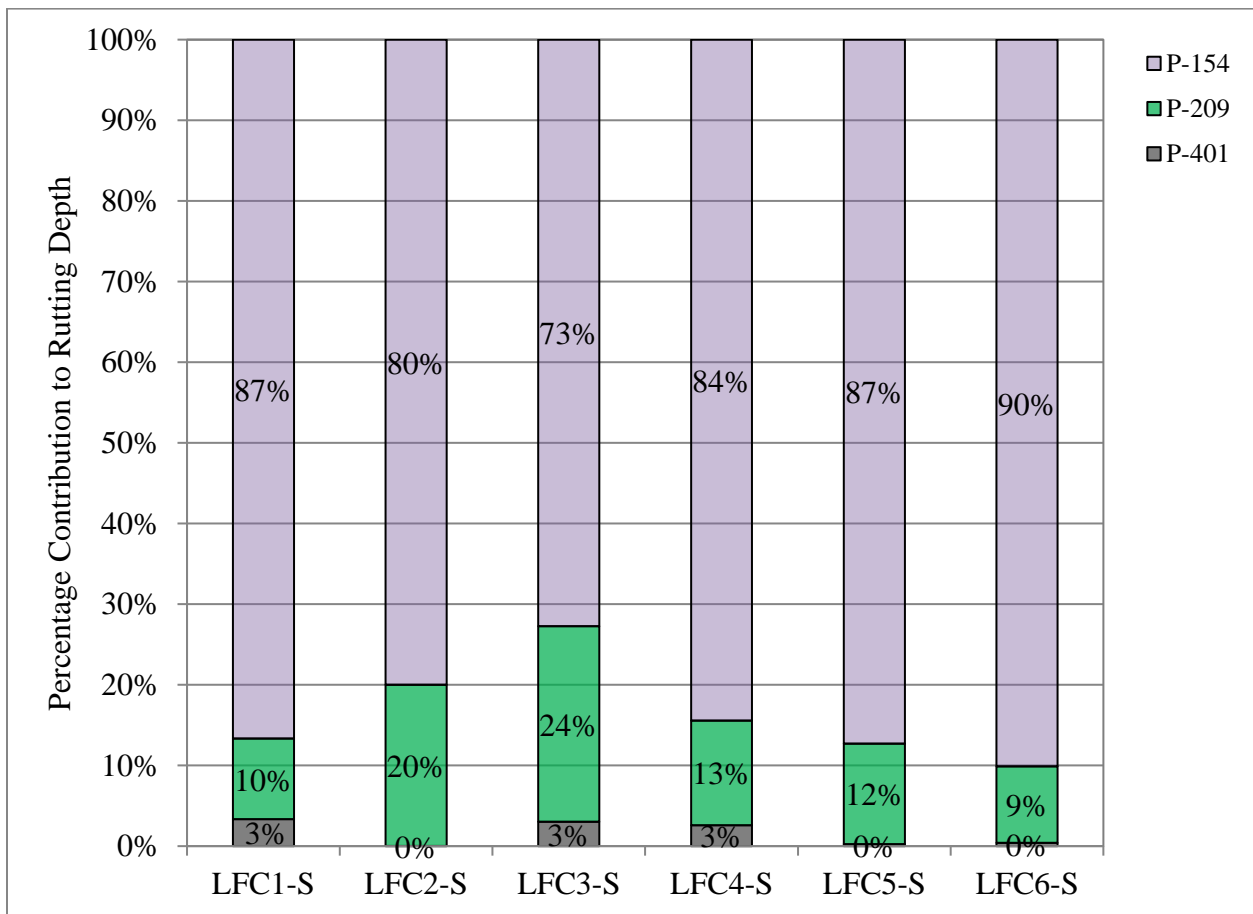


Figure 91. Percent Contribution to Rut Depth (CC7 South)

8. SUMMARY

- Six trenches were dug to investigate the failure mechanism of the pavement structure.
- A series of field tests were performed on each layer of the pavement structure. The test results were analyzed and summarized in this report.
- P-401 and ATDB cores, P-209, P-154 and P-152 materials were collected for laboratory testing.
- Layer profile measurements were taken from trench walls using a laser straight line to obtain the post-traffic pavement profile in all the test items.

9. REFERENCES

1. Gemini Technologies Inc. Construction Cycle 7 Post-Traffic Report – Laboratory Testing. Deliverable No. 4.9.3.1. July, 2019.